Common architecture between the flagellar type III ATPase complex and F_1-ATPase revealed by the structure of FliJ

Doctoral Thesis
September 2010

Tatsuya Ibuki

Graduate School of Frontier Biosciences
Osaka University

Abstract

The flagellum is a motile organelle composed of the basal body rings and the tubular axial structure. The axial component proteins synthesized in the cytoplasm are transferred into the central channel of the flagellum by the flagellar type III protein export apparatus for self-assembly at the growing end of the flagellum. The export apparatus is composed of six transmembrane proteins (FlhA, FlhB, FliO, FliP, FliQ, FliR) and three soluble components (FliH, FliI, FliJ). FliI is the ATPase and forms a hetero-trimer complex with a dimer of its regulator FliH in the cytoplasm. The $FliH_2FliI$ complex recruites export substrates to the proton-driven export gate made of the transmembrane proteins and helps the initial entry of the substrate into the gate. FliJ is an essential component for protein export. Since FliJ interacts with flagellar axial proteins and prevents their premature aggregation in the cytoplasm, FliJ has been postulated to be a general chaperone for the substrates. However, it remains unknown how these reactions proceed within the cell.

To elucidate the function of FliJ and molecular mechanism of flagellar protein export across the cell membrane, I determined the crystal structure of FliJ at 2.1 Å resolution. FliJ has a remarkable structural similarity to the γ-subunit of F_oF_1-ATP synthase. Although no apparent sequence similarity has been found between FliJ and the γ-subunit, a structure-based sequence alignment revealed regions that are conserved between them. Interestingly, it has already been shown that the FliI structure closely resembles those of the α/β-subunits of F_oF_1-ATP synthase, which form $\alpha_3\beta_3$ hexameric ring structure and that FliI forms a hexameric ring structure. These similarities suggest that FliI and FliJ may form a complex just like F_1-ATPase. I therefore analyzed the interaction between FliJ and FliI by electron microscopy and biochemical techniques. FliJ formed a complex with the FliI hexameric ring and facilitated the ring formation

and ATPase activity of FliI. These observations suggest that the flagellar type III protein export involves a mechanism similar to that of F_1-ATPase and that the flagellum and F_oF_1-ATP synthase are evolutionally related.

The conserved region between FliJ and the γ-subunit is highly conserved among their homologs as well and corresponds to the surface interacting with the ε-subunit of F_1-ATPase, suggesting that FliJ may have binding partner corresponding to the ε-subunit. To identify the function of these conserved residues, site-directed mutation experiments were performed for eight highly conserved, surface-exposed residues of FliJ. The F72A and L76A mutations abolished the interaction between GST-FliJ and FlhA. In the recent paper, it has been shown that an interaction between FliJ and a gate-forming protein FlhA facilitates an inward-directed proton flow through the gate. These results suggest that Phe-72 and Leu-76 of FliJ are essential for the interaction with FlhA to facilitate proton translocation-coupled protein export through the gate.

Table of contents

Introduction **1**

1. Bacterial flagella 1
2. Assembly process of the flagellum 2
3. Flagellar type III protein export apparatus 3
4. Role of FliJ 4
5. Focuses of my Ph. D. work 5

Chapter 1. X-ray structure analysis of FliJ **12**

1.1. Introduction 12
1.2. Materials and Methods 13
1.2.1. Protein expression and purification 13
1.2.2. Crystallization of FliJ 14
1.2.3. Preparation and crystallization of mercury derivative 15
1.2.4. X-ray diffraction data collection of FliJ 15
1.2.5. Mass spectrometry 16
1.2.6. Phasing, model building and refinement of FliJ 17
1.3. Results 26
1.3.1. Crystal structure of FliJ 26
1.3.2. Comparison with γ-subunit of F_1-ATPase 26
1.4. Discussion 31
1.4.1. High solubility of GSH-FliJ 31
1.4.2. Crystal packing of FliJ 31
1.4.3. Structural insight of FliJ and FliI 32

Chapter 2. Interaction between FliJ and FliI, and their complex **37**

2.1. Introduction 37
2.2. Materials and Methods 40
2.2.1. Bacterial strains, plasmids and primer 40
2.2.2. Preparation and purification of FliI 40
2.2.3. Preparation and purification of FliJ mutants 40
2.2.4. *In vitro* reconstruction of the FliI ring structure and electron microscopy 41

2.2.5. Preparation of FliJ labeled with Cy3 41
2.2.6. Analytical gel-filtration chromatography of FliI-FliJ complex 42
2.2.7. Preparation of FliJ labeled with Streptavidin 42
2.2.8. Electron cryomicroscopy and image processing 42
2.2.9. ATPase activity measurement of FliI 43
2.3. Result 47
2.3.1. FliJ affects the hexameric ring formation of FliI 47
2.3.2. Gel-filtration analysis of the FliI-FliJ complex labeled with Cy3 47
2.3.3. Observation of the FliI-FliJ complex labeled with streptavidin 48
2.3.4. Electron cryomicroscopy and image analysis of the FliI-FliJ complex 49
2.3.5. Effect of FliJ on the ATPase activity of FliI 50
2.4. Discussion 60
2.4.1. ATPase activity of FliI-FliJ complex 60
2.4.2. Similarities between flagellar protein export apparatus and F_oF_1-ATP synthase 60
Chapter 3. Role of the highly conserved residues of FliJ on the flagellar typr III protein export 63
3.1. Introduction 63
3.2. Materials and Methods 64
3.2.1. Bacterial strains, plasmids, primer and media 64
3.2.2. Construction of plasmids 64
3.2.3. Motility assay 65
3.2.4. Preparation of whole cell and culture supernatant fractions 65
3.2.5. Immunoblotting 65
3.2.6. Pull-down assays by GST affinity chromatography 66
3.2.7. Preparation and purification of $FlhA_C$ 66
3.2.8. ATPase activity measurement of FliI 67
3.3. Result 71
3.3.1. Alanine scanning analysis of highly conserved residues of FliJ 71
3.3.2. Dominant-negative effect of GST-FliJ mutants 72
3.3.3. Interaction between FlhA and GST-FliJ mutants 72
3.3.4. Interaction between $FlhA_C$ and GST-FliJ mutants (F72A and L76A) 73
3.3.5. $FlhA_C$ activates the ATPase activity of the $FliI_6FliJ$ complex 73

3.4. Discussion 80
3.4.1. The FliH-FliI complex overcomes the FliJ defects 80
3.4.2. Interaction between FliJ and FlhA 80
3.4.3. Role of the interaction between FliJ and FlhA in protein export. 81
Chapter 4. Conclusion 84
Acknowledgement 90
Reference 91
Publication 98

Abbreviations

ATP : adenosine triphosphate

ADP : adenosine diphosphate

DNA : deoxyribonucleic acid

DTT : dithiothreitol

EDTA : ethylenediaminetetraacetic acid

GST : glutathione-S-transferase

IPTG : isopropyl-1-thio-β-D-galactopyranoside

LB : Luria-Bertani broth

MALDI-TOF : matrix assisted laser desorption ionization time of flight

MES : 2-morpholino-4-ethanesulfonic acid

NADH : nicotinamide adenine dinucleotide

OD_{600} : optical density (wavelength 600 nm)

PBS : phosphate buffered saline

PCR : plymerase chain reaction

PEG : polyethylene glycol

PMF : proton motive force

RMS : root mean square

SAD : single-wavelength anomalous dispersion

S/N : signal/noise

SDS-PAGE : sodium dodecyl sulfate polyacrylamide gel electrophoresis

Tris : tris (hydroxymethyl) aminomethane

WT : wild type

Introduction

1. Bacterial flagella

Bacteria actively swim in liquid environments by rotating long, helical, filamentous organelle called the flagellum (Figure 1a). At the base of each filament, there is a rotary motor powered by proton or sodium ion motive force across the cytoplasmic membrane. When bacteria swim straight, the motors rotate counterclockwise (CCW) and the filaments form a bundle to produce thrust. By quick reversal of the motor rotation to clockwise (CW), the bundle is disrupted so that bacteria tumble and change their swimming direction to move toward more favorable environments from less favorable ones.

The flagellum is a large molecular assembly composed of nearly 30 different proteins and can be roughly divided into the basal body rings and the tubular axial structure (Figure 1b). The basal body rings, which are embedded in the cell envelope, work as a reversible rotary motor with stator units composed of trans-membrane proteins, MotA and MotB (Berg and Anderson, 1973; Silverman and Simon, 1974). The basal body rings include the C-ring, the MS-ring and the LP-ring. The C-ring, which is in the cytoplasm, regulates the reversal frequency of the motor and facilitates flagellar protein export for flagellar morphogenesis (Yamaguchi *et al*., 1986). The MS-ring, which is present in the cytoplasmic membrane, acts as the base for flagellar assembly. The LP-ring, which spans through the peptidoglycan layer and the outer membrane, functions as a bushing by encapsulating the drive shaft called the rod. The MS-ring and the C-ring form the rotor, which is surrounded by the stator units, and torque is believed to be generated by the interaction between the rotor and the stator. The tubular axial structure can be divided into three substructures: the filament, the hook and the rod (DePamphilis and Adler, 1971a, 1971b). The filament with typical lengths of 10 - 15

μm is a helical assembly made of a few tens of thousands of flagellin (FliC) molecules, and propels the cell by its rotation driven by the rotary motor. The hook, whose length is 55 ± 6 nm, acts as a universal joint that smoothly transmits torque generated by the motor to the filament regardless of its orientation. The hook is a helical assembly of about 120 copies of a single protein, FlgE. The rod is a drive shaft connecting the rotor rings and the hook. The rod with an approximate length of 30 nm is a complex structure composed of five proteins (FliE, FlgB, FlgC, FlgF and FlgG). The axial structure includes three more proteins: HAP1 (FlgK) and HAP3 (FlgL), which form a joint connecting the filament and the hook; and HAP2 (FliD), which forms a pentameric cap at the distal end of the filament to assist filament growth (as review articles, see Macnab, 2003; Berg, 2003).

2. Assembly process of the flagellum

The first step of flagellar assembly is the MS-ring formation by self-association of FliF protein in the cytoplasmic membrane (Figure 2-(A)). The C-ring, which is composed of FliG, FliM and FliN, is then formed onto the cytoplasmic face of the MS-ring, and the flagellar protein export apparatus is assembled somewhere within the MS-C-ring, most likely in the central pore of the MS-ring (Figure 2-(B)). The export apparatus consists of six integral membrane proteins (FlhA, FlhB, FliO, FliP, FliQ, FliR) and three soluble proteins (FliH, FliI, FliJ) (Figure 2-(C)) (Minamino and Macnab, 1999, 2000a). The axial structure component proteins are translocated across the cytoplasmic membrane through the export apparatus. After completion of the export apparatus, the rod proteins (FliE, FlgB, FlgC, FlgF and FlgG) and the putative rod cap protein (FlgJ) are exported to form the rod onto the periplasmic side of the MS-ring. The rod grows through the peptidoglycan layer with the help of FlgJ, which shows a

peptidoglycan hydrolyzing activity (Nambu *et al*., 1999) (Figure 2-(D)). Upon formation of the rod, FlgH and FliI are exported into the periplasmic space by the Sec export system, and assemble around the rod to form the LP-ring (Figure 2-(E, F)). After the rod completion, the hook (FlgE) is assembled with the help of the pentameric hook cap complex composed of FlgD until its length reaches ca. 55 nm (Figure 2-(G, H)) (Ohnishi *et al*., 1994; Hirano *et al*., 1994).

Then, the substrate specificity of the export apparatus switches from the rod/hook type to the filament type, by which the elongation of the hook stops. The hook cap complex is displaced by HAP1 (FlgK) (Figure 2-(I)) followed by the attachment of HAP3 (FlgL) on the HAP1 layer to form the hook-filament junction structure (Figure 2-(J)). Then, the pentameric filament cap complex composed of HAP2 (FliD) is formed on the hook-filament junction (Figure 2-(K, L)), and flagellin (FliC) subunits are incorporated onto the distal end of the growing flagellum just below the filament cap (Figure 2-(M-R)). During the filament growth, the stator units assemble around the rotor, and the motor begins to rotate (Kubori, *et al.,* 1992; Namba and Vonderviszt, 1997; Minamino and Namba, 2004).

3. Flagellar type III protein export apparatus

In general, most proteins to be secreted out of the cell are synthesized as precursor proteins with signal peptides at their amino termini and translocated across the cytoplasmic membrane by the Sec secretion apparatus. The signal peptides are the acceptance signal for translocation across the membrane and cleaved off by the signal peptidase during the export (Schatz and Beckwith, 1990). Among flagellar proteins, only FlgH (the L-ring protein), FlgI (the P-ring protein) and FlgA (the periplasmic chaperone for the assembly of the P-ring) have the signal peptides and are exported to

the periplasm by the Sec export pathway (Homma *et al*., 1987; Jones *et al*., 1987, 1989; Kutsukake *et al*., 1994a; Nambu *et al*., 2000; Schoenhals and Macnab, 1996). All the component proteins of the flagellar axial structure are translocated into the central channel of the growing flagellum by the flagellar specific type III protein export apparatus and then travel through the channel to the growing end for their self-assembly (Figure 3) (Macnab, 2004; Minamino *et al*., 2008). The membrane components of the export apparatus are believed to be located within the annular pore of the basal-body MS-ring to form the export gate. FliI is an ATPase (Fan *et al*., 1996), and its entire molecular structure highly resembles that of the α- and β-subunits of F_1-ATPase (Imada *et al*., 2007). FliH binds to the extreme N-terminal region of FliI to form the $FliH_2FliI$ complex in the cytoplasm and suppresses the ATPase activity of FliI (Auvray *et al*., 2002; Gonzalez-Pedrajo *et al*., 2002; Minamino and Macnab, 2000b). FliI forms a hexameric ring to fully exert its ATPase activity when the $FliH_2FliI$ complexes bind to the export gate (Minamino *et al*., 2006). FliI facilitates only the initial entry of the substrates into the narrow pore of the gate. The unfolding and translocation of the substrates through the gate is driven by proton motive force across the cytoplasmic membrane while the chemical energy derived from ATP hydrolysis by FliI is used for the release of FliH and FliI from the gate (Minamino and Namba, 2008).

4. Role of FliJ

FliJ is a 147 amino acid soluble protein and its structure is predicted to be an α-helical coiled coil (Figure 4). From a sequence analysis, FliJ is found to show similarities with flagellar specific chaperones, FliS, FlgN, and FliT, which are specific chaperones for FliC, FlgK and FlgL, and FliD, respectively. These chaperones are small α-helical proteins (ca. 15 to 20 kDa) including amphipathic helices in their C-terminal

regions (Figure 5).

FliJ is an essential component for protein export and interacts with FliH, FliI and the $FliH_2FliI$ complex. Since FliJ interacts with flagellar axial proteins and prevents their premature aggregation in the cytoplasm, it has been postulated to be a general chaperone for export substrates (Minamino *et al*., 2000). FliJ interacts not only with flagellar axial proteins and the soluble components of the export apparatus but also with FlhA and FlhB, which are export gate components (Minamino and Macnab, 2000a; Fraser *et al*., 2003), FliM, which is a component of the C-ring (Gonzalez-Pedrajo *et al*., 2006), and FliT and FlgN, which are chaperones for FliD and FlgK/FlgL, respectively (Evans *et al*., 2006). Thus, FliJ seems to regulate the entire export process through the dynamic interactions with its binding partners.

5. Focuses of my Ph. D. work

FliJ interacts with many flagellar proteins involved in protein export. However, its function was still obscure. To elucidate the function of FliJ and molecular mechanism of the flagellar protein export across the cell membrane, its structural information was imperative. Therefore I first determined the crystal structure of FliJ at 2.1 Å resolution, which revealed a remarkable structural similarity to the γ-subunit of F_oF_1-ATP synthase (Chapter 1). Since it has already been shown that the FliI structure closely resembles those of the α/β-subunits of F_oF_1-ATP synthase and that FliI forms a hexameric ring structure, these similarities suggest that FliI and FliJ may form a complex just like F_1-ATPase. I therefore analyzed the interaction between FliJ and FliI by electron microscopy and biochemical techniques (Chaper 2). Also, a structure based sequence alignment study allowed me to find a conserved region between FliJ and the γ-subunit. The role of highly conserved residues in this region was analyzed by

mutation analysis (Chapter 3). Based on these experimental results, I will discuss the function of FliJ and the molecular mechanism of flagellar protein export.

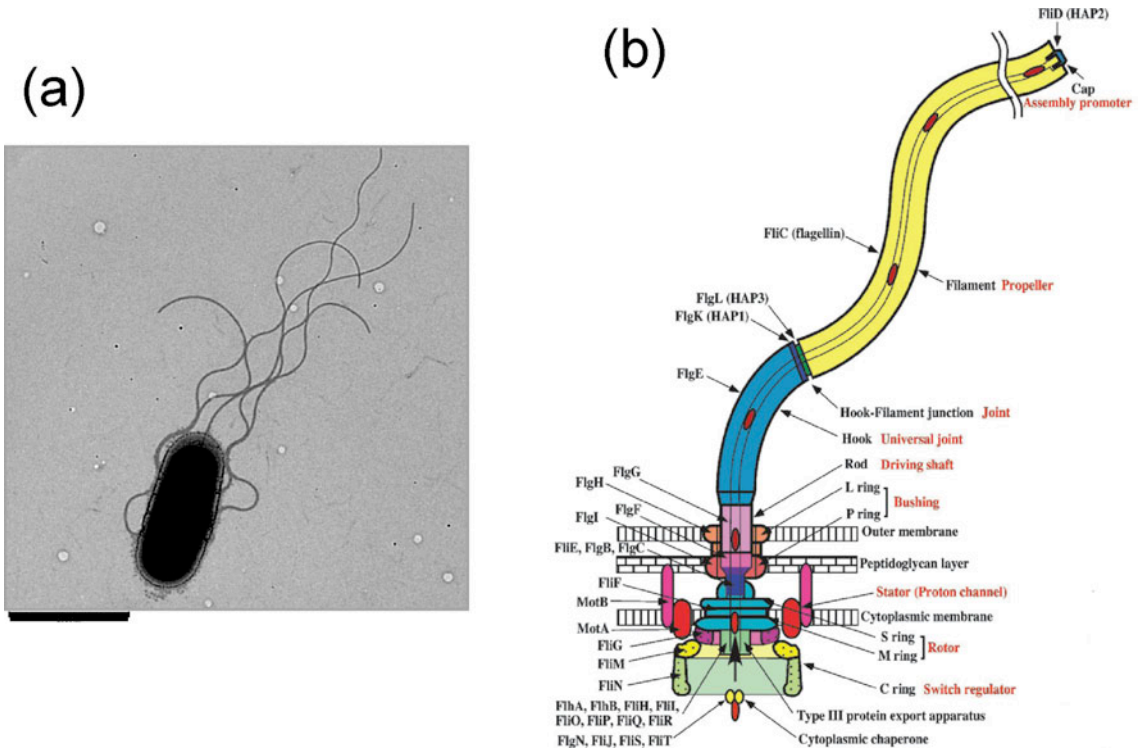

Figure 1. Bacterial flagellum. (a) Electron micrograph of *Salmonella typhimurium*, which has several flagella per cell. The length of the flagellum ranges from 10 to 15 μm, but the diameter is only about 20 nm. (b) Schematic diagram of the bacterial flagellum. The flagellum is a supra-molecular structure composed of nearly 30 different proteins. Most of the components are translocated by the export apparatus at the flagellar base into the central channel of the flagellum and assemble at its distal and with help of a capping protein.

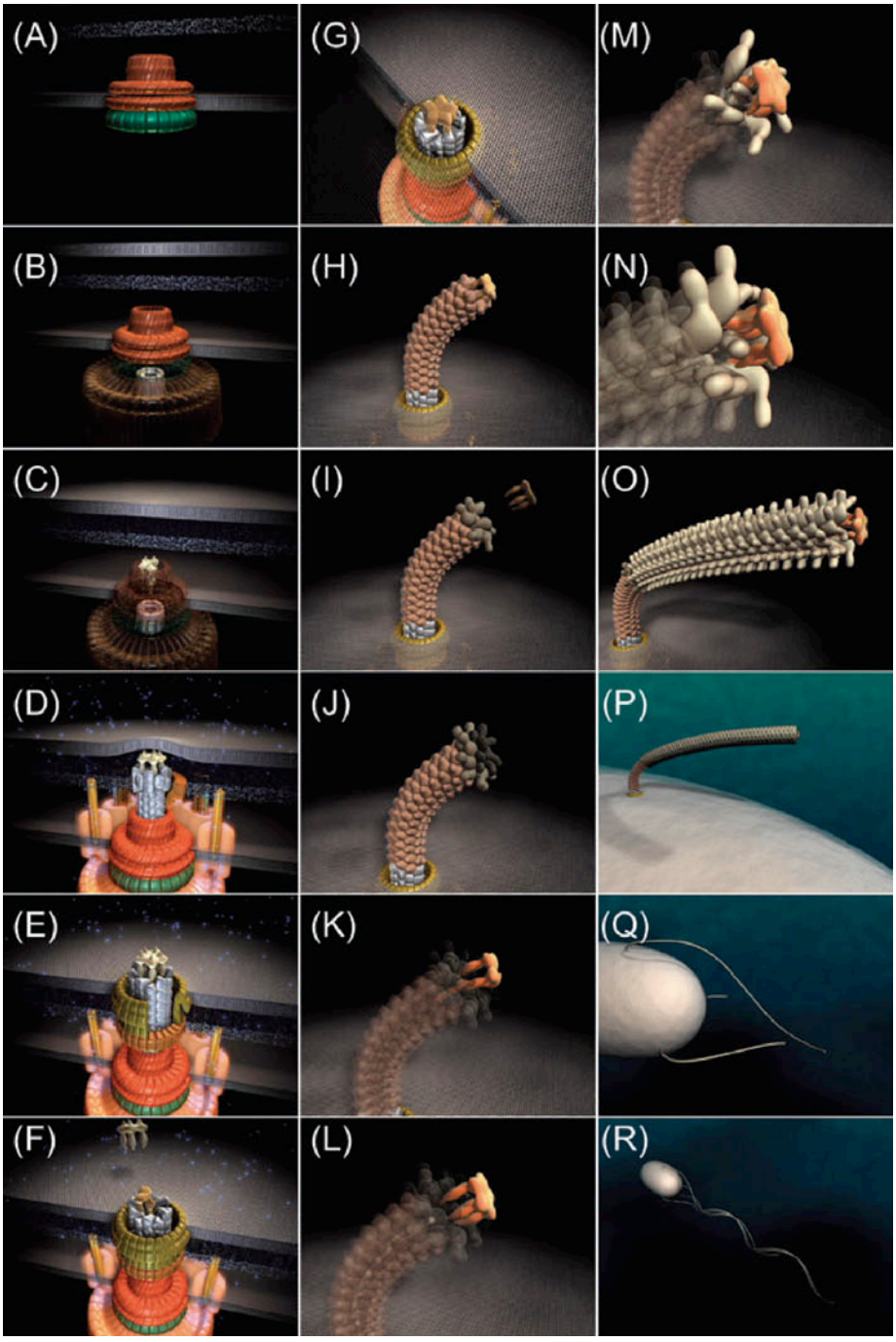

Figure 2. The assembly process of the flagellum proceeds from (a) to (r).

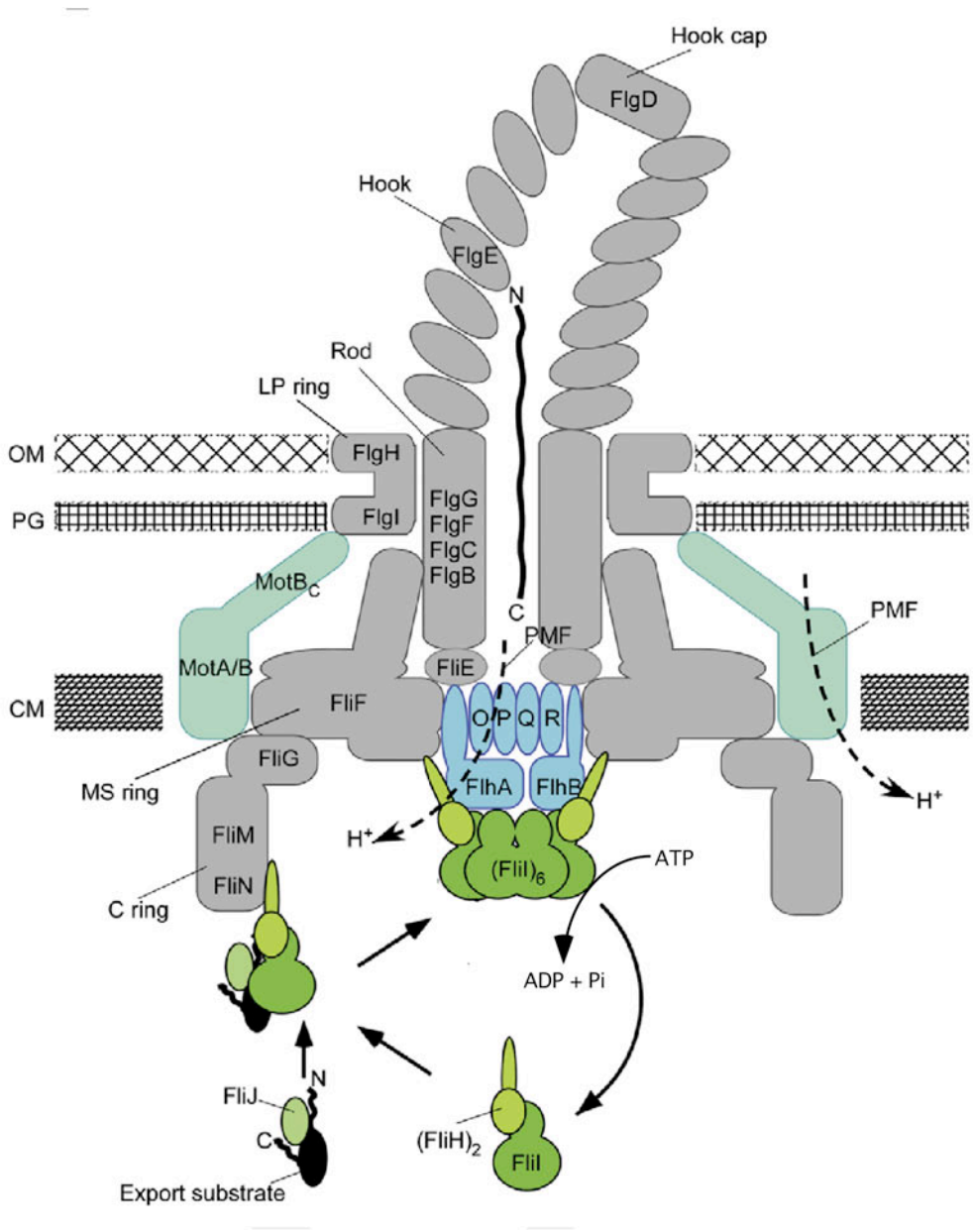

Figure 3. Schematic drawing of the flagellar type III protein export apparatus. The flagellar protein export apparatus consists of six integral membrane proteins (FlhA, FlhB, FliO, FliP, FliQ, and FliR), which are colored cyan, and three soluble proteins (FliH, FliI, and FliJ), which are colored green, and is believed to be at the center of the cytoplasmic face of the MS-ring. The assembly/disassembly cycle of the FliH/FliI ATPase complex is driven by the process of ATP hydrolysis by FliI homo-hexamer, which is formed upon docking of the FliH/FliI complex to the platform of the export gate made of the six integral membrane proteins (Minamino *et al*., 2008).

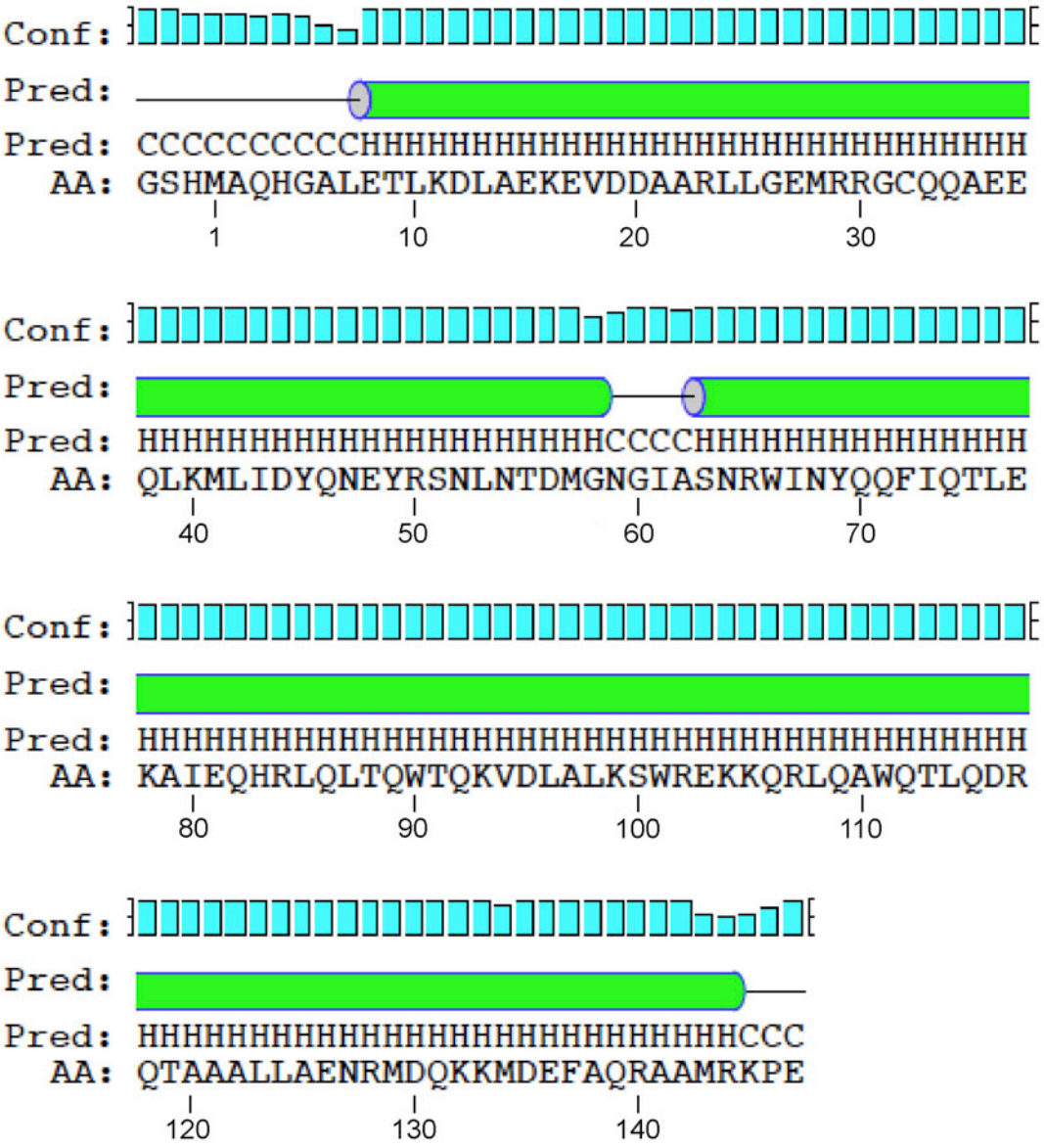

Figure 4. Secondary structure prediction of FliJ molecule. The secondary structure prediction of FliJ by using the PSIPRED protein structure prediction server (McGuffin *et al*., 2000). Conf shows confidence of prediction. Pred means prediction secondary structure, and Green cylinder of upper and character of lower denote a helices and secondary structure. AA shows amino acid sequence of FliJ.

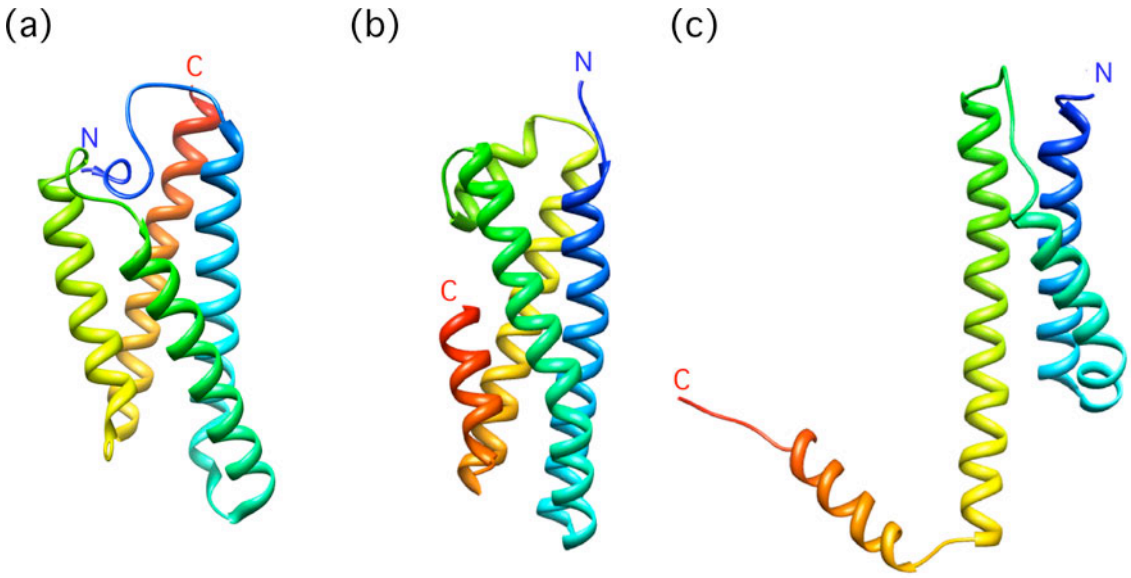

Figure 5. Crystal structures of flagellar specific chaperones. Cα ribbon drawing of the crystal structure of (a) FliS (PDB ID code 1ORJ) (b) FlgN (PDB ID code 2FUP) (c) FliT (PDB ID code 3A7M) (Imada *et al*., 2010). These three molecules are α-helical proteins and form a helix bundle structure.

Chapter 1
X-ray structure analysis of FliJ

1.1. Introduction

FliJ was difficult to handle because of its strong tendency to form insoluble aggregates. I found that FliJ with extra three residues attached to the N-terminus as a remainder of His-tag is highly soluble. I obtained hexagonal bi-pyramid crystals from this FliJ variant, and determined the structure at 2.1 Å resolution using anomalous diffraction data from a mercury derivative crystal collected at SPring-8 beamline BL41XU (Ibuki *et al*., 2009). The crystal structure revealed that FliJ consists of two α-helices, which form a coiled-coil structure. The structure also showed a remarkable similarity to that of the γ-subunit of F_oF_1-ATP synthase. The other soluble export apparatus components FliH and FliI are also known to have similarity to other components of F_oF_1-ATP synthase. The structure of FliI closely resembles those of the α/β-subunits of F_oF_1-ATP synthase, and the amino-acid sequence of FliH includes regions that are homologous to the b- and δ-subunits. In this chapter, I will show the details of the FliJ structure and discuss the complex formation of FliJ with FliI and the similarity between the complex and F_1-ATPase.

1.2. Materials and Methods

1.2.1. Protein expression and purification

A *Nde*I-*Bam*HI fragment encoding the *fliJ* gene (GenBank accession No. M62408) from pMM405 (Minamino and Macnab, 2000a) was inserted into the *NdeI*-*Bam*HI site of pET15b (Novagen) to create a plasmid pMMIJ001 (Ibuki *et al*., 2009). A 30 ml overnight culture of BL21(DE3)pLysS carrying pMMIJ001, which encodes FliJ with an N-terminal hexa-histidine (His-FliJ), was inoculated into 3 l LB medium (10 g bacto trypton, 5 g yeast extract, 10 g NaCl per litter) containing 50 μg/ml ampicillin and 30 μg/ml chloramphenicol. Cells were grown at 303 K until the culture density reached an OD_{600} of 0.6. Expression of His-FliJ was induced with isopropyl-1-thio-β-D-galactopyranoside (IPTG) at a final concentration of 1 mM and the culture was continued for 4 h. The cells were harvested by centrifugation (6400*g*, 10 min, 277 K) and stored at 193 K. The cells were thawed, suspended in a binding buffer (50 mM Tris-HCl pH 8.0, 500 mM NaCl, 50 mM imidazole) with a tablet of the Complete protease-inhibitor cocktail (Boehringer Mannheim), and sonicated (ASTRASON model XL2020 sonicator, Misonix Inc.). The cell lysate was centrifuged (19000*g*, 20 min, 277 K) to removed cell debris. The supernatant was loaded onto a HiTrap chelating column (GE Healthcare) equilibrated with the binding buffer. Proteins were eluted using a linear gradient of 50 - 500 mM imidazole, and fractions containing His-FliJ were collected. The His-tag was removed using proteolytic cleavage by adding 50 units of thrombin (GE Healthcare) to the His-FliJ solution. The protease cleavage produced FliJ with extra three residues, glycine, serine and histidine, attached to its N-terminus as a remainder of His-tag (GSH-FliJ). The reaction was carried out at 277 K in a solution dialyzed against the binding buffer overnight, and the reactant was purified by the HiTrap chelating column followed by a HiTrap Benzamidine FF column (GE

Healthcare) to remove the N-terminally His-tagged peptide, non-cleaved His-FliJ, and thrombin. The eluate was dialyzed against 50 mM MES-NaOH pH 6.0, 5 mM EDTA for 3 h at 277 K, and then GSH-FliJ (hereinafter referred to as FliJ) was further purified by cation-exchange chromatography with a HiTrap SP HP column (GE Healthcare). The peak fractions were applied to a HiLoad Superdex 75 (26/60) column (GE Healthcare) in 50 mM Tris-HCl pH 8.0, 2 mM EDTA, 500 mM NaCl. The purity of the product was examined by SDS-PAGE and MALDI-TOF mass spectrometry (Voyager DE/PRO, Applied Biosystems). The purified protein sample was concentrated to 5.0-6.0 mg/ml for further use.

1.2.2. Crystallization of FliJ

Initial crystallization screening of FliJ was performed at 293 K by the sitting-drop vapour-diffusion technique using the following screening kit: Wizard I and II, Cryo I and II (Emerald Biostructures) and Crystal Screen I and II (Hampton Research). Each drop was prepared by mixing 1 μl protein solution (4-8 mg/ml FliJ, 50 mM Tris-HCl pH 8.0, 2 mM EDTA, 500 mM NaCl) with 1 μl reservoir solution, and equilibrated against 150 μl reservoir solution. Within a week, small hexagonal bi-pyramid crystals appeared in several drops containing PEG-300 or PEG monomethyl ether 2000 at pH 4.2-5.2 (Figure 1-1a, b). I optimized the conditions by varying the precipitant concentration, pH and additives using the sitting-drop method. Finally, crystals suitable for X-ray analysis were obtained from drops prepared by mixing 1 μl protein solution (4.5 mg/ml) with 1 μl reservoir solution containing 0.1 M Phosphate-citrate pH 3.8, 20-30% (*v*/*v*) PEG-300 and 200-300 mM NaCl at 293 K. The crystals appeared within one week and grew to typical dimensions of 0.05 × 0.05 × 0.3 mm (Figure 1-1c).

1.2.3. Preparation and crystallization of mercury derivative

FliJ contains a single cysteine residue in its sequence, and hence mercury derivatives were prepared by adding methylmercury chloride to the purified FliJ solution to a final concentration of 1 mM for 15 h at 277 K. Prior to the treatment with the mercury compound, the purified FliJ solution was stored with 1 mM DTT for 3 h at 277 K for complete reduction of the cysteine side chain, and was dialyzed against 50 mM Tris-HCl pH 8.0, 500 mM NaCl to remove DTT. After treatment with mercury, the protein solution was dialyzed against 50 mM Tris-HCl pH 8.0, 500 mM NaCl to remove unbound methylmercury chloride. Although crystals of the mercury derivative appeared under the same conditions as the native FliJ crystals, a number of small and highly stacked crystals were grown (Figure 1-2a). I therefore added 100 μl silicon oil on the reservoir solution to reduce the nucleation and growth speed by slowing down the vapor exchange rate (Cheayen, 1997). Finally, single crystals with typical size of 0.1 × 0.1 × 0 0.4 mm were grown from a solution containing 0.1 M Phosphate-citrate pH 3.8, 25-35% (*v*/*v*) PEG-300 and 200-300 mM NaCl with a protein concentration of 5.7 mg/ml (Figure 1-2b). I also tried to prepare Se-Met labeled FliJ crystals, but purified Se-Met FliJ formed stable cysteine dimer, and no crystal was obtained.

1.2.4. X-ray diffraction data collection of FliJ

All X-ray diffraction data were collected at SPring-8 beamline BL41XU (Harima, Japan). Since the concentration of PEG-300 in the crystallization drops was high enough for cryo-protection, the crystals were directly transferred into liquid nitrogen for vitrification and mounted in a cryo-gas flow. The diffraction data were recorded on an ADSC Quantum 315 CCD detector (Area Detector Systems

Corporation) at 35 K using a helium-cryocooling device (Rigaku). The diffraction data were indexed, integrated and scaled using the programs *MOSFLM* (Leslie, 1992) and *SCALA* from the *CCP4* program suite (Collaborative Computational Project, Number 4, 1994).

The FliJ crystals diffracted to 3.3 Å resolution (Figure 1-3). The native crystals belong to the hexagonal space group $P6_122/P6_522$, with unit-cell parameters a = b = 52.9, c = 193.6 Å, γ = 120°. The Matthews coefficient (V_M; Matthews, 1968) suggests that the presence of a single FliJ molecule in the asymmetric unit, with a solvent content of 53%. The FliJ mercury derivative crystals grew larger than the native ones and diffracted to 2.1 Å resolution (Figure 1-4). The unit cell parameters of the derivative crystals (a = b = 52.9, c = 192.6 Å, γ = 120°) were the same as those of the native ones within the experimental error. The dramatic improvement of the resolution limit is probably due to the enhancement of molecular packing interactions in the crystal through the bound mercury atoms.

MALDI-TOF mass measurement of the mercury derivative crystals indicated that about 1/3 of FliJ molecules did not bind mercury (Figure 1-5). But, Bijvoet and isomorphous difference Patterson maps of the derivative showed common significant clear peaks on the Harker sections (Figure 1-6), suggesting that the usefulness of these data for phasing by the SAD or the SIRAS method. The statistics of data collection are summarized in Table 1-1.

1.2.5. Mass spectrometry

The purified proteins and the crystals were analyzed by MALDI-TOF mass spectrometer (Voyager-DE PRO, Applied Biosystems) operated in linear mode. 0.5 μl of sample solution or a single crystal were mixed with 0.5 μl of matrix solution (10

mg/ml sinapinic acid, 50% acetonitrile, 0.1% trifluoroacetic acid) and dried before measurement.

1.2.6. Phasing, model building and refinement of FliJ

The initial SAD (single-wavelength anomalous dispersion) phase was calculated from the anomalous data of a mercury derivative crystal using SOLVE (Terwilliger and Berendzen, 1999) and improved by density modification using DM (Collaborative Computational Project, Number 4, 1994). The atomic model was constructed with COOT (Emsley *et al*., 2010) and refined against the mercury derivative data to 2.1 Å with CNS (Brunger, 1998). During the refinement process, manual modification was performed by using omit map. The refinement converged to an R factor of 23.3% and a free R factor of 25.5%. The ramachandran plot showed that 95.2% and 4.8% residues were located in the most favorable and allowed region, respectively. Structural refinement statistics are summarized in Table 1-2.

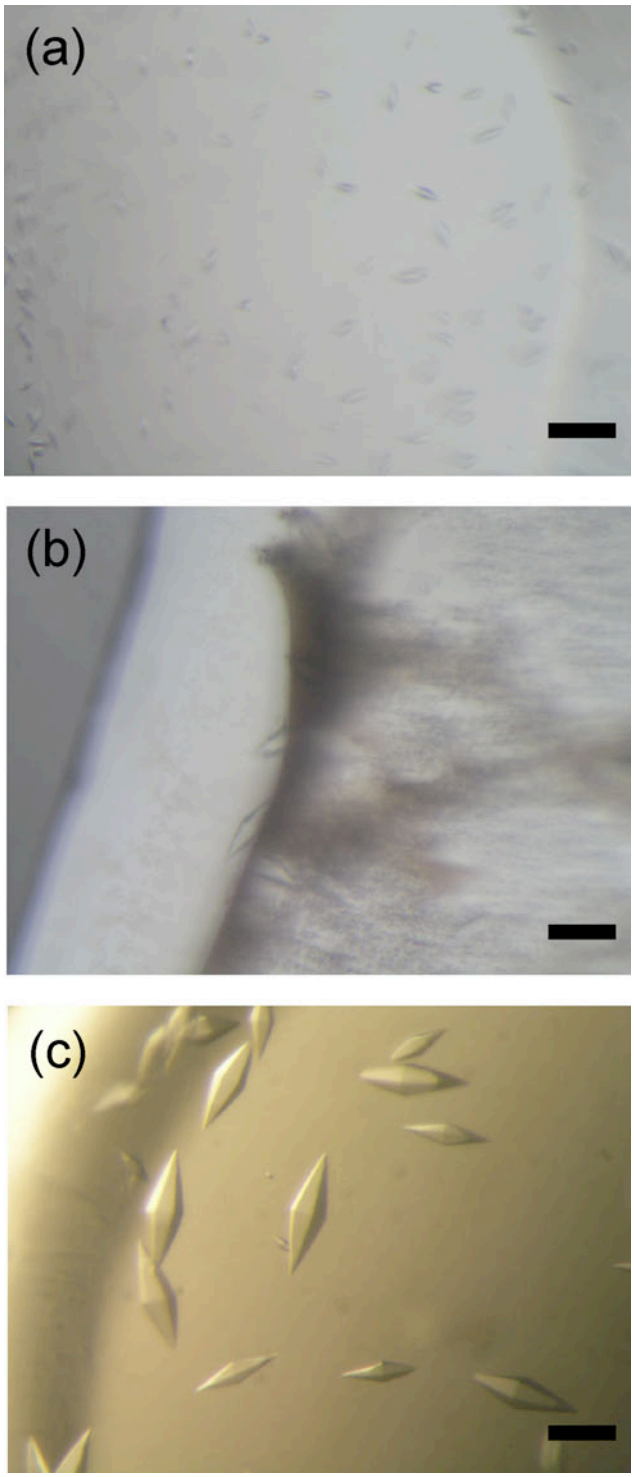

Figure 1-1. Crystals of native FliJ. Crystals of FliJ appeared in drops containing (a) PEG-300 (b) PEG monomethyl ether 2000. These small crystals were obtained during initial screening. (c) These hexagonal bi-pyramid crystals were obtained after optimization. The scale bar is 0.1 mm in length.

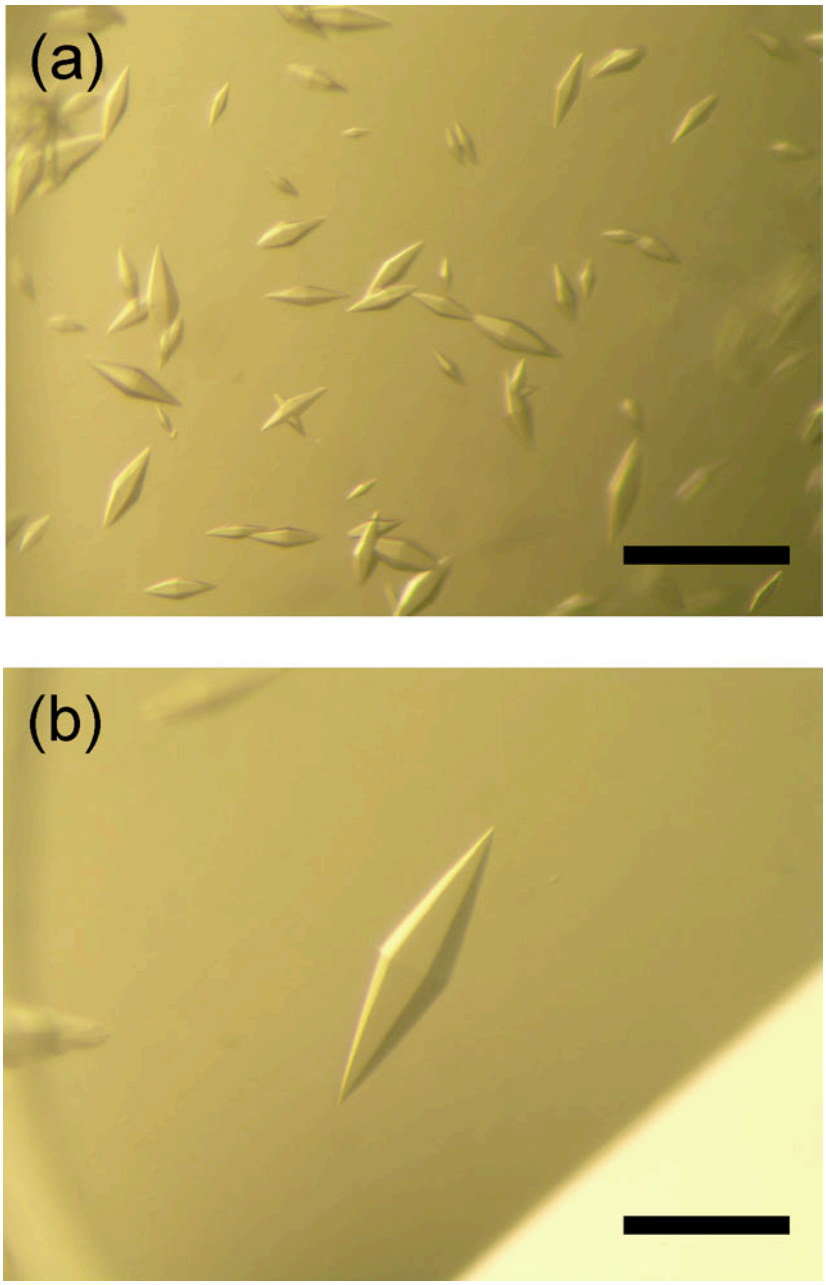

Figure 1-2. Crystals of the FliJ mercury derivative. (a) Crystals of the mercury derivative appeared under the same conditions as the native FliJ crystals. (b) Crystals were obtained by adding silicon oil on the reservoir solution. The scale bar is 0.2 mm in length.

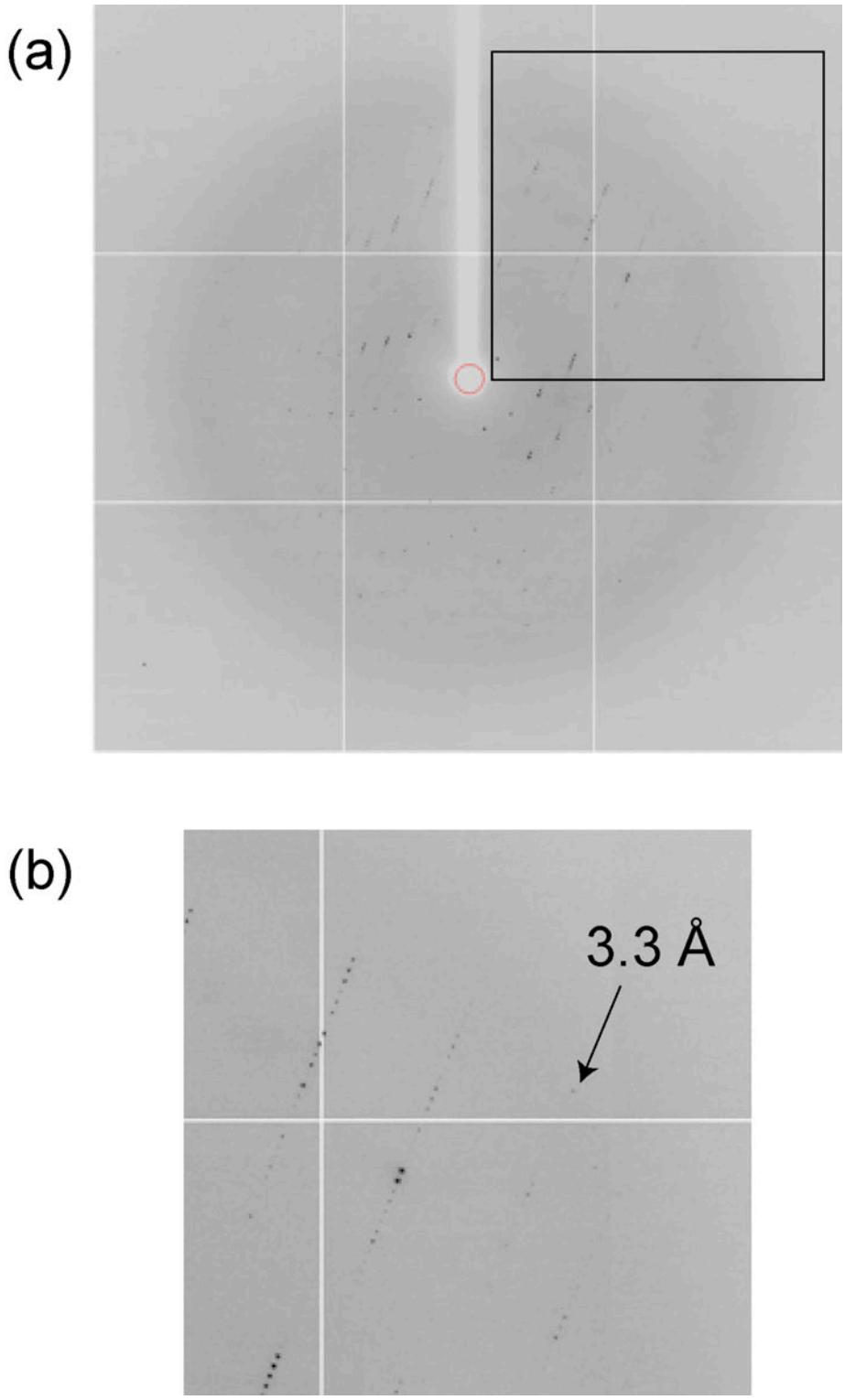

Figure 1-3. X-ray diffraction pattern of a native FliJ crystal. (a) A 1° oscillation image taken at the BL41XU in SPring-8. (b) Magnified X-ray pattern of the boxed region of image (a).

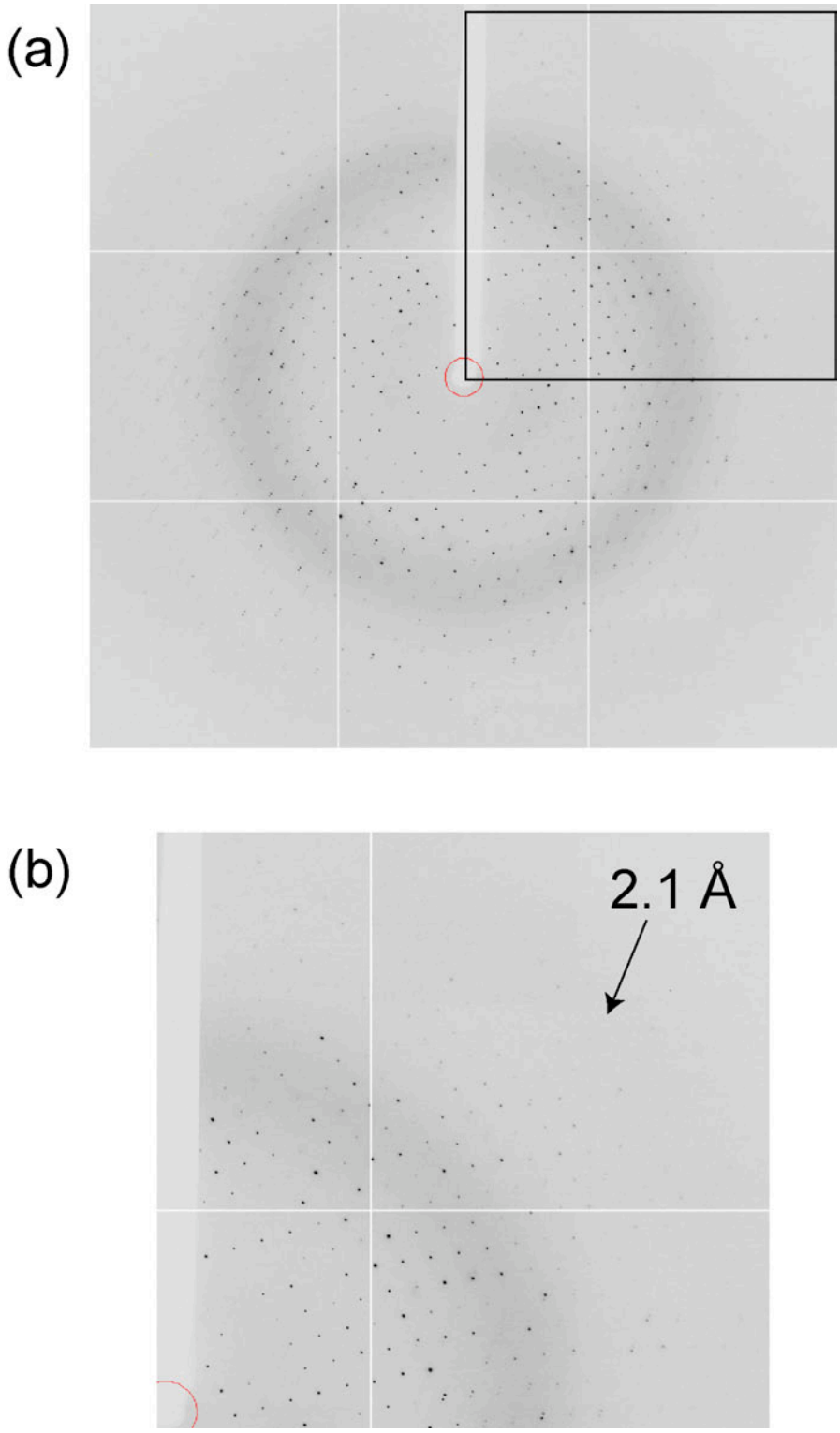

Figure 1-4. X-ray diffraction pattern of a mercury derivative crystal of FliJ. (a) A 1° oscillation image taken at the BL41XU in SPring-8. (b) Magnified X-ray pattern of the boxed region of image (a).

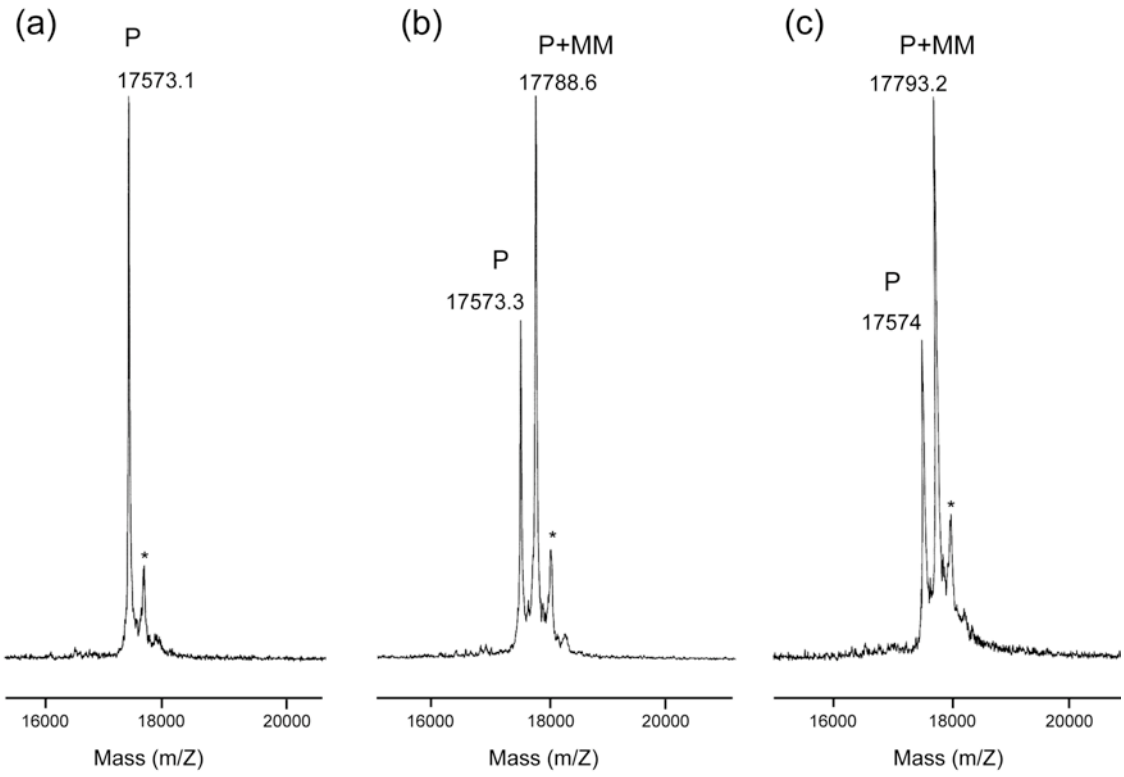

Figure 1-5. Mass spectrograms of native and mercury derivative FliJ. MALDI-TOF mass spectrogram of (a) native FliJ and (b) the methylmercury-derivative of FliJ and (c) the methylmercury-derivative of FliJ from a crystal. Peaks corresponding to native (P) and methylmercury-derivative (P+MM) FliJ are labeled. Peaks labeled with an asterisk (*) represent matrix-related adduct peaks. Native FliJ has a mass around 17573 Da, and the methylmercury-derivative has a mass around 17788 Da. The difference between native and derivative FliJ is about 215 Da, corresponding to a single methylmercury molecule (215.5 Da). Thus the methylmercury-derivative of FliJ has a single methylmercury molecule. The derivative crystals contain both native and methylmercury-derivative FliJ molecules.

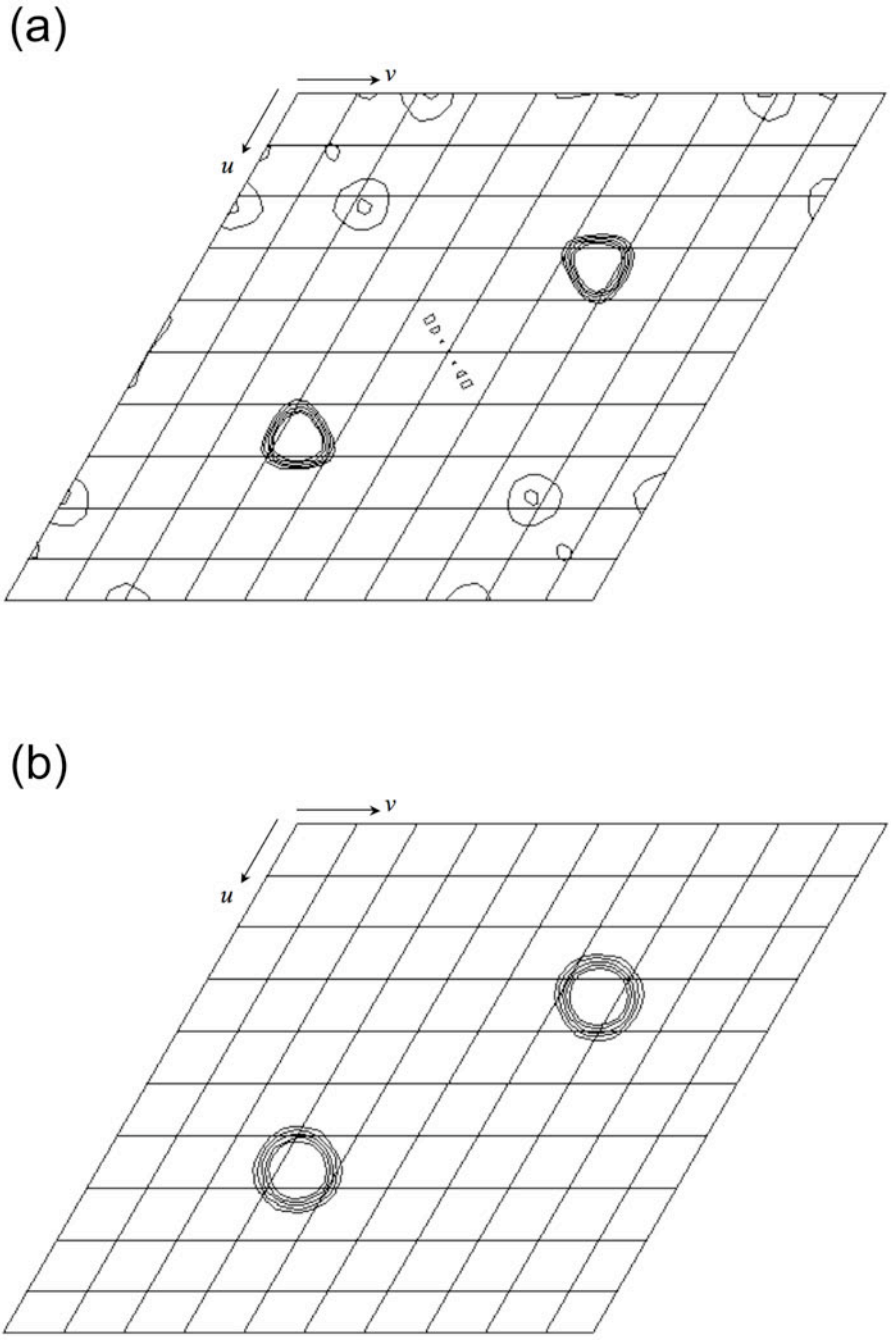

Figure 1-6. Difference Patterson maps. (a) Bijvoet and (b) isomorphous difference Patterson maps (w = 1/3 Harker section) calculated using the data from the mercury derivative at 3.5 Å resolution. The contour lines are drawn from 2.0 σ to 6.0 σ, with an increment of 1.0 σ.

Table 1-1. Summary of the data statistics.

Values in parentheses indicate statistics for the highest resolution shell.

	Native	Mercury derivative
Space group	$P6_522$	$P6_522$
Unit-cell parameters (Å, º)	a = b = 52.9	a = b = 52.9
	c = 193.6	c = 192.6
	γ = 120	γ = 120
Wavelength	1.0000	1.0082
Resolution (Å)	48.4-3.3 (3.48-3.3)	38.5-2.1 (2.21-2.1)
Observations	38500 (5686)	109081 (15888)
Unique reflections	2825 (378)	10037 (1426)
Completeness (%)	100 (100)	99.7 (100)
Redundancy	13.6 (15.0)	10.9 (11.1)
$I/\sigma(I)$	3.4 (1.9)	4.7 (2.2)
R_{merge} [#] (%)	8.1 (39.7)	8.0 (31.7)
R_{anom} [+] (%)		5.6 (11.2)

[#] $R_{\text{merge}} = \Sigma_{\mathbf{h}} \Sigma_l |I_{\mathbf{h}l} - \langle I_{\mathbf{h}} \rangle| / \Sigma_{\mathbf{h}} \Sigma_l \langle I_{\mathbf{h}} \rangle$, where I_l is the lth observation of reflection **h** and $\langle I_{\mathbf{h}} \rangle$ is the weighted average intensity for all observations l of reflection **h**.

[+] $R_{\text{ano}} = \Sigma_{\mathbf{h}} |\langle I(\mathbf{h}+) \rangle - \langle I(\mathbf{h}-) \rangle| / \Sigma_{\mathbf{h}} (\langle I(\mathbf{h}+) \rangle + \langle I(\mathbf{h}-) \rangle)$, where $\langle I(\mathbf{h}+) \rangle$ and $\langle I(\mathbf{h}-) \rangle$ correspond to the average intensities of each Friedel pair for reflection **h**.

Table 1-2. X-ray refinement statistics.

Values in parentheses indicate statistics for the highest resolution shell.

Measurement	Value
Resolution range (Å)	37.3-2.1 (2.23-2.1)
No. of reflections working	10032 (1531)
No. of reflections test	480 (76)
R_w, (%)	23.3 (21.6)
R_{free}, (%)	25.5 (25.2)
Rms deviation bond length (Å)	0.005
Rms deviation bond angle (˚)	1.0
B factor	
Protein atoms	36.8
Ligand atoms	32.1
Solvent atoms	52.6
Ramachandran plot (%)	
Most favored	95.2
Additionally allowed	4.8
Generously allowed	0
Disallowed	0
No. of protein atoms	1107
No. of ligand atoms	1
No. of solvent atoms	158

$R_w = \Sigma \; ||F_o| - |F_c|| \; / \; \Sigma \; |F_o|$, same as R_{free} but calculated on 5% of data set aside for refinement.

1.3. Results

1.3.1. Crystal structure of FliJ

The atomic model of FliJ was built for residues from Gln-3 to Ala-138. FliJ adopts an anti-parallel coiled-coil structure composed of two long α-helices, α1 and α2 (Figure 1-7a). α1 is eight turns shorter than α2, and hence the C-terminal segment of α2 is protruding from the coiled-coil core. The N-terminal five residues including the residues of the reminder of a His-tag (Ibuki *et al*., 2009), the C-terminal nine residues, and Thr-58 and Asp-59, which lie in the loop connecting α1 and α2, were invisible in the electron density map. The binding regions for FlgN and FliT (Evans *et al*., 2006) are assigned on α1 and the N-terminal portion of α2, respectively. The binding region for FliH (Fraser *et al*., 2003) is on the C-terminal region of α2 and slightly overlaps with the FliT-binding region (Figure 1-7a).

Highly conserved residues among FliJ homologs are located on two exposed surfaces of the FliJ structure (Figure 1-7b, c). One is located between the C-terminal region of α1 (38-49) and the N-terminal region of α2 (72-83) and mainly formed by hydrophobic residues. The other is formed by three hydrophilic residues, Gln-131, Asp-135 and Glu-136, located on the C-terminal single helical region of α2.

1.3.2. Comparison with γ-subunit of F_1-ATPase

The structure of FliJ shows a marked similarity with the coiled coil structure formed by the N- and the C-terminal helices of the γ-subunit of F_1-ATPase (Abrahams *et al*., 1994). The length of the coiled-coils as well as the length of each helix is comparable. While the coiled-coil structure of FliJ extends in a relatively straight form, that of the γ-subunit is bent around residue 24 in the N-terminal helix and residue 234 in the C-terminal helix. Therefore the whole FliJ structure cannot be fitted well onto the

γ-subunit. However, when the structure is divided into two regions at the bending point, the upper and the lower parts of FliJ and the γ-subunit (PDB ID code 1E79) (Figure 1-8a, b) (Gibbons *et al*., 2000) are nicely superimposed to each other. The upper (residues 26-45 and 65-98) and lower (residues 6-25 and 99-136) regions of FliJ can be superimposed to those of the γ-subunit (upper; residues 25-44 and 200-233, lower; residues 5-24 and 234-271) with RMS deviations of 1.9 Å and 1.6 Å, respectively, for corresponding Cα atoms. The bending of the coiled-coil of the γ-subunit seems to be caused by the interaction with its own α/β domain. The C-terminal helix of the γ-subunit is bent along the α/β domain and the N-terminal helix, the coiled-coil partner, is also bent accordingly. Recently, a crystal structure of V_1-ATPase at 4.5 Å resolution has been reported (Numoto *et al*., 2009). The coiled-coil region of D-subunit, the central stalk of V_1-ATPase, is straight and its conformational resemblance seems to be closer to FliJ than the γ-subunit (Figure 1-8a, c).

Although no apparent sequence similarity has been found between FliJ and the γ-subunit, structure based sequence alignment revealed a region conserved between them (Figure 1-9a, c). The conserved residues are located on the surface interacting with the ε-subunit of F_1-ATPase (Figure 1-9b) (Gibbons *et al*., 2000), suggesting that FliJ may have binding partners corresponding to the ε-subunit.

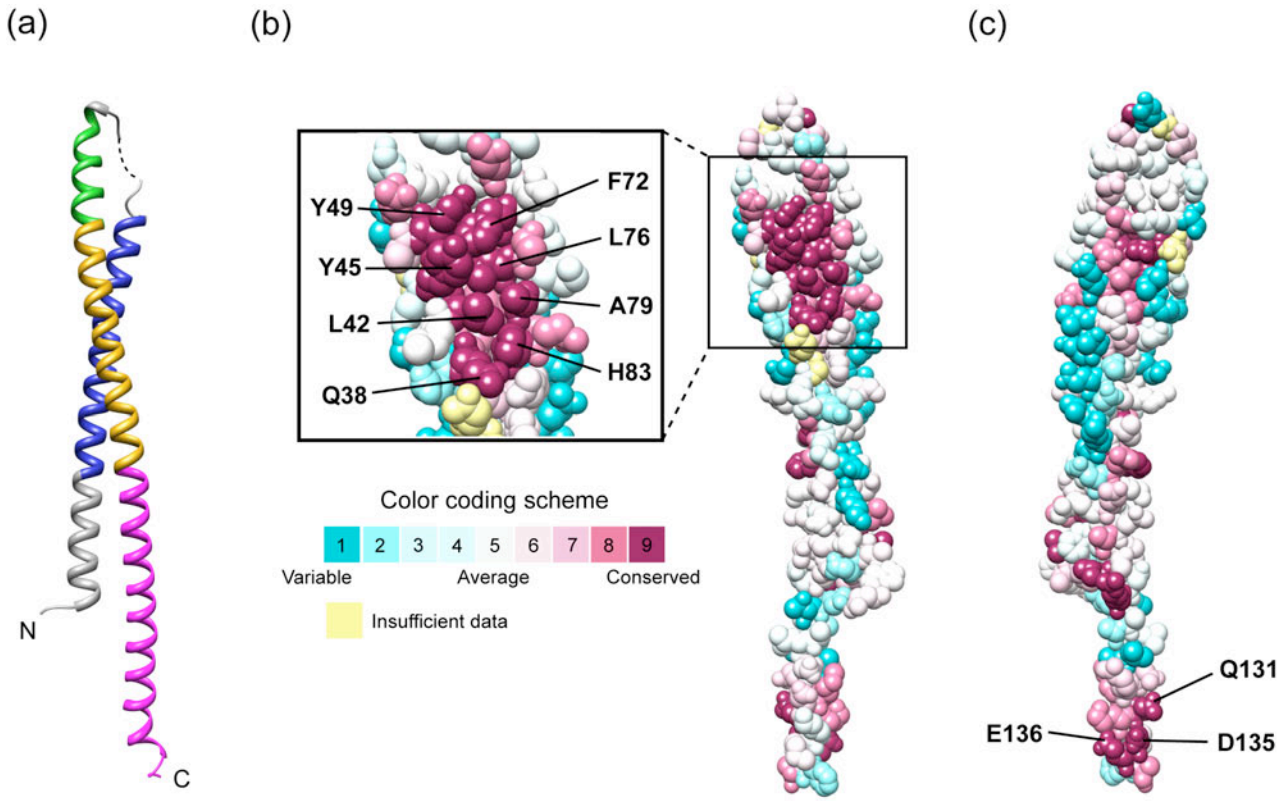

Figure 1-7. Structure of FliJ. (a) Cα ribbon drawing of FliJ. The binding regions for FlgN, FliT, FliH and both FliT and FliH are highlighted with blue, green, magenta and yellow. (b),(c), Evolutionary conserved residues of FliJ. The figures were prepared by ConSurf [http://consurf.tau.ac.il/]. Residues are colored in accordance with conservation among amino acid sequences of FliJ from 50 different bacteria. (c), The back side view of (b).

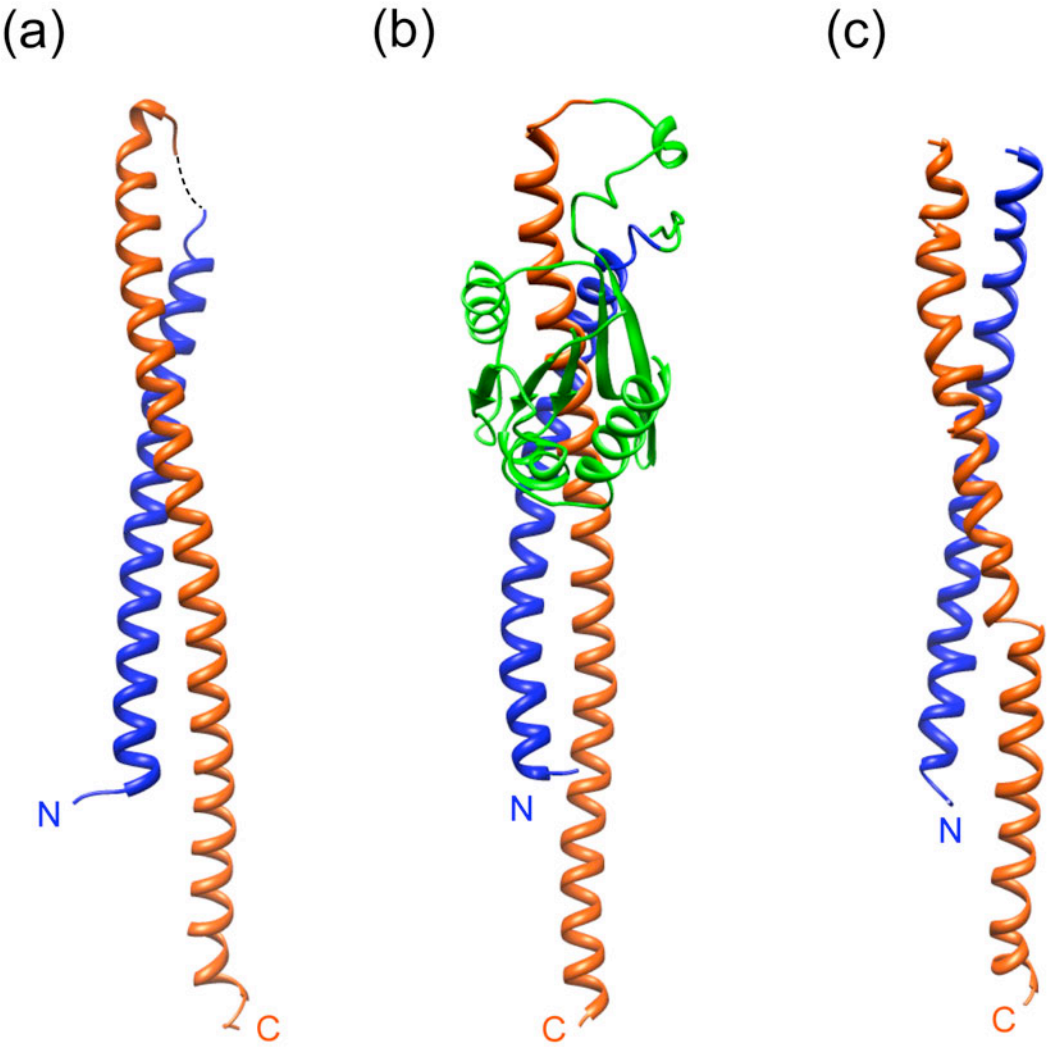

Figure 1-8. Structural comparison between FliJ and central stalks of F_1- and V_1-ATPase. Cα ribbon drawing of crystal structures of (a) FliJ, (b) the γ-subunit from bovine mitochondria at 2.4 Å resolution (PDB ID code 1E79) (Gibbons *et al*., 2000), (c) the D-subunit from *Thermus thermophilus* at 4.5 Å resolution (PDB ID code 3A5D) (Numoto *et al*., 2009).

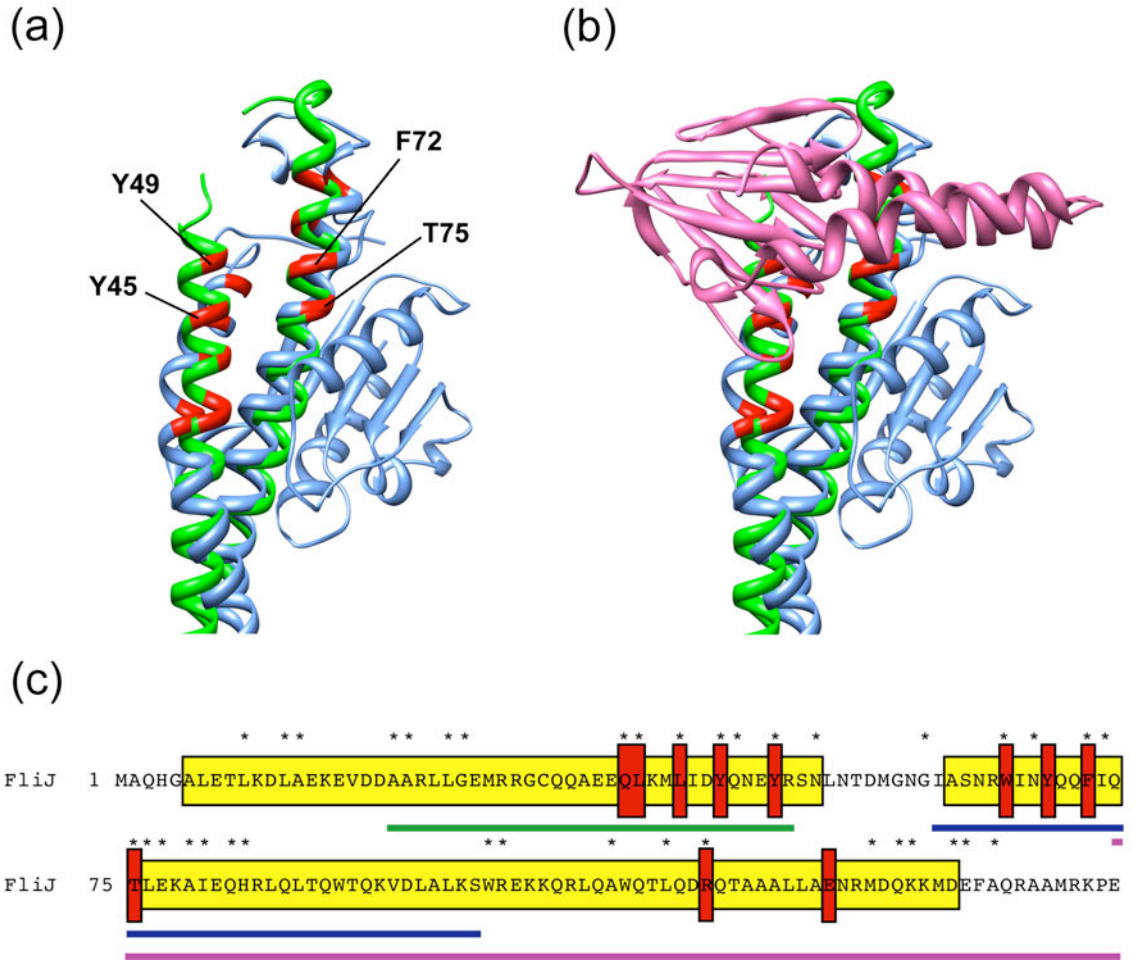

Figure 1-9. Structural similarity between FliJ and the γ-subunit of F_1-ATPase. (a) Close-up view of the conserved region between FliJ and the γ-subunit. FliJ (green) is superimposed to the γ-subunit (light blue) from bovine mitochondria (PDB ID code 1E79). The highly conserved residues between FliJ homologs and γ-subunits are shown in red. (b) The ε-subunit (pink) (PDB ID code 1E79) was displayed with FliJ and the γ-subunit. (c) The amino-acid sequence of FliJ is shown with various information. Yellow boxes denote α-helices. The highly conserved residues between FliJ and γ-subunit are indicated by red boxes. The binding regions for FlgN, FliT and FliH are shown by green, blue and purple bars below the sequence, respectively. Asterisks above the sequence represent highly conserved residues among FliJs from various organisms.

1.4. Discussion

1.4.1. High solubility of GSH-FliJ

The protease cleavage of His-FliJ produced FliJ with extra three residues, glycine, serine and histidine, attached to its N-terminus as a remainder of His-tag. We call this GSH-FliJ. While both FliJ and His-FliJ tend to form insoluble aggregates, GSH-FliJ is highly soluble, which led me to the success in crystallization, although the reason why the N-terminal three residues dramatically change the solubility is unclear. I expected that the structure of GSH-FliJ would provide clues to this question. But, the N-terminal five residues including these extra three residues were invisible in the electron density map, indicating that these residues are flexible and not stably folded.

FliJ has six hydrophobic residues (Ala-120, Ala-121, Ala-122, Leu-123, Leu-124, Ala-125) lined up in the C-terminal segment of α2 protruding from the coiled-coil core but still near the N-terminal segment of α1 (Figure 1-10). The three extra residues GSH may reach and hover over this hydrophobic region to prevent FliJ from aggregation. In addition, MGSH-FliJ (GSH-FliJ with an N-terminal methionine residue) restored the swarming motility of a *Salmonella* Δ*fliJ* mutant to the wild-type level (data not shown), indicating that these extra amino acid residues do not interfere with the function of FliJ.

1.4.2. Crystal packing of FliJ

The mercury derivative crystals grew larger than the native ones and diffracted to 2.1 Å resolution. The unit cell parameters of the derivative crystals (a = b = 52.9, c = 192.6 Å, γ = 120°) were the same as those of the native ones within the experimental error. In the crystal, twelve FliJ molecules are present in a unit cell (Figure 1-11a, b). When searching for the position of a mercury atom, two FliJ molecules seem

to bind to each other through two mercury atoms bound to Cys-32 of FliJ in the crystal. The mercury atom bound to Cys-32 is also coordinated by Asn-127 and Gln-131 of a neighboring FliJ molecule related by the crystallographic symmetry (Figure 1-11c). The dramatic improvement in the resolution is probably due to the enhancement of molecular packing interactions in the crystal through bound mercury atoms.

1.4.3. Structural insight of FliJ and FliI

The structural similarities between FliJ and the γ-subunit of F_1-ATPase shown in this work and between FliI and the α/β-subunits of F_1-ATPase (Figure 1-10a, b) shown previously suggest that FliJ and FliI may form a ring complex with a central stalk similar to the structure of F_1-ATPase. FliI is known to form a hexamer to exert its full enzyme activity. Although the atomic structure of FliI was solved in monomeric form, a FliI hexamer model was built using the F_1-ATPase structure as a template (Figure 1-10c, d). The model clearly revealed that the main chain structures constructing the subunit interface and those surrounding the central channel of the ring are well conserved, while the regions that differ between FliI and the F_1-α/β-subunits are all located on the outer surface of the hexamer ring (Figure 1-11). The structure of the ATP binding site of F_1-ATPase as well as the amino acid residues of the α/β-subunits involved in ATP hydrolysis are highly conserved in FliI, suggesting that the FliI family and F_1-ATPase share a similar catalytic pathway for ATP hydrolysis. These observations suggest that FliJ and FliI form a complex like the $\alpha_3\beta_3\gamma$ complex of F_1-ATPase. I therefore analyzed the interaction between FliJ and FliI by electron microscopy and biochemical techniques in the next chapter.

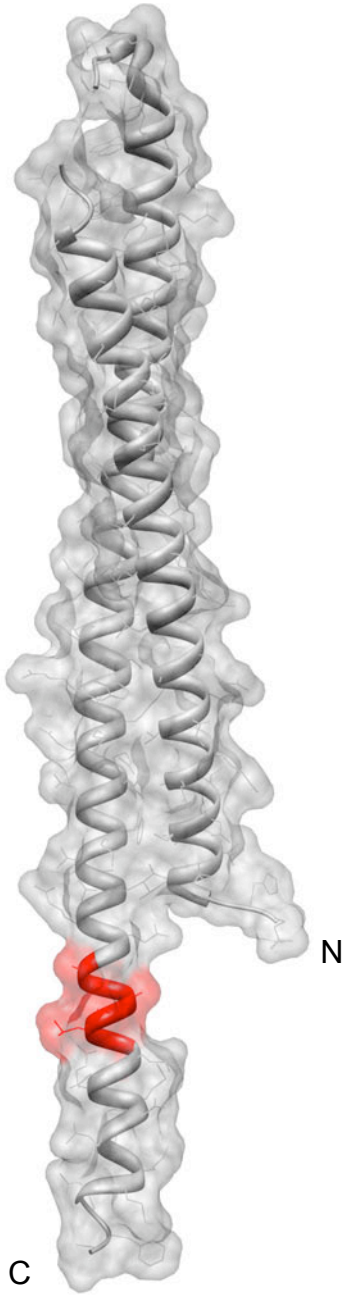

Figure 1-10. Hydrophobic surface of FliJ molecule. Cα ribbon drawing of FliJ with a gray, semi-transparent solid surface of the space-filling model. The six consecutive hydrophobic residues (Ala-120, Ala-121, Ala-122, Leu-123, Leu-124, Ala-125) in the C-terminal segment of α2 protruding from the coiled-coil core are shown in red. Note that they are close to the N-terminal segment of α1.

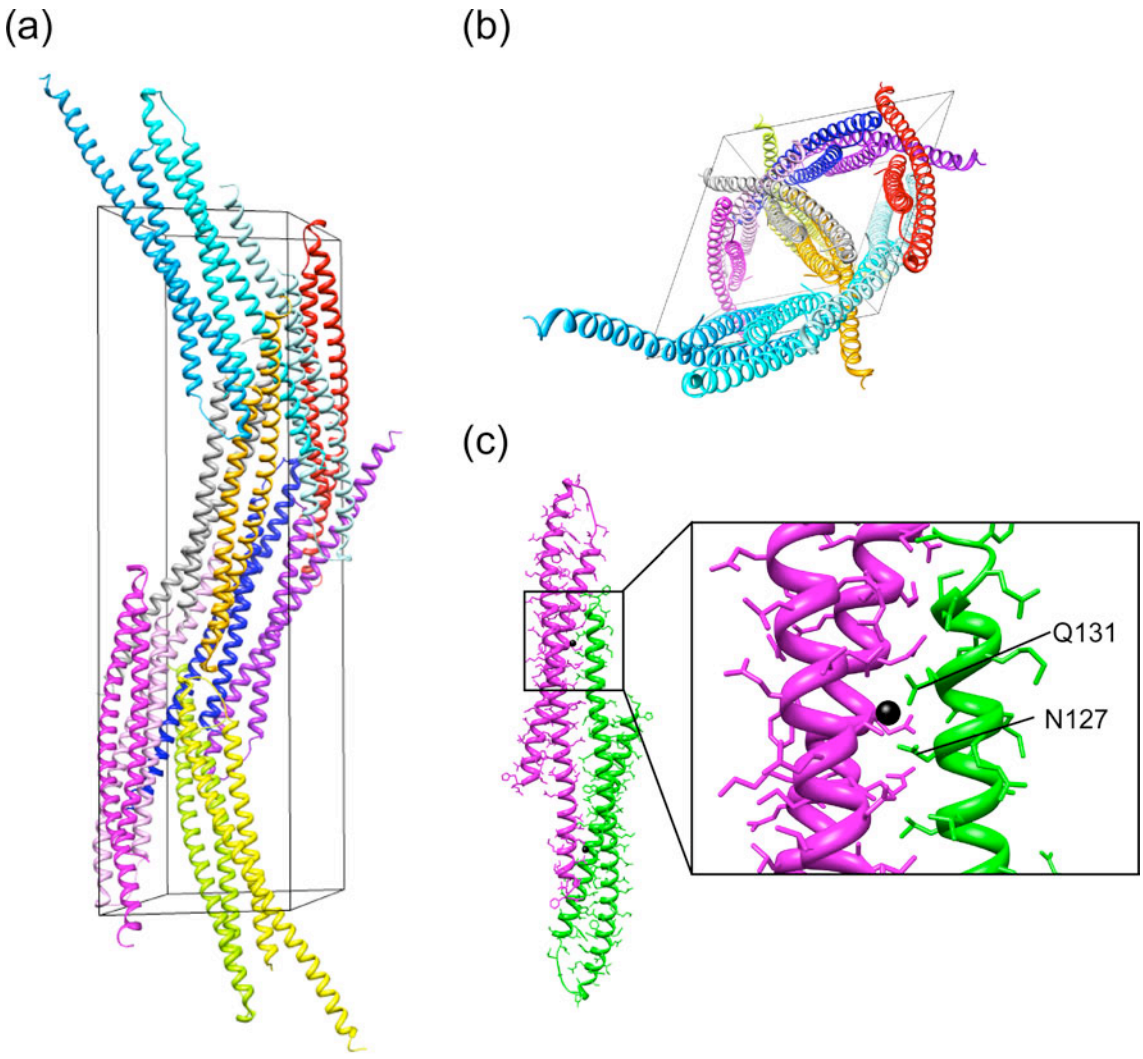

Figure 1-11. Crystal packing of FliJ molecules. (a), (b) Twelve molecules present in a unit cell in side view (a) and end-on view (b) of a unit cell. (c) Close-up view of two molecules related by the crystallographic 2-fold symmetry. The black ball represents a mercury atom.

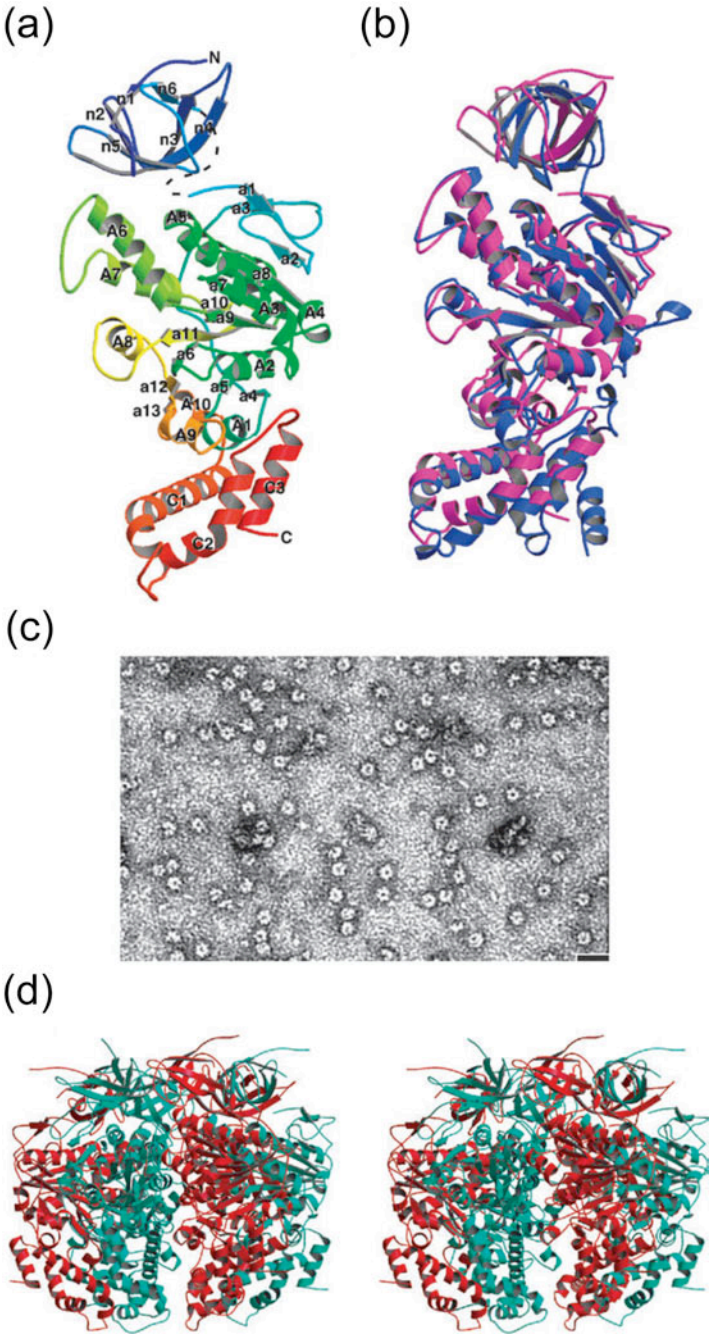

Figure 1-12. Structural similarities between FliI ATPase and F1-ATPase subunits. (a) Cα ribbon drawing of the crystal structure of FliI(Δ1-18). The linker connecting the N-terminal and ATPase domains, which is missing in the model due to disorder, is indicated by dashed line. (b) Comparison of the relative domain orientation. FliI(Δ1-18) (cyan) is superimposed on the F_1-β-subunits without any nucleotide. (c) Electron micrograph of the FliI ring particles. Scale bar, 200 Å. (d) FliI hexamer model. Stereo view of the Cα ribbon diagram (Minamino *et al*., 2008).

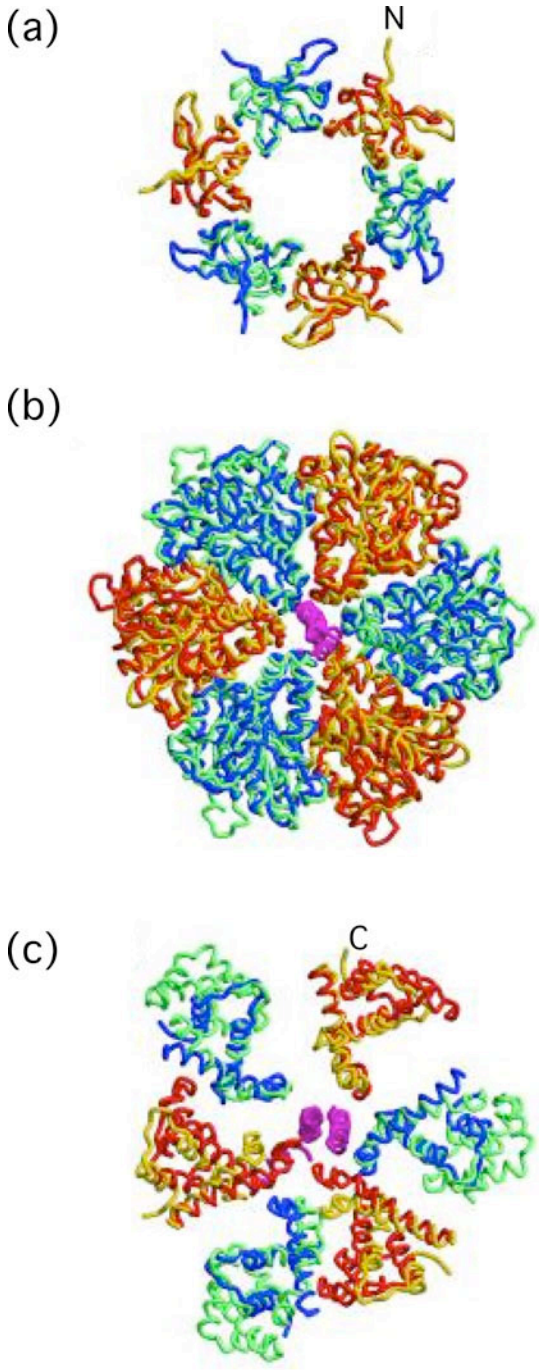

Figure 1-13. The FliI hexamer model. Superposition of FliI (blue and yellow) onto the α- (blue green) and β- (orange) subunits of F_1-ATPase (PDB ID code 1BMF) (Abrahams *et al*., 1994). (a) N-terminal domain. (b) ATPase domain. (c) C-terminal domain. The N- and C-termini of the model are labeled for one subunit in (a) and (c), respectively. (Imada *et al*., 2007)

Chapter 2
Interaction between FliJ and FliI, and their complex

2.1. Introduction

The structural similarity between FliJ and the γ-subunit of F_1-ATPase was shown in the previous chapter. Together with the similarity between FliI and the α/β-subunits, FliI and FliJ are expected to form a complex similar to the $\alpha_3\beta_3\gamma$ complex of F_1-ATPase. The crystal structure of a major part of the bovine heart F_1 including the $\alpha_3\beta_3$ and part of the γ-subunit has been determined at 2.8 Å resolution (Abrahams *et al*., 1994). The overall structure of F_1-ATPase is shown in Figure 2-1. The three α- and three β-subunits associate just like the segments of an orange to form a roughly spherical assembly of about 10 nm in diameter. The left-handed coiled coil part of the γ-subunit runs approximately along the axis of the $\alpha_3\beta_3$ ring complex and protrudes from the ring by about 30 Å, while the reminder forms a small α-helical segment (Figure 2-1).

In this chapter, I examined the interaction and complex formation of FliJ with the FliI hexamer ring. The structure of the FliI-FliJ complex is analyzed by electron microscopy. FliJ formed a complex with the FliI hexamer ring and facilitated the ring formation and the ATPase activity of FliI. From the results of genetic analyses of FliI, we determined the region involved in the FliI-FliJ interaction. I will discuss the structure of the $FliI_6FliJ$ complex, possible roles of FliJ in protein export, and

similarities between the flagellar protein export apparatus and F_oF_1-ATP synthase.

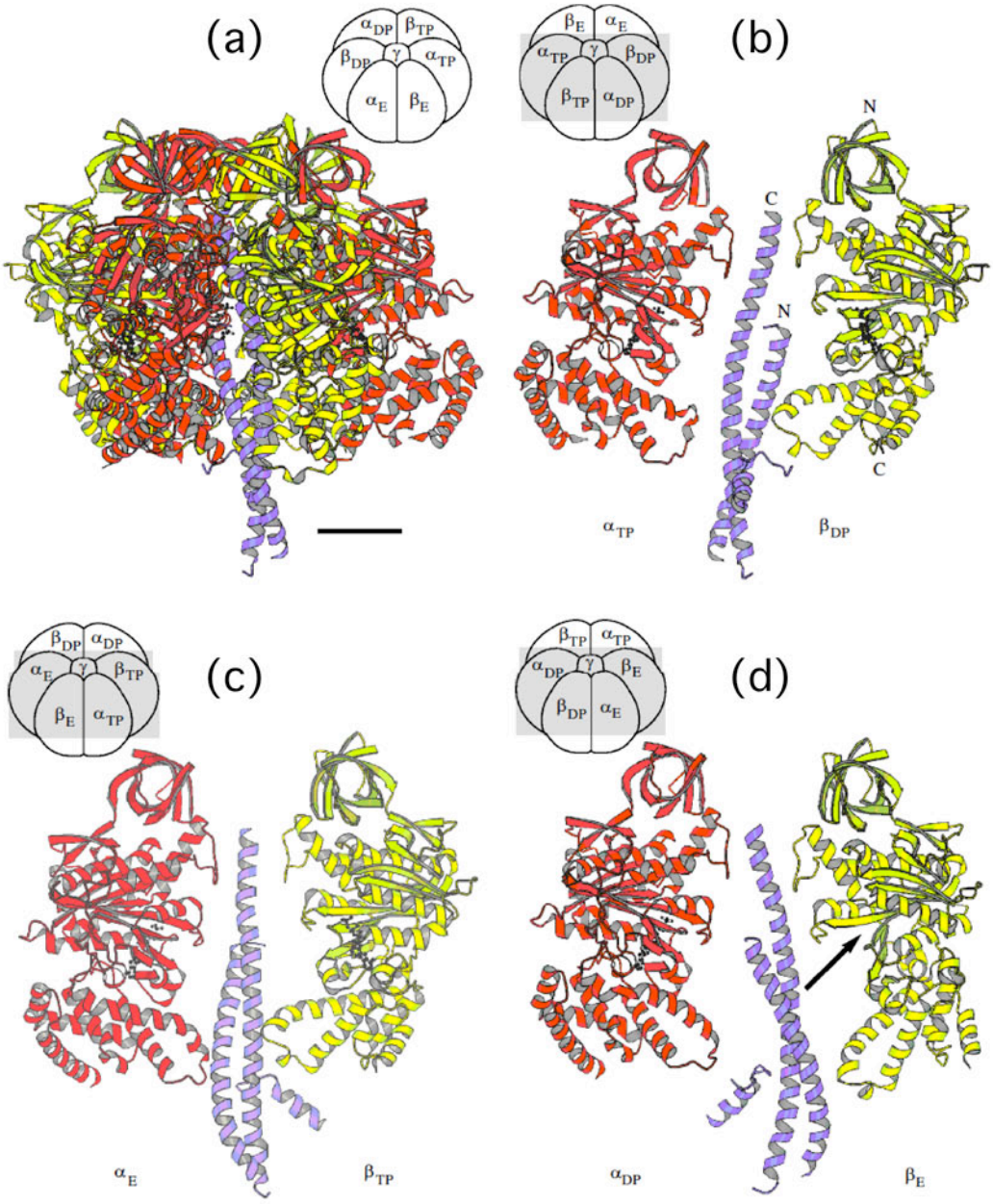

Figure 2-1. The crystal structure of bovine mitochondrial F_1-ATPase. Nucleotides are drawn in a 'ball and stick' representation. The relative positions of α- and β-subunits labeled as described in the text, are indicated in the schematic diagram in the upper left or right of the figures. (a) The entire structure of F_1-ATPase. Scale bar, 20 Å. (b) The α_{TP}, β_{DP} and γ-subunits. The N- and C-termini of the β- and γ-subunits are shown. (c) The α_E, β_{TP} and γ-subunits. (d) The α_{DP}, β_E and γ-subunits. The arrow indicates the point at which the β-sheet of the nucleotide binding domain is disrupted in β_E (Abrahams *et al*., 1994).

2.2. Materials and Methods

2.2.1. Bacterial strains, plasmids and primer

The bacterial strains, plasmids and primers used in the experiments described in this chapter are listed in Table 2-1 and 2-2.

2.2.2. Preparation and purification of FliI

A 30 ml overnight culture of BL21(DE3)pLysS carrying pMM1771, which encodes FliI with an N-terminal hexa-histidine (His-FliI) followed by a thrombin-cleavage site on pTrc99A (GE Healthcare), was inoculated into 1 l LB medium containing 50 μg/ml ampicillin and 30 μg/ml chloramphenicol. Cells were grown at 296 K until the culture density reached an OD_{600} of 0.6. Expression of His-FliI was induced with IPTG at a final concentration of 0.1 mM. Overnight culture was centrifuged (6400*g*, 10 min, 277 K) and the cells were stored at 193 K. The cells were thawed, suspended in binding buffer (50 mM Tris-HCl pH 8.0, 500 mM NaCl, 80 mM imidazole) with a tablet of the Complete protease-inhibitor cocktail, and sonicated. After centrifugation (19000*g*, 20 min, 277 K), the supernatant was loaded onto a HiTrap chelating column (GE Healthcare) equilibrated with the binding buffer. Proteins were eluted using a linear gradient of imidazole. Fractions containing His-FliI were kept with 50 units of thrombin (GE Healthcare) at 277 K overnight and applied to a HiLoad Superdex 75 (26/60) column (GE Healthcare) in 50 mM Tris-HCl pH 8.0, 150 mM NaCl. The purity of the product was examined by SDS-PAGE and MALDI-TOF mass spectrometry (Voyager DE/PRO, Applied Biosystems).

2.2.3. Preparation and purification of FliJ mutants

The mutant variants of His-FliJ (FliJ(C32T) and FliJ(C32T, I67C)) were

generated by the QuikChange site-directed mutagenesis method (Stratagene). Site-directed mutagenesis was performed by inverse PCR method (Imai *et al.* 1991). The DNA sequence encoding *fliJ*(C32T) was produced and amplified by PCR from plasmid pMMIJ001 with the primers PIJ001 and PIJ002 using *PfuTurbo* DNA polymerase (Stratagene), and ligated to create plasmid pTIJ001. A plasmid pTIJ002, which encodes FliJ mutants (C32T, I67C), was produced in the same protocol used for pTIJ001 construction with the primers PIJ003 and PIJ004. Primers used to create plasmids encoding the FliJ mutants were listed in Table 2-2. DNA sequences of the final products were analyzed with a 3130 Genetic Analyzer (Applied Biosystems). The mutant proteins were expressed in BL21(DE3)pLysS and purified as the same protocol used for native FliJ (see Section 1.2.1 of Chapter 1).

2.2.4. *In vitro* reconstruction of the FliI ring structure and electron microscopy

Purified FliI or the mixtures of FliI and FliJ(C32T) with various molar ratios were incubated in 35 mM Tris-HCl (pH 8.0), 113 mM NaCl, 0 or 1 mM DTT, 5 mM ADP, 5 mM $AlCl_3$, 15 mM NaF, 5 mM $MgCl_2$, and 100 μg/ml acidic phospholipids at 310 K for a few minutes. The final concentration of FliI in each solution was adjusted to 50 μg/ml. Samples were applied to carbon-coated copper grids and negatively stained with 0.5% (w/v) uranyl acetate. Micrographs were recorded at a magnification of ×25,000 with a JEM-1011 transmission electron microscope (JEOL, Tokyo, Japan) operated at 100 kV.

2.2.5. Preparation of FliJ labeled with Cy3

Crude FliJ(C32T, I67C) with His-tag solution was mixed with 1 mM Cy3-maleimide (GE Healthcare) in a HiTrap chelating column and incubated for 3 h at

room temperature. Then, the FliJ(C32T, I67C)-Cy3 was purified as the same method used for native FliJ (see Section 1.2.1 of Chapter 1). The purity of the product was examined by SDS-PAGE and MALDI-TOF mass spectrometry (Voyager DE/PRO, Applied Biosystems).

2.2.6. Analytical gel-filtration chromatography of FliI-FliJ complex

Purified FliI and FliJ(C32T, I67C)-Cy3 were mixed at the molar ratio with 6 to 1, and was incubated in 35 mM Tris-HCl (pH 8.0), 113 mM NaCl, 5 mM ADP, 5 mM $AlCl_3$, 15 mM NaF, 5 mM $MgCl_2$, and 100 μg/ml acidic phospholipids at 310 K for a few minutes. The samples applied to a Superdex^{TM} 200 HR 10/30 column (GE Healthcare). The protein solution was eluted with 50 mM Tris-HCl (pH 8.0), 150 mM NaCl, 5 mM $MgCl_2$, 1 mM AMP-PNP.

2.2.7. Preparation of FliJ labeled with Streptavidin

Crude FliJ(C32T, I67C) with His-tag solution was mixed with 1 mM biotin-PEG2-Maleimide (Thermo) in a HiTrap chelating column and incubated for 3 h at room temperature. Then, the biotinated FliJ(C32T, I67C) was purified as the same method used for native FliJ (see Section 1.2.1 of Chapter 1) and mixed with small amount of Streptavidin (Thermo) and incubated for 4 h at 277 K. The FliJ(C32T, I67C) in complex with Streptavidin was purified with a HiLoad Superdex 75 (26/60) column in 50 mM Tris-HCl pH 8.0, 150 mM NaCl. The purity of the product was examined by SDS-PAGE.

2.2.8. Electron cryomicroscopy and image processing

Sample grids for electron cryomicroscopy were prepared by applying a 4 μl of

protein solution (150 μg/ml) onto a holey carbon grid (Quantifoil R0.6/1.3, Quantifoil Micro Tools, Jena, Germany), which had been glow discharge in a weak vacuum for 20 s immediately before use. The grids were blotted for 3 s and quick-frozen in liquid ethane using Vitrobot (FEI, Eindhoven, Netherlands) before transfer to a liquid nitrogen storage capsule. Images were recorded using a TVIPS 4K × 4K CCD camera on a JEM-3200FSC electron microscope (JEOL, Tokyo, Japan), equipped with a liquid-helium cooled specimen stage, an Ω-type energy filter and a field-emission electron gun operated at an accelerating voltage of 200 kV. Micrographs were recorded at 50 K with a magnification of ×140,000, corresponding to 1.07 Å/pixel. Focal pairs of micrographs were recorded at a defocus between 1.5 and 2.5 μm with an electron dose of 40 $e^-/Å^2$ for the first micrograph, and a defocus between 3.5 and 5.5 μm with an electron dose of 40 $e^-/Å^2$ for the second. They were merged using the FOCALPAIR (Ludtke *et al*., 1999, 2003). The defocus amplitude, envelope and noise values were determined using CTFIT (Ludtke *et al*., 1999). Micrographs showing significant astigmatism or drift were discarded. The particle images were selected with BOXER (Ludtke *et al*., 1999) and the boxed particle images were aligned and classified using the REFINE2D.PY (Ludtke *et al*., 1999).

2.2.9. ATPase activity measurement of FliI

ATPase activity of FliI was measured at 310 K with an enzyme-coupled ATP-regenerating system by using a spectrophotometer V-630BIO (JASCO). The reaction mixture contained 50 mM Tris-HCl (pH 8.0), 100 mM KCl, 4 mM ATP-Na, 4 mM $MgCl_2$, 2 mM phosphoenolpyruvate, 50 μg/ml pyruvate kinase, 50 μg/ml lactate dehydrogenase, and added NADH until the mixture density reached an OD_{340} of 1.0 - 1.2 in a final volume of 1.0 ml. The reaction was initiated by addition of FliI (340

μg/ml) or the mixtures of FliI (340 μg/ml) and FliJ in various molar ratios dissolved in 50 mM Tris-HCl (pH 8.0), 150 mM NaCl to 1.0 ml of the assay mixture, and the rate of ATP hydrolysis was monitored as the rate of oxidation of NADH determined by the absorbance decrease at 340 nm.

Table 2-1. Strains and plasmids used in this study of this chapter

Strains or Plasmids	Relevant properties	Source or ref.
E.coli		
BL21(DE3)pLysS	Host for overexpression from the T7 promoter	Novegen
Salmonella		
SJW1368	Δ(*cheW-flhD*); master operon mutant	(Ohnishi *et al*., 1994)
Plasmids		
pET15b	Expression vector	Novegen
pGEX6p-1	Expression vector	GE Healthcare
pTrc99A	Expression vector	GE Healthcare
$pBGtI_{CAT}$	pTrc99AFF4/His-FliI(111-456)	(Minamino *et al*., 2003)
pMM1702	pTrc99AFF4/His-FliI	(Minamino *et al*., 2000)
pMM1771	pTrc99A/ His-FliI	This study
pMMI100	pTrc99AFF4/His-FliI(1-100)	This study
pMMI38	pTrc99AFF4/His-FliIΔ(381-390)	This study
pMMI39	pTrc99AFF4/His-FliIΔ(391-400)	This study
pMMI43	pTrc99AFF4/His-FliIΔ(431-440)	This study
pMMIJ001	pET15b/His-FliJ	(Ibuki *et al*., 2009)
pMMJ1001	pGEX6p-1/GST-FliJ	(Minamino *et al*., 2010)
pTIJ001	pET15b/His-FliJ(C32T)	This study
pTIJ002	pET15b/His-FliJ(C32T, I67C)	This study

Table 2-2. Primers used in this study of this chapter

Primer		Sequence
PIJ001	-C32T-Fw	ctgggcgaaatgcgtcgcggcacccaacaggcggaagaacagctc
PIJ002	-C32T-Rv	gagctgttcttccgcctgttgggtgccgcgacgcatttcgcccag
PIJ003	-I67C-Fw	ggcatcgccagtaatcgctggtgcaactatcagcagtttattcag
PIJ004	-I67C-Rv	ctgaataaactgctgatagttgcaccagcgattactggcgatgcc

2.3. Result

2.3.1. FliJ affects the hexameric ring formation of FliI

FliI forms a hexameric ring structure in the presence of ATP or its analog, and phospholipids facilitate the hexamer formation (Claret *et al*., 2003). The yield of the FliI ring structure is higher in the presence of a non-hydrolyzable ATP analog, AMP-PNP, than ATP, indicating that the stability of the ring states is regulated by the ATP hydrolysis process (Kazetani *et al*., 2009). Therefore I mixed FliJ and FliI with various molar ratios in the presence of Mg^{2+}-ADP-AlF_4, and observed the mixtures by electron microscopy. The result shows that FliJ strongly affects the hexamric ring formation of FliI (Figure 2-2). When FliI and FliJ were mixed with molar ratio of 1:1, only few rings were observed (Figure 2-2b), indicating that the interaction between FliI and FliJ is stronger than that between FliI subunits. On the contrary, when they were mixed with the molar ratio of 6:1, the ring formation is greatly enhanced (Figure 2-2a). These results indicate that FliJ interacts with FliI and acts as a nucleus for the FliI ring formation.

2.3.2. Gel-filtration analysis of the FliI-FliJ complex labeled with Cy3

The FliI hexamer ring is very unstable in solution. Even in the presence of ATP analogues and phospholipids, the equilibrium is almost entirely biased to the monomeric state. That is why FliI hexameric ring structure has been observed only by electron microscopy (Minamino *et al*., 2006. Kazetani *et al*., 2009). In this study, I found that addition of FliJ with the molar ratio of 1:6 to FliI greatly enhance the FliI ring formation and stabilize the FliI hexamer. To examine the complex formation of FliJ with the FliI ring in solution, I prepared FliJ labeled with the Cy3-maleimide, mixed it with FliI and observed the mixture by analytical gel-filtration chromatography. Since

the presence of nucleotides disturbs the protein detection at OD_{280}, elution peaks were observed by fluorescence emission at 570 nm of FliJ-Cy3 (ex. 500 nm) to detect a small amount of FliJ-Cy3. Ile-67 of FliJ was selected as a labeling target because its corresponding residue of the γ-subunit of F_1-ATPase is exposed on the outside of the F_1 α/β ring structure. Ile-67 was substituted to cysteine (I67C) for labelling with Cy3-maleimide, and the intrinsic cystein residue Cys-32 was substituted to threonine (C32T) to avoid undesirable side reaction. Purified FliJ-Cy3 was then mixed with FliI in the presence of Mg^{2+}-ADP-AlF_4 and phospholipids and applied to a Superdex^{TM} 200 HR 10/30 column.

Figure 2-3 shows the elution profile of FliJ-Cy3, FliI, FliI-FliJ-Cy3 and the A_3B_3 ring of V_1-ATPase. The FliI and FliI-FliJ-Cy3 samples were prepared in the presence of ADP-AlF_4 and phospholipids and were eluted in the presence of AMP-PNP. In the elution profile of FliJ-Cy3, a single peak was observed (Figure 2-3). On the contrary, the mixture of FliI and FliJ-Cy3 showed another peak at a corresponding to the A_3B_3 ring of V-ATPase (Figure 2-3). These results indicate that FliJ forms complex with the FliI ring in solution.

2.3.3. Observation of the FliI-FliJ complex labeled with streptavidin

To further analyze the complex formation of FliJ with the FliI ring, I prepared FliJ decorated with the biotin-streptavidin label, mixed it with FliI and observed the mixture by electron microscopy. Biotinated FliJ(C32T, I67C) was then mixed with a small amount of streptavidin (ST), and the FliJ/ST complex was purified by gel filtration chromatography to remove excess biotinated FliJ(C32T, I67C). Based on the molar contents of FliJ and ST in the complex, two FliJ molecules were estimated to bind to the streptavidin tetramer ($FliJ_2/ST_4$) (Figure 2-4). The $FliJ_2/ST_4$ complex was

then mixed with FliI in the presence of Mg^{2+}-ADP-AlF_4 and observed by electron microscopy. A number of pairs of rings that are bridged by an extra density were seen (Figure 2-5). The bridging density probably corresponds to streptavidin. This result indicates that FliJ associates with the FliI hexamer ring structure.

2.3.4. Electron cryomicroscopy and image analysis of the FliI-FliJ complex

To clarify the location of FliJ in the $FliI_6FliJ$ complex, I analyzed the images of frozen-hydrated $FliI_6FliJ$ and FliI ring particles embedded in vitreous ice by electron cryomicroscopy. Figure 2-6 shows an electron micrograph of the FliI ring particles, recorded at a magnificent of ×140,000, with underfocus between 1.5 and 2.5 μm, and an electron dose of 40 $e^-/Å^2$ (Figure 2-6a). Because of the relatively small size of the particles, they were mostly invisible due to the extremely low contrast and low S/N. Since larger amounts of defocus are known to enhance the contrast and S/N, the second micrograph was recorded from the same area of the specimen with underfocus between 3.5 and 5.5 μm and an electron dose of 40 $e^-/Å^2$ (Figure 2-6b). Despite such large amounts of underfocus, the contrast and S/N enhancement were not high enough to allow particle image selection. The contrast and S/N were then further enhanced by applying a focal-pair merging technique (Ludtke *et al*., 1999, 2003) (Figure 2-6c) and the results were dramatic; I was able to determine the position of the FliI rings in the focal-pair merged micrographs. I used this information to pick up particle images from the first micrographs of each pair, that is, those recorded with smaller underfocus and less radiation damage.

Since the distribution of the particle orientation was strongly biased to end-on view, we aligned and averaged the end-on images of each particle. The averaged image of FliI shows a hexameric ring structure with a central hole of 2 nm in diameter (Figure

2-7a), which is consistent with previous reports (Claret *et al*., 2003. Minamino *et al*., 2006. Kazetani *et al*., 2009). On the contrary, the averaged image of the $FliI_6FliJ$ complex clearly shows an extra density in the interior of the central hole but located off the center and close to one of the peripheral subunits (Figure 2-7b). These observations suggest that FliJ penetrates into the central hole of the FliI ring in a similar way to the γ-subunit of F_1-ATPase (Abrahams *et al*., 1994). Pull-down assays by GST affinity chromatography revealed that FliJ binds to the C-terminal region of the C1 α-helix of FliI, which corresponds to the region of the β-subunit that interacts with the γ-subunit in the F_1-ATPase structure (Figure 2-8).

2.3.5. Effect of FliJ on the ATPase activity of FliI

It has been reported that FliJ stimulates the ATPase activity of FliI (Evans *et al*., 2006) although the details have not been shown. Therefore I examined the effect of FliJ addition on the ATPase activity of FliI. FliI is believed to self-assemble into a homo-hexamer to fully exert its ATPase activity. Thus, the highest ATPase activity is expected when FliJ is added to FliI with the molar ratio of 1:6, and the addition of excess amount of FliJ is expected to reduce the ATPase activity. However, the ATPase activity increased according to the amount of FliJ added (Figure 2-9). This result suggests that the hexamer ring structure is not indispensable for the ATPase activity of FliI.

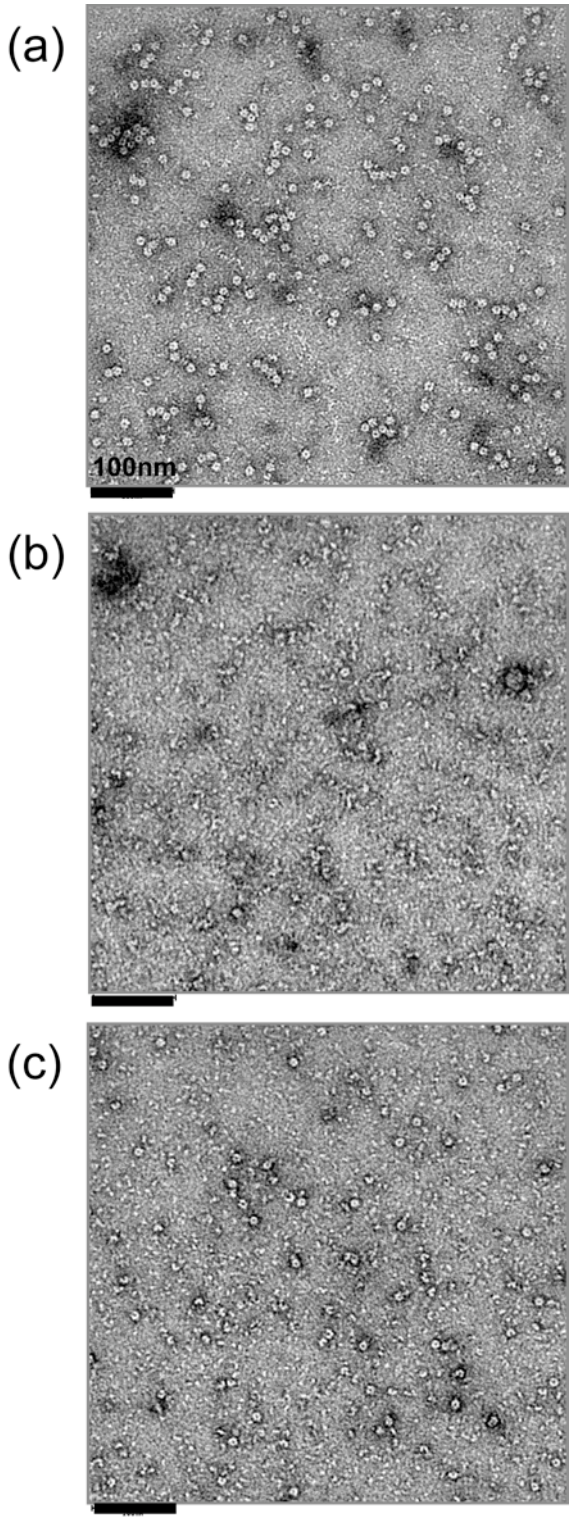

Figure 2-2. Effect of FliJ on the FliI ring formation. Negatively stained electron micrographs of FliI and FliI-FliJ mixtures. FliI and FliJ were mixed with molar ratio of (a) 6:1, (b) 1:1, and (c) 1:0.

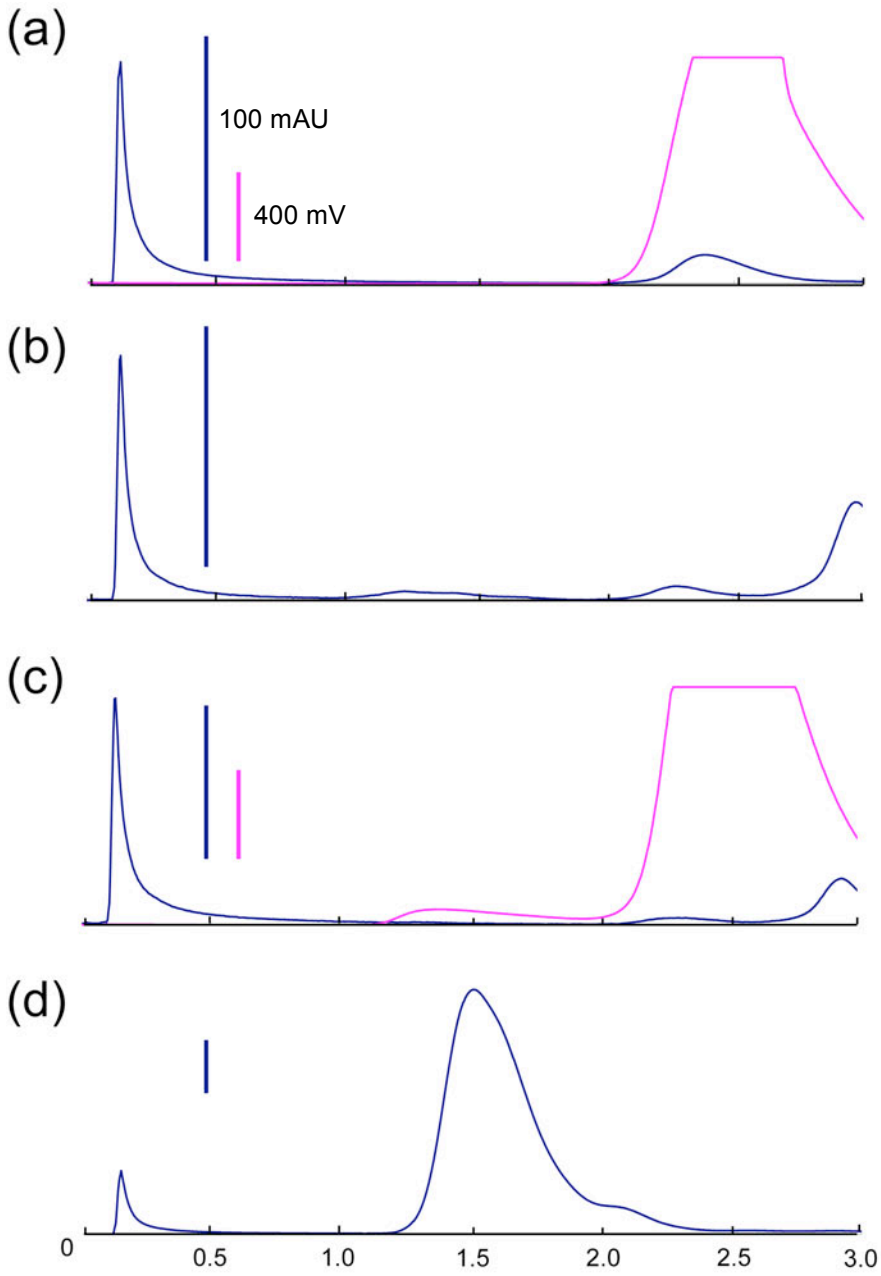

Figure 2-3. Analytical gel-filtration chromatography of the FliI-FliJ complex. Gel-filtration (Superdex 200) profile of (a) FliJ-Cy3, (b) FliI, (c) FliI-FliJ-Cy3 and (d) the A_3B_3 ring of V-ATPase. For (b) FliI and (c) FliI-FliJ-Cy3, the samples were prepared in the presence of ADP-AlF_4 and phospholipids and eluted in the presence of AMP-PNP. Blue and pink lines represent absorbance at 280 nm and fluorescence at 570 nm (ex. 500 nm), respectively.

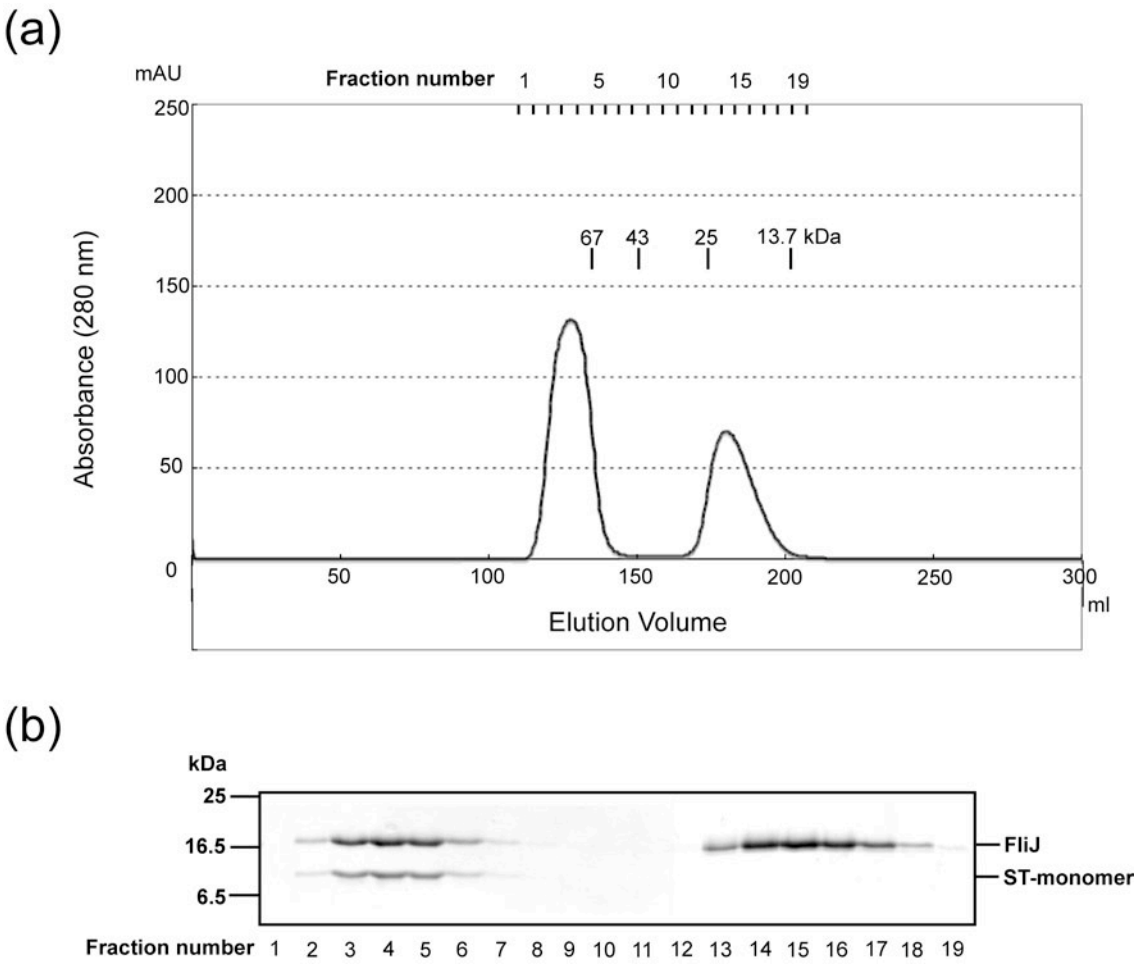

Figure 2-4. Isolation of the FliJ labeled with streptavidin. (a) Elution profile of the mixture of the biotinated FliJ(C32T/I67C) and streptavidin (ST) by gel-filtration chromatography. Elution peak positions of the size marker proteins are shown: albumin (67 kDa), ovalbumin (44 kDa), chymotrypsinogen A (25 kDa) and ribonuclease A (13.7 kDa), with fraction numbers and molecular-mass protein standards indicated in the chromatogram. (b) SDS-PAGE analysis of the fractions of the gel-filtration chromatography. Only the earlier elution peak contains FliJ and ST.

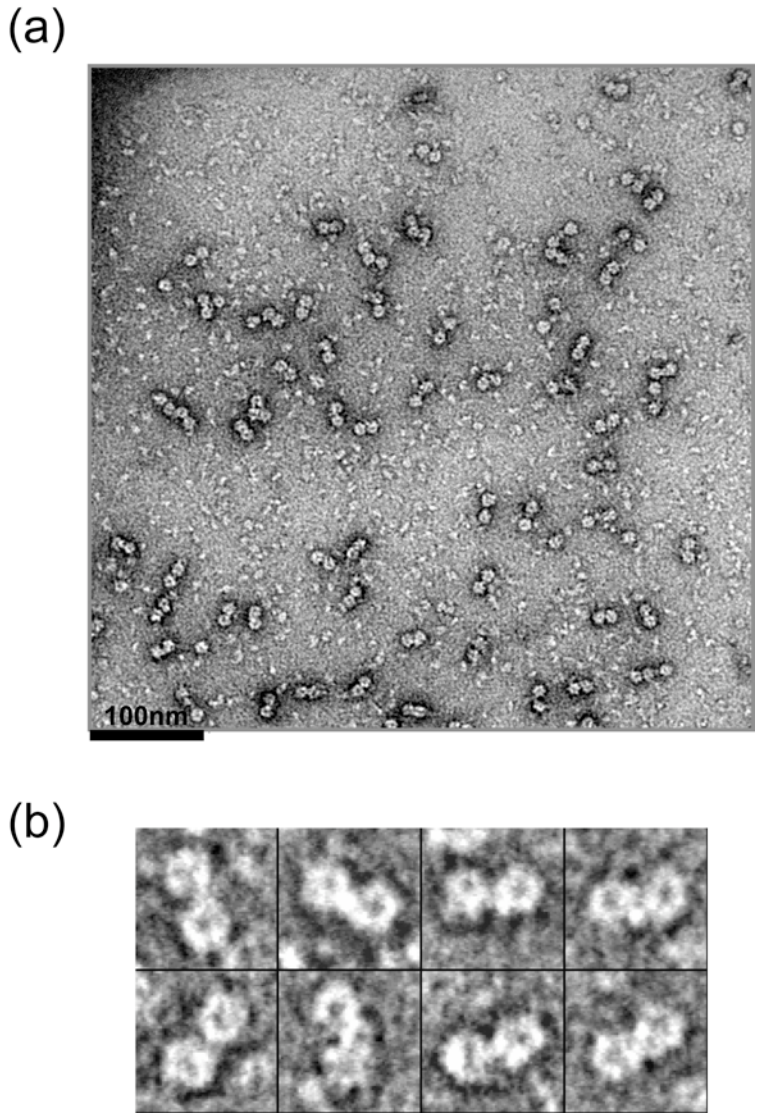

Figure 2-5. Electron micrographs of the FliI-FliJ complex. (a) Negatively stained electron micrographs of the mixture of FliI and FliJ labeled with streptavidin. (b) Close-up views of the paired FliI hexameric rings.

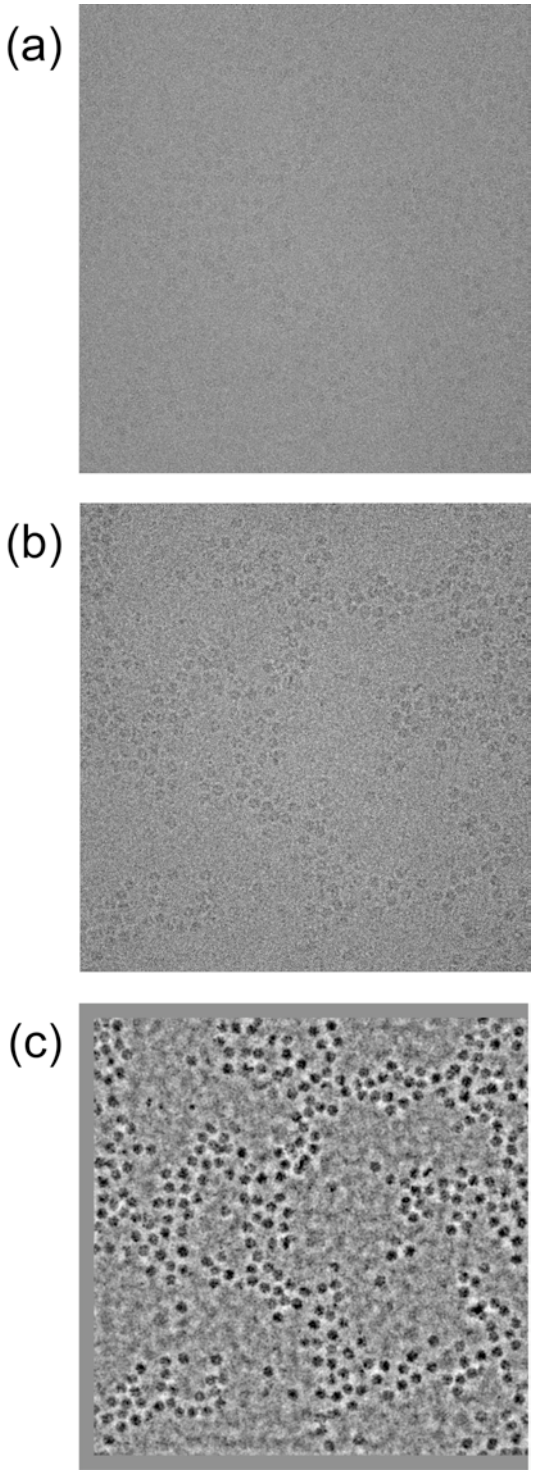

Figure 2-6. Contrast enhancement by focal pair merging of electron cryomicrographs for particle selection. (a) Micrograph recorded at 40 $e^-/Å^2$ between 1.5 and 2.5 μm underfocus. (b) Micrograph recorded at 40 $e^-/Å^2$ between 3.5 and 5.5 μm underfocus from the same area as panel (a). (c) Contrast-enhanced image by focal pair merging of panel (a) and (b).

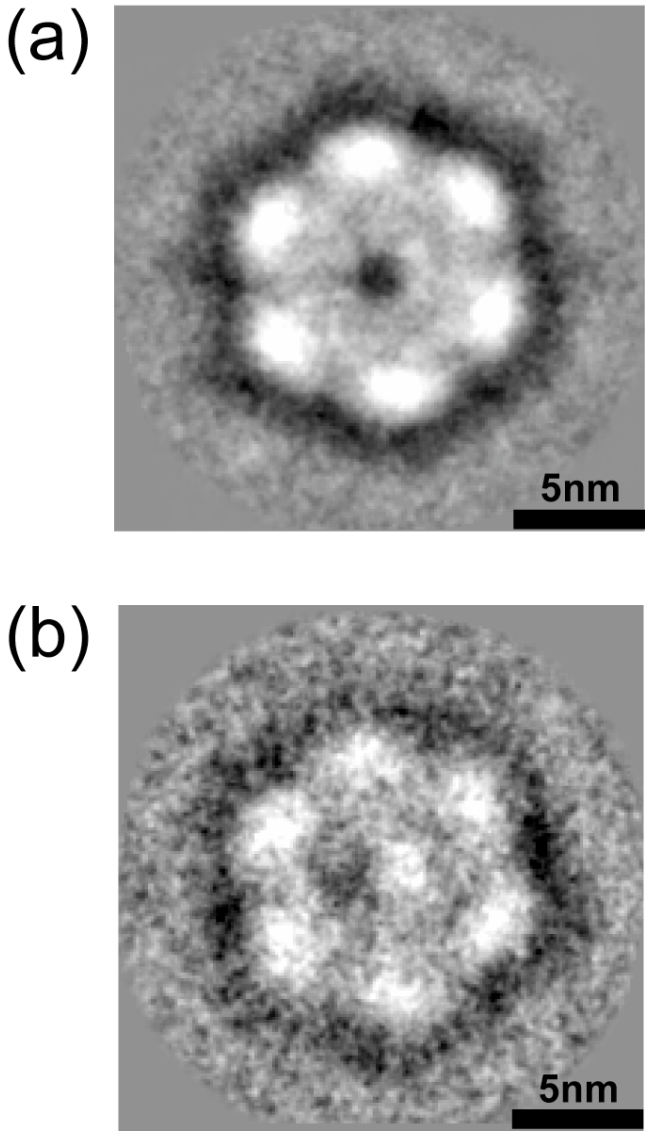

Figure 2-7. Comparison of the FliI ring and the FliJ-FliI ring complex. Averaged end-on view images of (a) the FliI hexameric ring and (b) the FliJ-FliI ring complex.

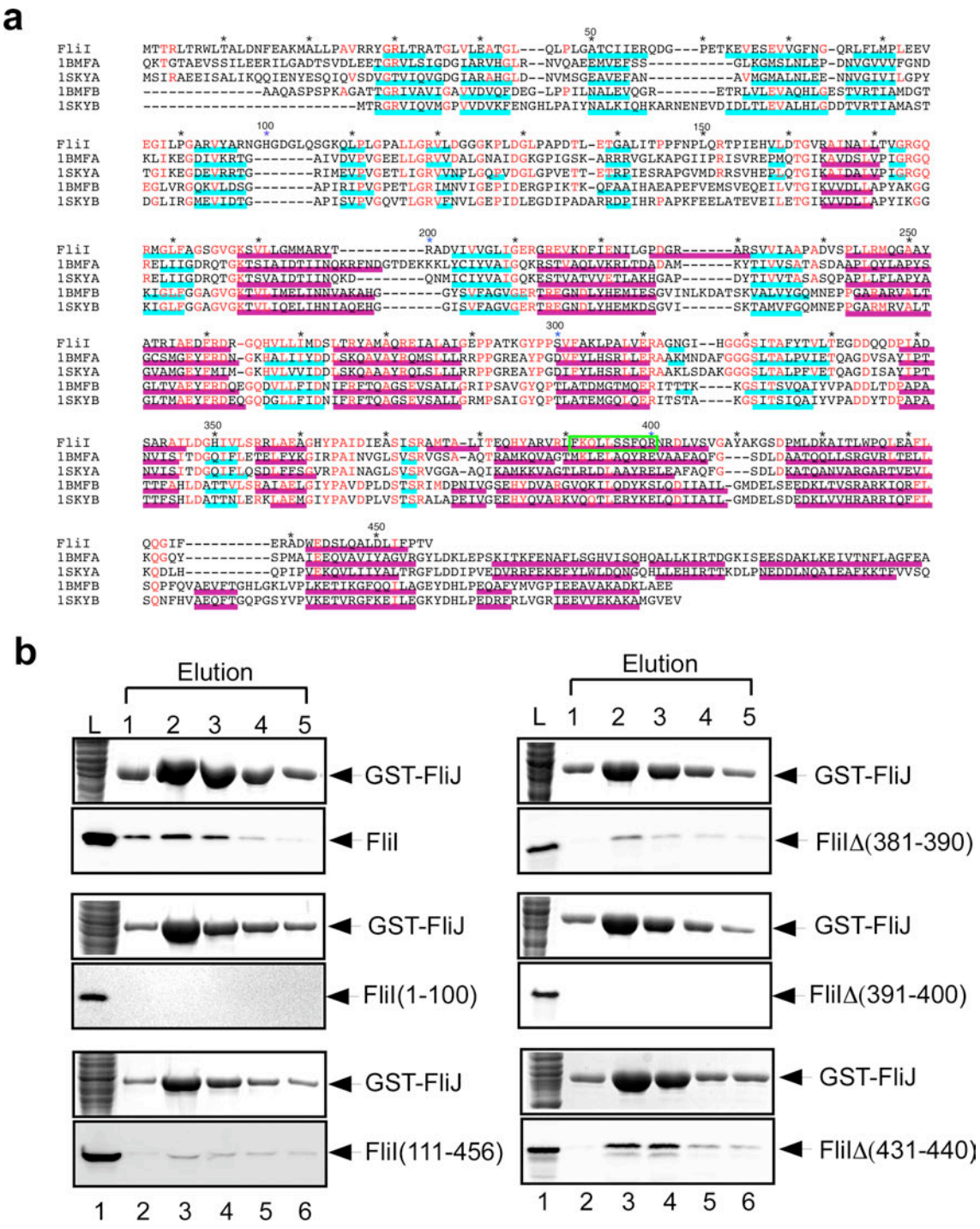

Figure 2-8. The FliJ binding site of FliI. (a) Structure-based sequence alignment of FliI and the α/β-subunits of F_1-ATPase from bovine mitochondria (1BMFA and 1BMFB) and the thermophilic *Bacillus* PS3 (1SKYA and 1SKYB). Bars in purple and cyan below each sequence indicate α-helix and β-strand, respectively. The region interacting with FliJ is shown by the green box. The residues conserved between FliI

and any of the F_1 subunits are highlighted in red. (b) Interaction of FliJ with FliI and FliI mutants revealed by pull-down assay using GST affinity chromatography. The mixture of the soluble fractions prepared from SJW1368 (Δ*flhDC-cheW* mutant) expressing GST-FliJ with those from SJW1368 producing His-FliI (left upper two panels), His-FliI(1-100) (left middle two panels), His-FliI(111-456) (left lower tow panels), FliIΔ(381-390) (right upper two panels), FliIΔ(391-400) (right middle two panels) and FliIΔ(431-440) (right lower two panels) were loaded onto a GST column. After extensive washing, proteins were eluted with a buffer containing 10 mM reduced glutathione. The eluted fractions were analyzed by both CBB staining and immunoblotting with polyclonal anti-FliI antibodies. (Experimented by T. Minamino)

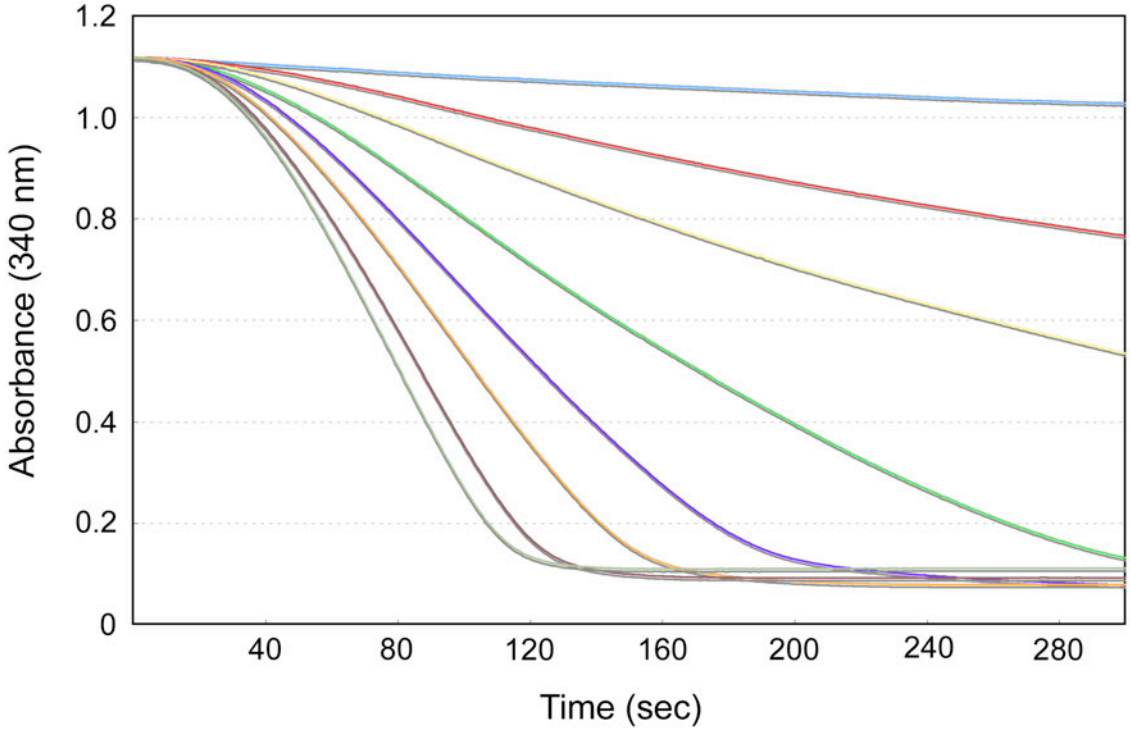

Figure 2-9. ATPase activity of FliI in the presence of FliJ. ATP hydrolysis was monitered at 310 K in the presence of an ATP regenerating system. The reactions were started by the addition of 100 μl of 340 μg/ml FliI or the mixtures of FliI and FliJ in various molar ratios solution to 1.0 ml of the reaction mixture. Blue line represents the ATPase activity of FliI alone; red, yellow, green, purple, orange, brown and dark green lines represent that of the mixture FliI and FliJ at the moler ration of 1:1/12, 1:1/6, 1:1/3, 1:1/2, 1:1, 1:2, 1:3 respectively.

2.4. Discussion

2.4.1. ATPase activity of FliI-FliJ complex

The number of FliI rings observed by electron microscopy of negatively stained specimens increased by the addition of FliJ to FliI, but only upto the ratio of 1:6; the number decreased by the further addition of FliJ (Figure 2-2). However, the ATPase activity of FliI increased according to the amount of FliJ added (Figure 2-9). These results suggest that the complete hexameric ring structure is not indispensable for the full ATPase activity. Because the catalytic site is located at the inteface of the neighboring FliI subunits and since FliJ facilitates the assembly of FliI, an increased probability of small oligomer formation of FliI, such as dimer or trimer, may be sufficient to increase the ATPase activity. An increased level of the ATPase activity may facilitate the cyclic process of protein export consisting of initial docking, unfolding and translocation of export subustrates. However, the overexpression of FliJ is actually deletrious for protein export, as demonstrated by the strong inhibition on the motility (Minamino and Macnab, 2000). This inhibitory effect implies that it is the FliI hexameric ring that is essential for protein export, probably to facilitate the initial insertion of export substrate into the export gate by docking of the ring with bound export substrate to the FlhA-FlhB platform. So the expression of FliJ must be controlled to an appropriate level not to suppress the rate of protein export. Although no solid evidence is available, it is thought that the expression level of FliJ is lower than that of FliI.

2.4.2. Similarities between flagellar protein export apparatus and F_oF_1-ATP synthase

The structural similarity between the $FliI_6FliJ$ complex and the $\alpha_3\beta_3\gamma$ complex

of F_1-ATPase implies a close relationship between the bacterial flagellum and F_oF_1-ATP synthase. Moreover, the N-terminal and C-terminal regions of FliH are homologous to the b- and δ-subunits of F_oF_1-ATP synthase, respectively (Pallen *et al*., 2006). The b- and δ-subunits form the peripheral stalk essential for connecting F_1 with F_o (Dunn *et al*., 2000). Both FliH and the b subunit share an elongated structure and form homodimer (Minamino *et al*., 2001, 2002). A right-handed α-helical coiled coil structure with its intrinsic asymmetry is responsible for the dimerization of the b-subunit (Pallen *et al*., 2006). Since the central region of FliH between residues 101 and 140, which is responsible for FliH dimerization, contains a sequence with a significant probability of forming α-helical coiled coil (González-Pedrajo *et al*., 2002), the FliH dimer may form in a similar manner to the b-subunit dimer. The δ-subunit binds to the extreme N-terminal region of the α-subunit or α/β pair (Dunn *et al*., 2000). Similarly, the C-terminal region of FliH binds to the extreme N-terminal region of FliI (Minamino *et al*., 2000, 2001. Lane *et al*., 2006). Since FliI is not able to associate efficiently with the FlhA-FlhB platform of the export gate in the absence of FliH, these similarities strongly suggest that FliH acts as a peripheral stalk to anchor the $FliI_6FliJ$ complex to the platform (Minamino *et al*., 2003).

Although FliJ has been postulated to be a general chaperone for export substrates (Minamino *et al*., 2000), the structure of the $FliI_6FliJ$ complex suggests a novel role of FliJ in protein export. The structural similarity between the $FliI_6FliJ$ complex and F_1-ATPase indicates that they share a common mechanism for their distinct functions. F_1-ATPase involves a rotational mechanism for hydrolyzing ATP. Rotation of the γ-subunit synchronously drives a series of conformational changes of the α/β-subunits that leads to the sequential ATP hydrolysis at the three catalytic sites (Noji *et al*., 1997. Yoshida *et al*., 2001). Then, does FliJ rotate in the $FliI_6FliJ$ complex? That

may be possible, although we do not have any solid evidence. In fact, the addition of FliJ increases the ATP hydrolyzing activity of FliI. Since ATP hydrolysis promotes the dissociation of the FliI ring structure (Minamino *et al*., 2008), the ATP hydrolyzing activity of FliI in the hexameric ring should be well organized. FliJ may harmonize the reactions at the six possible catalytic sites and control the association/dissociation of the FliI subunit into/from the ring structure at the export gate.

In F_oF_1-ATP synthase, rotation of the c-subunit ring in the F_o region, which is energized by proton motive force across the inner membrane, drives the rotation of the γ-subunit, leading to ATP synthesis (Yoshida *et al*., 2001). In other words, the γ-subunit couples proton motive force with the chemical synthesis of ATP. Many such similarities between the flagellar export system and F_oF_1-ATP synthase suggest that FliJ couples ATP hydrolysis by FliI with the proton flow. Recently, it has been shown that the interaction between FliJ and a gate-forming protein FlhA facilitates an inward-directed proton flow (Minamino and Namba. In preparation), suggesting that FliJ couples the proton flow and translocation of export substrates through the gate.

Chapter 3
Role of the highly conserved residues of FliJ on the flagellar type III protein export

3.1. Introduction

The homologous region between FliJ and the γ-subunit corresponds to the surface the γ-subunit interacting with the ε-subunit of F_1-ATPase, suggesting that FliJ may have a binding partner corresponding to the ε-subunit. To identify the function of the residues in the homologous region, site-directed mutation experiments were performed for eight highly conserved, surface-exposed residues of FliJ (Figure 1-7b). The F72A and L76A mutations abolished the interaction between GST-FliJ and FlhA. These results indicate that Phe-72 and Leu-76 of FliJ are essential for the interaction with FlhA to facilitate the protein export process. In this chapter, I will discuss the roles of these highly conserved residues on the protein export.

3.2. Materials and Methods

3.2.1. Bacterial strains, plasmids, primer and media

The bacterial strains, plasmids and primers used in the studies of this chapter are listed in Table 3-1 and 3-2. Soft tryptone agar plates were prepared by mixing 10 g of Bacto-Tryptone, 5 g of NaCl and 3.5 g of Bacto-agar in 1 l of water, and ampicillin was added at a final concentration of 50 μg/ml.

3.2.2. Construction of plasmids

Site-directed mutagenesis was performed by inverse PCR method. The DNA sequence encoding *fliJ* (Q38A) was produced and amplified by PCR from plasmid pMMIJ001 with the primers PIJ005 and PIJ006, and ligated to create plasmid pTIJ003. Plasmids pTIJ004 to pTIJ010, which encodes His-FliJ mutants (L42A, Y45A, Y49A, F72A, L76A, A79S and H83A), were produced in the same protocol used for pTIJ003 construction.

Plasmids from pTIJ003 to pTIJ010 was digested with *Nde*I and *Bam*HI, and ligated into *Trc* expression vector pTrc99AFF4 (Ohnishi *et al*., 1994) to create pTIJ101 to pTIJ108.

To create *Bam*HI and *Eco*RI sites, the DNA sequence encoding each mutants of *fliJ* were amplified by PCR from plasmids pTIJ003 to pTIJ010. Plasmids pTIJ003 to pTIJ010 was digested with *Bam*HI and *Eco*RI, and ligated into GST-tag fusion protein expression vector pGEX6p-1 (GE Healthcare) to create pTIJ201 to pTIJ208.

Primers used to create plasmids encoding the FliJ mutants were listed in Table 3-2. DNA sequence of the final products was analyzed with a 3130 Genetic Analyzer (Applied Biosystems).

3.2.3. Motility assay

pTrc99AFF4-based and pGEX6p-1-based plasmids encoding wild type FliJ and its various point mutants were transformed into a *ΔfliJ* strain, MKM40, a *ΔfliH-fliI-fliJ* bypass (Δ*fliH-I-J flhB*(P28T)) mutant strain, MMHIJ0117, and the wild type strain SJW1103, respectively. Fresh overnight colonies were picked into soft tryptone agar plates containing ampicillin and incubated at 303 K, and the motility was assessed by examining the migration of bacteria through the agar from the center toward the periphery of the plate.

3.2.4. Preparation of whole cell and culture supernatant fractions

Salmonella cells were grown at 303 K with shaking until the cell density had reached an OD_{600} of ca. 1.0 - 1.2. Aliquots of culture containing a constant number of cells were clarified by centrifugation. Cell pellets were resuspended in SDS-loading buffer normalized by the cell density to give a constant amount of cells. The proteins in the culture supernatants were precipitated by 10% trichloroacetic acid, suspended in a Tris-SDS loading buffer and heated 368 K for 5 min. After SDS-PAGE, immunoblotting with polyclonal anti-FliC, anti-FlgD and anti-FliJ antibodies was carried out and signals were detected with an ECL immunoblotting detection kit (GE Healthcare).

3.2.5. Immunoblotting

After the proteins in each fraction had been separated by SDS-PAGE, they were transferred onto a nitrocellulose membrane (BIO RAD) with a transblotting apparatus (GE Healthcare). The membrane was blocked for 1 h with 25 ml of TBS-T (20 mM Tris-HCl, pH 7.5, 500 mM NaCl, 0.1% Tween 20) containing 1.0% skim milk.

After washing with 25 ml of TBS-T three times by shaking (5 min × 3), the membrane was soaked with 10 ml of TBS-T containing 1 μl of polyclonal antibody for 1 h, then washed with 25 ml of TBS-T three times. After removing unreacted primary antibody, the membrane was soaked with 10 ml of TBS-T containing 1.7 μl of secondary antibody for 1 h, then washed 3 times with 25 ml of TBS-T. Immunodetection was performed with an ECL immunoblotting kit (GE Healthcare).

3.2.6. Pull-down assays by GST affinity chromatography

SJW1103 cells transformed with pGEX-6p-1 (GST), pMMJ1001 (GST-FliJ) or pTIJ201 to pTIJ208 (GST-FliJ (Q38A, L42A, Y45A, Y49A, F72A, L76A, A79S and H83A)) were suspended in PBS (8 g of NaCl, 0.2 g of KCl, 3.63 g of $Na_2HPO_4 \cdot 12H_2O$, 0.24 g of KH_2PO_4, pH 7.4 per liter) and sonicated. After the centrifugation of cell lysates to remove undisrupted cells and insoluble membrane fractions, the soluble fractions were loaded onto a glutathione sepharose 4B column (GE Healthcare). After extensively washing the column with PBS, proteins were eluted with 50 mM Tris-HCl, pH 8.0, 10 mM reduced glutathione. Fractions containing GST, GST-FliJ, or GST-FliJ point mutation variants were indentified by SDS-PAGE and immnoblotting.

For co-purification of His-$FlhA_C$ with GST, GST-FliJ or GST-FliJ point mutation variants, The soluble fractions prepared from BL21(DE3)pLysS cells expressing GST, GST-FliJ or GST-FliJ point mutation variants were mixed with those from BL21(DE3)pLysS cells transformed with pMM102 (His-$FlhA_C$) and then the mixtures were loaded onto a GST column. After washing with PBS, bound proteins were eluted.

3.2.7. Preparation and purification of $FlhA_C$

A 30 ml overnight culture of BL21(DE3)pLysS carrying pMM102 (Minamino and Macnab, 1999), which encodes $FlhA_C$ with an N-terminal deca-histidine (His-$FlhA_C$) on pTrc99A (GE Healthcare), was inoculated into 1 l LB medium containing 50 μg/ml ampicillin and 30 μg/ml chloramphenicol. Cells were grown at 303 K until the culture density reached an OD_{600} of 0.6. The expression of His-$FlhA_C$ was induced with IPTG at a final concentration of 0.5 mM. Overnight culture was centrifuged (6400*g*, 10 min, 277 K) and the cells were stored at 193 K. The cells were thawed, suspended in the binding buffer (50 mM Tris-HCl pH 8.0, 500 mM NaCl, 50 mM imidazole) with a tablet of the Complete protease-inhibitor cocktail, and sonicated. After centrifugation (19000*g*, 20 min, 277 K), the supernatant was loaded onto a HiTrap chelating column (GE Healthcare) equilibrated with the binding buffer. Proteins were eluted using a linear gradient of imidazole. Fractions containing His-$FlhA_C$ applied to a HiLoad Superdex 75 (26/60) column (GE Healthcare) in 50 mM Tris-HCl pH 8.0, 150 mM NaCl. The purity of the product was examined by SDS-PAGE and MALDI-TOF mass spectrometry (Voyager DE/PRO, Applied Biosystems).

3.2.8. ATPase activity measurement of FliI

The ATPase activity was measured with an enzyme-coupled assay as described in 2.2.9. The reaction was started by the addition of FliI or the mixtures of FliI and FliJ, FliI and $FlhA_C$, FliI and FliJ and $FlhA_C$ at the molor ratios of 6:1, 6:1 and 6:1:1, respectively.

Table 3-1. Strains and plasmids used in this study of this chapter

Strains or Plasmids	Relevant properties	Source or ref.
E.coli		
BL21(DE3)pLysS	Host for overexpression from the T7 promoter	Novegen
Salmonella		
SJW1103	Wild-type for motility and chemotaxis	(Yamaguchi *et al*., 1984)
MKM40	Δ*fliJ*	(Minamino and Namba, In preparation)
MMHIJ0117	Δ*fliH-fliI-fliJ*, *flhB*(P28T)	(Minamino and Namba, In preparation)
Plasmids		
pET15b	Expression vector	Novegen
pGEX6p-1	Expression vector	GE Healthcare
pTrc99A	Expression vector	GE Healthcare
pTrc99AFF4	Modified trc expression vector	(Ohnishi *et al*., 1994)
pMMIJ001	pET15b/His-FliJ	(Ibuki *et al*., 2009)
pTIJ003	pET15b/His-FliJ(Q38A)	This study
pTIJ004	pET15b/His-FliJ(L42A)	This study
pTIJ005	pET15b/His-FliJ(Y45A)	This study
pTIJ006	pET15b/His-FliJ(Y49A)	This study
pTIJ007	pET15b/His-FliJ(F72A)	This study
pTIJ008	pET15b/His-FliJ(L76A)	This study
pTIJ009	pET15b/His-FliJ(A79S)	This study
pTIJ010	pET15b/His-FliJ(H83A)	This study
pMM404	pTrc99AFF4/FliJ	(Minamino *et al*., 2000)
pTIJ101	pTrc99AFF4/FliJ(Q38A)	This study
pTIJ102	pTrc99AFF4/FliJ(L42A)	This study
pTIJ103	pTrc99AFF4/FliJ(Y45A)	This study
pTIJ104	pTrc99AFF4/FliJ(Y49A)	This study
pTIJ105	pTrc99AFF4/FliJ(F72A)	This study
pTIJ106	pTrc99AFF4/FliJ(L76A)	This study

pTIJ107	pTrc99AFF4/FliJ(A79S)	This study
pTIJ108	pTrc99AFF4/FliJ(H83A)	This study
pMMJ1001	pGEX6p-1/GST-FliJ	(Minamino *et al*., 2010)
pTIJ201	pGEX6p-1/GST-FliJ(Q38A)	This study
pTIJ202	pGEX6p-1/GST-FliJ(L42A)	This study
pTIJ203	pGEX6p-1/GST-FliJ(Y45A)	This study
pTIJ204	pGEX6p-1/GST-FliJ(Y49A)	This study
pTIJ205	pGEX6p-1/GST-FliJ(F72A)	This study
pTIJ206	pGEX6p-1/GST-FliJ(L76A)	This study
pTIJ207	pGEX6p-1/GST-FliJ(A79S)	This study
pTIJ208	pGEX6p-1/GST-FliJ(H83A)	This study
pMM102	pTrc99A/His-FlhAc	(Minamino and Macnab, 1999)

Table 3-2. Primers used in this study of this chapter

Primer		sequence
PIJ005	-Q38A-Fw	cgcggctgccaacaggcggaagaagcgctcaaaatgctgatcgattatcag
PIJ006	-Q38A-Rv	ctgataatcgatcagcattttgagcgcttcttccgcctgttggcagccgcg
PIJ007	-L42A-Fw	caggcggaagaacagctcaaaatggcgatcgattatcagaatgagtatcgc
PIJ008	-L42A-Rv	gcgatactcattctgataatcgatcgccattttgagctgttcttccgcctg
PIJ009	-Y45A-Fw	gaacagctcaaaatgctgatcgatgctcagaatgagtatcgcagtaatttg
PIJ010	-Y45A-Rv	caaattactgcgatactcattctgagcatcgatcagcattttgagctgttc
PIJ011	-Y49A-Fw	gatcgattatcagaatgaggctcgcagtaatttgaacaccg
PIJ012	-Y49A-Rv	cggtgttcaaattactgcgagcctcattctgataatcgatc
PIJ013	-F72A-Fw	cgctggatcaactatcagcaggctattcagacactggaaaaggcg
PIJ014	-F72A-Rv	cgccttttccagtgtctgaatagcctgctgatagttgatccagcg
PIJ015	-L76A-Fw	ctatcagcagtttattcagacagcggaaaaggcgatagagcagcatc
PIJ016	-L76A-Rv	gatgctgctctatcgccttttccgctgtctgaataaactgctgatag
PIJ017	-A79S-Fw	gtttattcagacactggaaaagtcgatagagcagcatcgcctccagc
PIJ018	-A79S-Rv	gctggaggcgatgctgctctatcgacttttccagtgtctgaataaac
PIJ019	-H83A-Fw	ctggaaaaggcgatagagcaggctcgcctccagcttacgcagtgg
PIJ020	-H83A-Rv	ccactgcgtaagctggaggcgagcctgctctatcgccttttccag

3.3. Result

3.3.1. Alanine scanning analysis of highly conserved residues of FliJ

To investigate the roles of highly conserved residues (Gln-38, Leu-42, Tyr-45, Tyr-49, Phe-72, Leu-76, Ala-79 and His-83) of FliJ on the flagellar protein export, I performed site-directed mutagenesis. Each residue was replaced with alanine except for Ala-79, which was replaced with threonine. The pTrc99AFF4-based plasmids encoding these FliJ point mutation variants were introduced into MKM40 (Δ*fliJ*), and the motility of the resulting transformants was examined on soft tryptone agar plates (Figure 3-1a). All mutants recovered the motility of the *fliJ* null mutant at the wild-type level. Recently, the FliH-FliI complex is proposed to increase the mutational robustness of the export apparatus from an evolutional aspect (Hara *et al*., personal communication). Thus, the effect of FliJ mutations on the export process might have been concealed by the FliH-FliI complex. Therefore, I further analyzed the effect of the FliJ point mutations in the *ΔfliH-fliI-fliJ* bypass (Δ*fliH-I-J flhB*(P28T)) mutant cells. The plasmids were introduced into MMHIJ0117, and the motility of the resulting transformants was examined on soft tryptone agar plates (Figure 3-1b). Although the motility of Q38A and H83A mutants were complemented to the wild-type level, the remaining six mutants (L42A, Y45A, Y49A, F72A, L76A, A79S) markedly reduced their motility. Among them, the motility of L42A, Y45A and Y49A was considerably reduced to even less than the negative control level (V). These results show that the six highly conserved residues play some important roles in the export process.

Next, I examined the secretion of the filament protein FliC and the hook-capping protein FlgD from the FliJ mutant cells by immunoblotting. Expression level of FliJ mutant variants was also analyzed by immunoblotting (Figure 3-2c). The Q38A and H83A mutants secrete FliC at the wild-type level, but the secretion by the

other FliJ point mutant variants was at the negative control level (Figure 3-2a). These results are consistent with those of the motility assay. On the other hand, the secretion level of FlgD was significantly reduced only in two mutants (F72A and L76A) (Figure 3-2b). These results indicate that FliJ interacts with export substrates in different ways.

3.3.2. Dominant-negative effect of GST-FliJ mutants

Recently, it has been shown that GST-FliJ is non-functional and exerts a strong dominant-negative effect on motility of wild-type cells, indicating that GST-FliJ albeit non-functional can be installed into the export gate. Pull-down assays showed that FlhA was co-purified with GST-FliJ but not with GST, indicating a specific interaction between FlhA and FliJ (Minamino and Namba, In preparation).

To analyze the negative dominance effect of GST-FliJ on the motility of the wild-type cells, I transformed *Salmonella* wild-type strain SJW1103 with the pGEX6p-1-based plasmids encoding FliJ point mutation variants and analyzed the motility of the transformants on soft agar plate (Figure 3-3). GST-FliJ(F72A) and GST-FliJ(L76A) did not inhibit wild-type motility, suggesting that these mutations suppress the interaction of FliJ with FlhA.

3.3.3. Interaction between FlhA and GST-FliJ mutants

To investigate whether Phe-72 and Leu-76 of FliJ are involved in the interaction with FlhA, I carried out pull-down assay using GST affinity chromatography. The F72A and L76A mutations abolished the interaction between GST-FliJ and FlhA, while the others demonstrated no effect (Figure 3-4), indicating that Phe-72 and Leu-76 are critical for binding to FlhA. These results also suggest that the interaction between FliJ and FlhA is important for the secretion of FlgD.

3.3.4. Interaction between $FlhA_C$ and GST-FliJ mutants (F72A and L76A)

FliJ is known to form a complex with $FlhA_C$ (Minamino *et al*., 2010). To investigate whether Phe-72 and Leu-76 of FliJ are involved in the interaction with $FlhA_C$, I carried out pull-down assays using GST affinity chromatography. Whereas the interaction of GST-FliJ (L76A) with His-$FlhA_C$ was detected at the wild-type level, the F72A mutant variant lost the interaction with His-$FlhA_C$ (Figure 3-5). This result indicates that Phe-72 is involved in the interaction between FliJ and $FlhA_C$ but that Leu-76 is involved in the interaction with the other portion of FlhA.

3.3.5. $FlhA_C$ activates the ATPase activity of the $FliI_6FliJ$ complex

$FlhA_C$ is thought to form a part of the platform of the export gate with the C-terminal cytoplasmic region of FlhB and interact with all the soluble components of the export apparatus (Minamino and Macnab, 2000a). So I examined whether $FlhA_C$ influences the ATPase activity of FliI. The ATPase activity of FliI was not affected by the addition of $FlhA_C$ alone. However, the ATPase activity increased in the presence of FliJ and $FlhA_C$ by about seven fold compared to that of FliI alone (Figure 3-6). The addition of FliJ alone increased the ATPase activity by only four fold. These results indicate that $FlhA_C$ accelerates the ATPase activity of FliI through the interaction with FliJ.

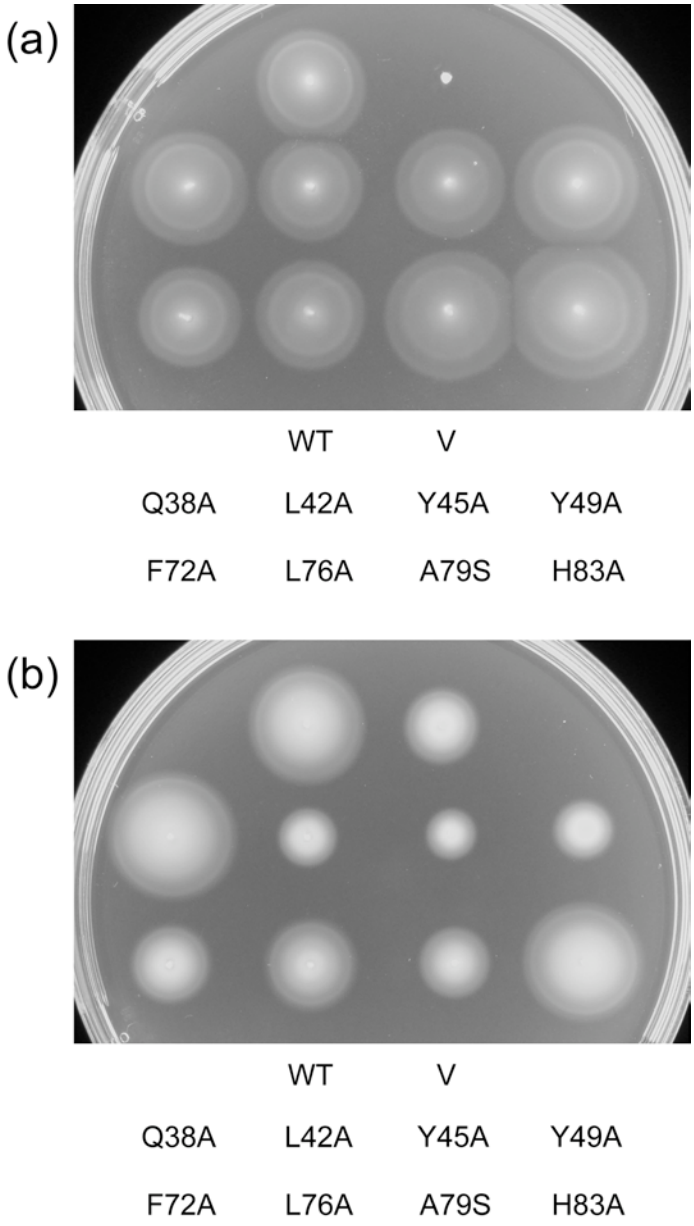

Figure 3-1. Swarming motility assay. Motility assays of (a) *ΔfliJ* strain MKM40 and (b) *ΔfliH-fliI-fliJ* bypass (Δ*fliH-I-J flhB*(P28T)) mutant strain MMHIJ0117 harboring various plasmids for mutant FliJ proteins on soft agar plates. MKM40 and MMHIJ0117 transformed with pMM404 (WT of FliJ) were inoculated as the positive control. MKM40 and MMHIJ0117 transformed with pTrc99AFF4 were inoculated as the negative control. MKM40 and MMHIJ0117 were transformed with the following plasmids: pTIJ101 (Q38A mutant of FliJ), pTIJ102 (L42A), pTIJ103 (Y45A), pTIJ104 (Y49A), pTIJ105 (F72A), pTIJ106 (L76A), pTIJ107 (A79S) and pTIJ108 (H83A). The plates were incubated at 303 K for (a) 8 hours and (b) 12 hours.

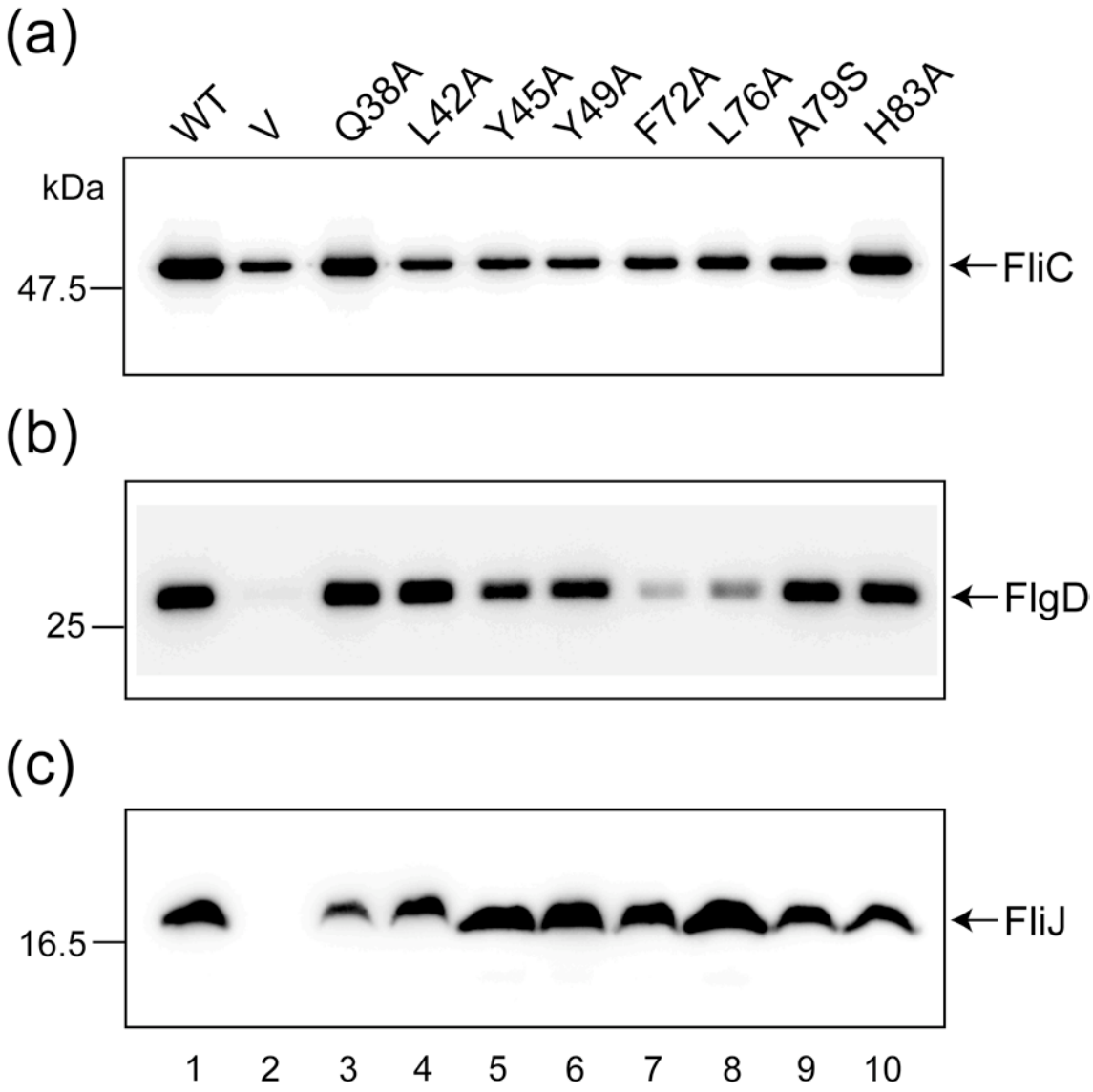

Figure 3-2. Export property of FliJ mutants. Secretion analysis of (a) FliC and (b) FlgD. Culture supernatant from the MMHIJ0117 strains transformed with pTIJ101 (Q38A mutant of FliJ), pTIJ102 (L42A), pTIJ103 (Y45A), pTIJ104 (Y49A), pTIJ105 (F72A), pTIJ106 (L76A), pTIJ107 (A79S) and pTIJ108 (H83A) were examined by using the polyclonal anti-FliC and anti-FlgD antibodies. (c) Expression level of the above FliJ mutant proteins in cells by using the polyclonal anti-FliJ antibody

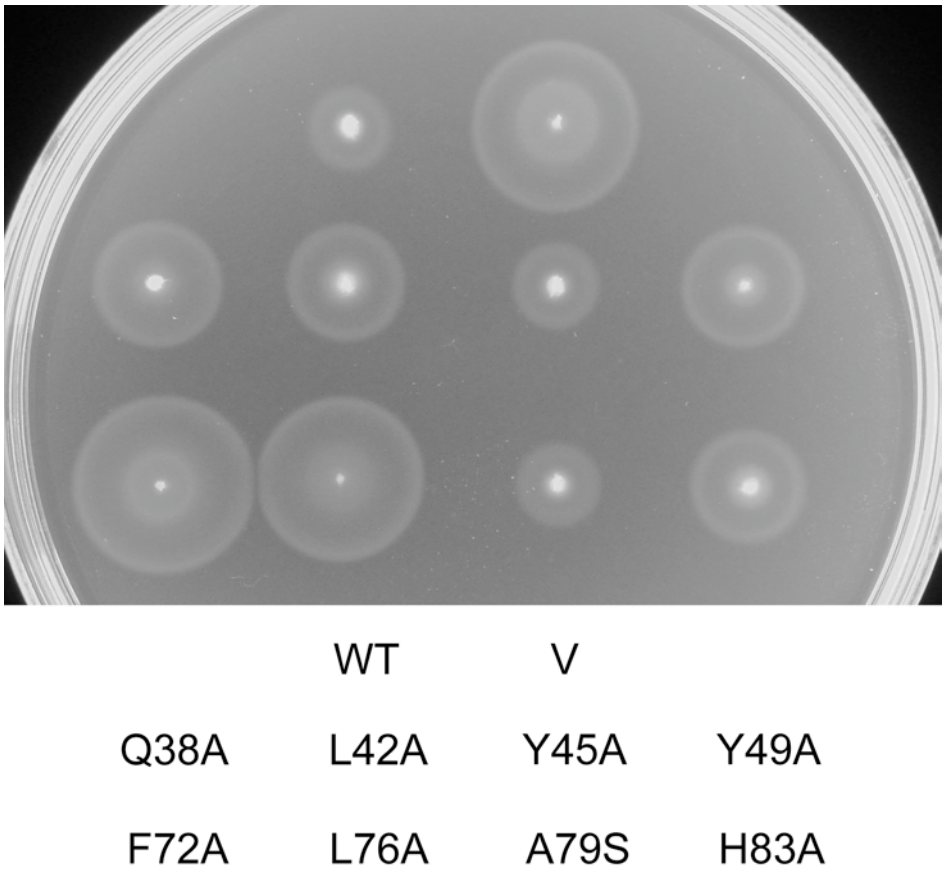

Figure 3-3. Negative-dominance effects of GST-FliJ mutants on wild-type motility. Dominance effects on the motility of the wild-type strain SJW1103 transformed with pGEX6p-1-based plasmids, pTIJ201 (Q38A mutant of GST-FliJ), pTIJ202 (L42A), pTIJ203 (Y45A), pTIJ204 (Y49A), pTIJ205 (F72A), pTIJ206 (L76A), pTIJ207 (A79S) and pTIJ208 (H83A), on soft agar plate.

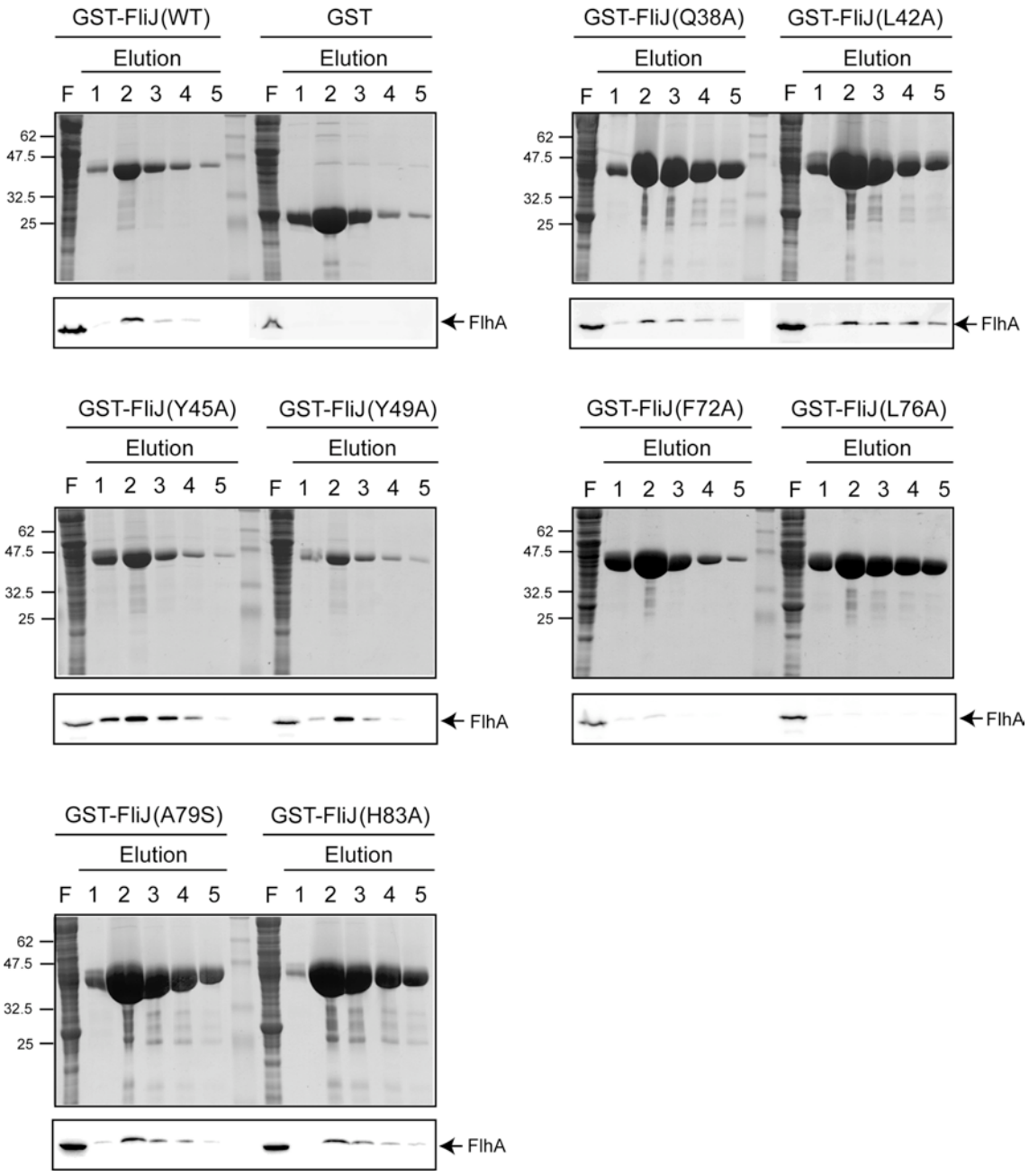

Figure 3-4. Interaction of FliJ with FlhA. The soluble fractions from the wild-type strain SJW1103 overproducing GST, GST-FliJ or GST-FliJ mutants were loaded onto a GST column. After washing, proteins were eluted with a buffer containing 10 mM reduced glutathione. The eluted factions of GST or GST-FliJ were analyzed by CBB staining (upper panels). The eluted FlhA protein was analyzed by immunoblotting with the polyclonal anti-FlhA antibody (lower panels).

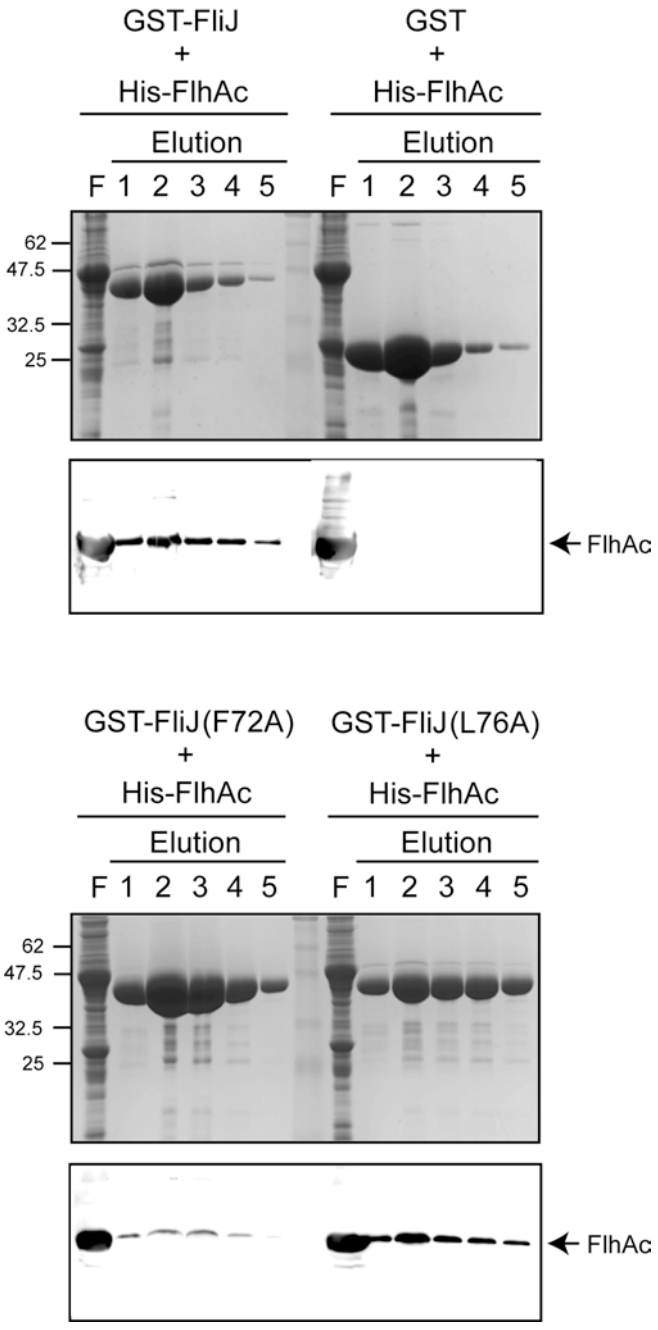

Figure 3-5. Interaction of FliJ with $FlhA_C$. The mixture of the soluble fractions prepared from BL21(DE3)pLysS strains expressing, GST-FliJ (upper left panels), GST (upper right panels), GST-FliJ(F72A) (lower left panels) and GST-FliJ(L76A) (lower right panels) with those from a BL21(DE3)pLysS strain producing His-$FlhA_C$ were loaded onto a GST column. After extensive washing, proteins were eluted with a buffer containing 10 mM reduced glutathione. The eluted fractions were analyzed by both CBB staining and immunoblotting with the polyclonal anti-FlhA antibody.

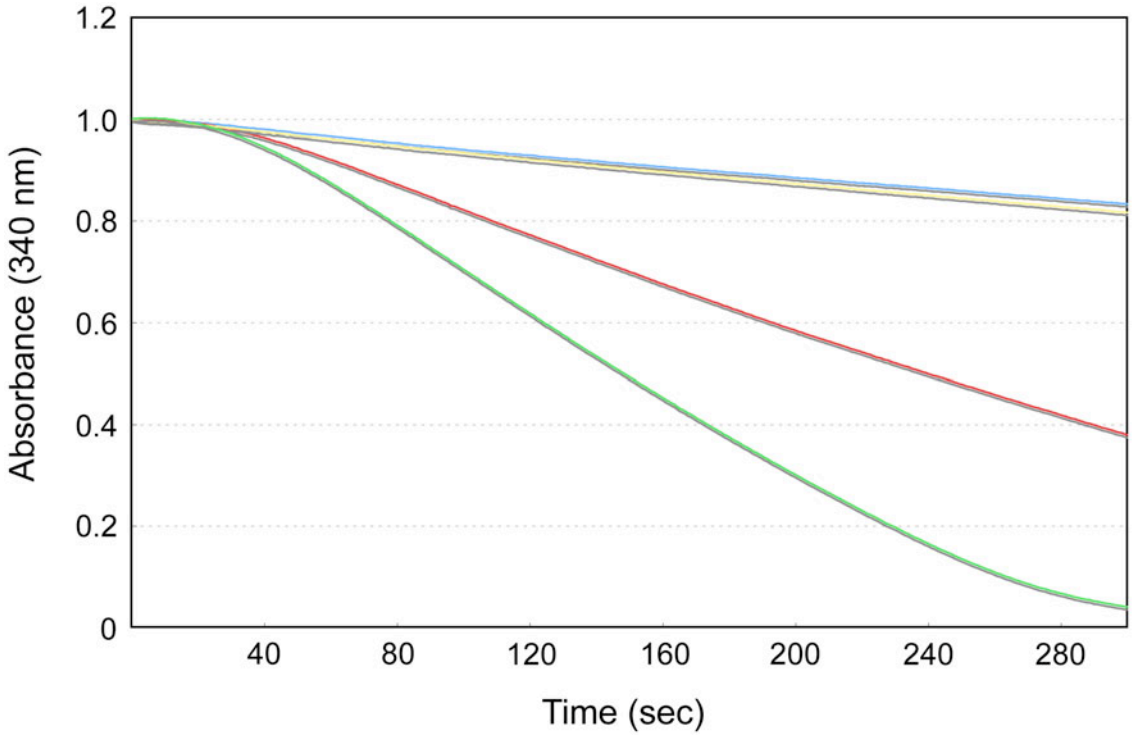

Figure 3-6. FliI ATPase activity measurement in the presence of FliJ and $FlhA_C$. ATP hydrolysis was monitered at 310 K in the presence of an ATP regenerating system. The reactions were started by the addition of 100 μl of 340 μg/ml FliI (blue line), the mixture of FliI and FliJ at the molar ratio of 6:1 (red line), the mixture of FliI and $FlhA_C$ at the molar ratio of 6:1 (yellow line), or the mixture of FliI, FliJ and $FlhA_C$ at the molar ratio of 6:1:1 (green line) to 1.0 ml of the reaction mixture.

3.4. Discussion

3.4.1. The FliH-FliI complex overcomes the FliJ defects

The highly conserved eight residues of FliJ (Figure 1-9b) might function directly in protein export process. To prove the importance of the conserved residues of FliJ, I carried out alanine scanning mutagenesis (Figure 3-1). Whereas many of these mutations did not impair the export function in the presence of FliH and FliI (Figure 3-1a), many of them abolished the motility in the absence of FliH and FliI (Figure 3-1b). It has been proposed recently that the FliH-FliI complex brings about a specific association between FliJ and FlhA (Minamino and Namba, In preparetion) and increases the mutational robustness of the export apparatus from an evolutional aspect (Hara *et al*., personal communication). From these results, it is thought that the FliH-FliI complex somehow conceals the effects of FliJ mutations on the export process. The present result also indicates that the FliH-FliI complex helps FliJ binds to FlhA.

3.4.2. Interaction between FliJ and FlhA

The highly conserved eight residues of FliJ (Gln-38, Leu-42, Tyr-45, Tyr-49, Phe-72, Leu-76, Ala-79 and His-83) correspond to the residues of the γ-subunit exposed on the outside of the F_1-α/β ring structure and interacting with the ε-subunit in F_1-ATPase (Figure 1-9b). The results of my study described in this chapter show that two residues, Phe-72 and Leu-76, on the conserved surface of FliJ interact with FlhA. FlhA is the largest integral membrane component of the flagellar protein export apparatus and is composed of an N-terminal transmembrane domain ($FlhA_{TM}$) and a C-terminal cytoplasmic domain ($FlhA_C$). $FlhA_C$ is thought to form a part of the platform of the export gate that the soluble components bind to. The interaction of GST-FliJ with $FlhA_C$ is not very strong but is much stronger with FlhA, indicating that $FlhA_{TM}$ is also

involved in the binding of FliJ. In other words, FliJ has at least two binding sites for FlhA, one for $FlhA_C$ and the other for $FlhA_{TM}$. In fact, the F72A mutation of FliJ abolishes the interaction with both FlhA and $FlhA_C$, but the L76A mutation abolishes it only with FlhA. Therefore, Phe-72 is responsible for the ineraction with $FlhA_C$, and Leu-76 with $FlhA_{TM}$.

Interestingly, other mutations (L42A, Y45A, Y49A and A79S) significantly reduced *ΔfliH-fliI* bypass mutant motility, but they retain the binding ability to FlhA to the wild type GST-FliJ level. Recently, the crystal structure of $FlhA_C$ at 2.8 Å resolution has been reported (Saijo-Hamano *et al.*, 2010). $FlhA_C$ consists of four subdomains (A_CD1, A_CD2, A_CD3 and A_CD4) and a linker connecting $FlhA_C$ to $FlhA_{TM}$ (Figure 3-7). Together with the genetic, biochemical and MD simulation studies, dynamic conformational change of $FlhA_C$ is expected in the export process (Saijo-Hamano *et al.*, 2010). The four residues (Leu-42, Tyr-45, Tyr-49 and Ala-79) might be important for the proper conformational change of $FlhA_C$.

$FlhA_C$ interacts with FliI and FliJ (Minamino *et al.*, 2010) and activates the ATPase activity of FliI only in the presence of FliJ. These results suggest that the ATPase activity becomes much higher when the $FliI_6FliJ$ complex docks onto the FlhA-FlhB platform. Thus, the ATP hydrolysis reaction in the export process appears to be well regulated through the dynamic interactions between the components of the export apparatus.

3.4.3. Role of the interaction between FliJ and FlhA in protein export.

To examine the effect of FliJ mutations on the export process, I analyzed the secretion levels of the filament protein FliC and hook-capping protein FlgD from the MMHIJ0117 strains transformed with FliJ mutants. Although the secretion level of FliC

decreased in all mutants that reduced their motility (Figure 3-2a), that of FlgD was significantly reduced only in two mutants (F72A and L76A) (Figure 3-2b). These results indicate that FliJ interacts with each export substrate in a different way or that the export of FlgD depends on the FliJ-FlhA interaction more strongly than that of FliC. FlgD belongs to the rod/hook-type export class, and FliC to the filament-type. It is possible that somewhat different mechanisms might be used for the export of rod/hook-type and filament-type substrates. To examine such differece further, I will measure the secretion level of other rod/hook-type and filament-type export substrates in the near future.

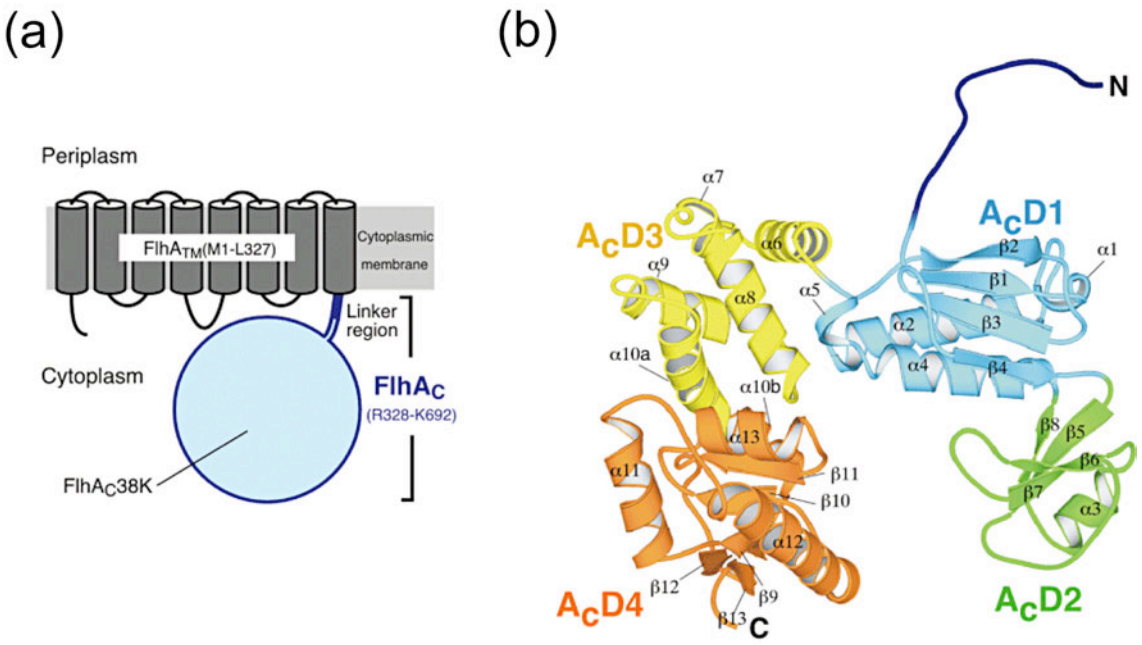

Figure 3-7. Crystal structure of FlhA$_C$. (a) Domain organization of FlhA. The region that corresponds to the atomic model is colored in light blue. (b) Cα ribbon diagram of FlhA$_C$. The linker region and the four domains are colored: dark blue, the linker; cyan, A$_C$D1; green, A$_C$D2; yellow, A$_C$D3; orange, A$_C$D4 (Saijo-Hamano *et al.*, 2010).

Chapter 4
Conclusion

Some of the components of the flagellar type III protein export apparatus are known to show amino acid sequence similarities with the F_oF_1-ATP synthase proteins. The flagellar specific ATPase FliI has marked structural/sequential similarities with the α/β-subunits of F_1-ATPase (Imada *et al*., 2006). The N-terminal and C-terminal regions of FliH have sequential similarities with the b- and δ-subunits of F_oF_1-ATP synthase (Pallen *et al*., 2006), respectively. On the contrary, FliJ has no apparent sequence similarity with any components of F_oF_1-ATP synthase. Although FliJ is known to interact with many flagellar proteins involved in protein export, its function is still obscure. In this study, I determined the crystal structure of FliJ at 2.1 Å resolution. FliJ shows a remarkable structural similarity with the γ-subunit of F_1-ATPase. Structure based sequence alignment between FliJ and the γ-subunit reveals a conserved surface that was not identified by the sequence analysis alone.

The structural similarities between FliJ and the γ-subunit and between FliI and the α/β-subunits suggested that FliJ and FliI form a complex similar to F_1-ATPase. I therefore analyzed the interaction between FliJ and FliI by electron microscopy and biochemical techniques. I found that FliJ and FliI form the $FliI_6FliJ$ complex, just like the F_1-$\alpha_3\beta_3\gamma$ complex. Moreover, the addition of FliJ to FliI facilitated the ring formation of FliI and increased its ATPase activity.

The structural similarity between the two systems suggest the functional similarity between FliJ and the γ-subunit. Stepwise rotation of the γ-subunit is coupled with conformational changes of the α/β-subunits that lead to sequential ATP hydrolysis at the three catalytic sites. Similarly, FliJ may rotate within the FliI ring for sequential ATP hydrolysis, although the role of FliJ rotation in protein export is not at all clear.

The homologous region between FliJ and the γ-subunit corresponds to the surface of the γ-subunit interacting with the ε-subunit of F_1-ATPase, suggesting that FliJ may have a binding partner corresponding to the ε subunit. To examine the functions of conserved residues in this region of FliJ, I selected eight highly conserved and surface-exposed residues and performed site-directed mutagenesis. I found that the conserved residues interact with FlhA. Phe-72 and Leu-76 are essential for the interaction with FlhA: Phe-72 with $FlhA_C$, and Leu-76 with $FlhA_{TM}$. Interstingly, FlhAc activates the ATPase activity of FliI through the interaction with FliJ. These results suggest that the $FliI_6FliJ$ complex docks onto the FlhA-FlhB platform of the export gate via the interaction between FliJ and FlhA to facilitate the initial insertion of export substrate into the gate.

Although I have shown the structural similarities between the $FliI_6FliJ$ complex and F_1-ATPase, the functions of the two systems are distinct. How does the export process proceed by the mechanism similar to F_1-ATPase? It has been suggested that export substrates are transferred to the export gate through the central hole of the FliI hexameric ring structure. However, I have also shown that FliJ penetrates into the central hole of the FliI ring in a similar manner to the γ subunit of F_1-ATPase. It appears to be difficult for export substrate to pass through the central hole. Then, how could the substrates be transported to the gate? Evans *et al*. have shown by genetic and

biochemical study that FliJ binds to FlgN and FliT, which are flagellar specific chaperones. The binding regions of FliJ for these two molecules are exposed on the outside of the FliI ring in the model of the $FliI_6FliJ$ complex (Figure 1-7). These results imply that export substrates might bind to the $FliI_6FliJ$ complex via flagellar specific chaperones such as FliT and FlgN and might be directly inserted to the export gate, just as shown in Figure 4-1.

Based on available information, I propose the following mechanism for flagellar protein export (Figure 4-1a). First, the $FliH_2FliI$-FliJ-substrate complex is formed in the cytoplasm, probably from a $FliH_2FliI$ complex and a FliJ-export substrate complex. The $FliH_2FliI$-FliJ-substrate complex binds to FliN of the C-ring to increase the local concentration of the complex to dock to the FlhA-FlhB platform efficiently (Minamino *et al.*, 2008). FliJ interacts with FliM of the C-ring, releasing the $FliH_2FliI$-FliJ-substrate complex from the C-ring to promote the docking of this complex to the FlhA-FlhB platform (Figure 4-1b). Upon this docking, the $FliH_xFliI_6$-FliJ-substrate complex forms on the platform via the interactions between FliJ and FlhA (Figure 4-1c), and the FliI ATPase is activated. Recently, it has been shown that proton motive force across the cell membrane is essential for flagellar protein export (Minamino and Namba, 2008; Paul *et al.*, 2008). The energy of ATP hydrolysis by FliI seems to be used to dissociate the $FliH_xFliI_6$-FliJ complex from the export gate and the substrate being translocated into the gate (Minamino and Namba, 2008). The export gate drives the successive unfolding/translocation of partially folded export substrates by the energy of proton motive force, although the mechanism of energy conversion is completely unknown. In this study, I have shown that FliJ and FliI form the $FliI_6FliJ$ complex, like the F_1-$\alpha_3\beta_3\gamma$ complex. It is therefore conceivable that the energy of ATP hydrolysis by FliI is converted into the mechanical motion of FliJ,

such as rotation or conformational change just like that of the γ-subunit in the F_1-$\alpha_3\beta_3\gamma$ complex. Moreover, the latest, unpublished study shows that the FliJ-FlhA interaction is required for efficient inward-directed proton influx (Minamino and Namba, personal communication). So, it would be possible that the conformational change of FliJ by the energy of ATP hydrolysis by FliI is transmitted to FlhA and somehow opens the proton channel of the export gate (Figure 4-1d). As a result, proton motive force drives the successive unfolding and translocation of the long polypeptide chain through the narrow pore of the export gate. The process must be a one-dimensional Brownian motion of the polypeptide chain biased by proton motive force. The ATP hydrolysis and/or the conformational change of FliJ induce the dissociation of the $FliH_xFliI_6$-FliJ complex from the gate (Figure 4-1e). To see the validity of this model of flagellar protein export mechanism, high-resolution structural information of the entire export apparatus including the transmembrane gate is essential. Together with furhter biochemical and genetic analyses, I would like to advance my study toward the comprehensive understanding of this highly sophisticated, dynamic and complex system.

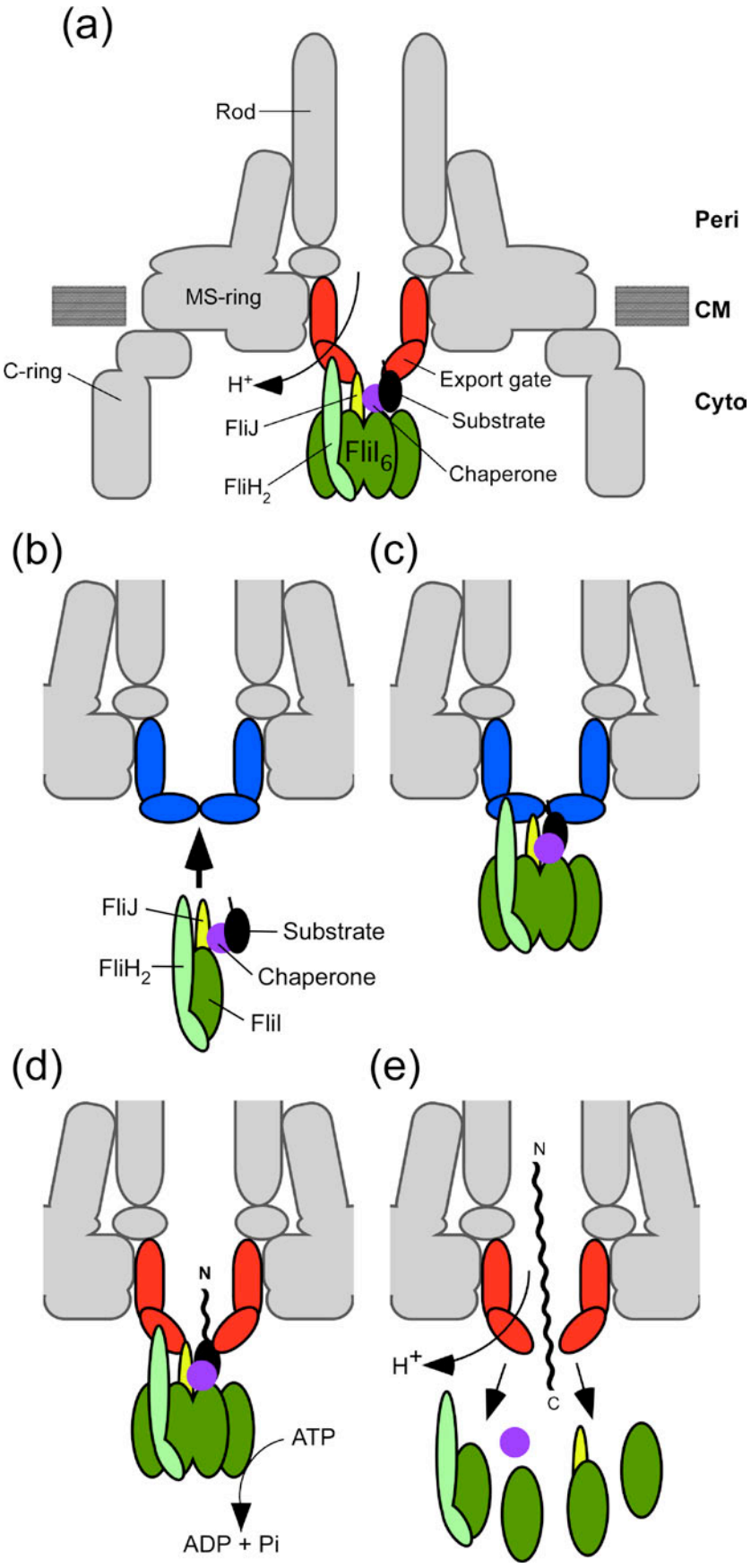
(a)
Rod
Peri
MS-ring
CM
C-ring
H+
Export gate
Cyto
FliJ
Substrate
FliI6
Chaperone
FliH2
(b)
(c)
FliJ
Substrate
FliH2
Chaperone
FliI
(d)
(e)
N
N
H+
C
ATP
ADP + Pi

Figure 4-1. Model for flagellar protein export. (a) The flagellar protein export apparatus in the basal body. (b) The $FliH_2FliI$ complex delivers the export substrates-specific chaperone complex to the export gate along with FliJ. (c) The $FliH_xFliI_6$-FliJ-substrate complex forms on the FlhA-FlhB platform via the interactions between FliJ and FlhA. (d) The conformational change of FliJ by the energy of ATP hydrolysis of FliI is transmitted to FlhA and opens the proton channel somewhere in the export gate. (e) The ATP hydrolysis or the conformational change of FliJ induces the dissociation of the $FliH_xFliI_6$-FliJ complex from the gate. Pi, inorganic phosphate.

Acknowledgement

This study has been carried out in the Protonic NanoMachine Laboratory, Graduate School of Frontier Biosciences, Osaka University.

I would like to express my sincere gratitude to my supervisor, Prof. Keiichi Namba and Associate Prof. Katsumi Imada for incessant guidance, discussion and encouragement throughout my Ph.D work. I wish to express my sincere thanks to Prof. Hiroyuki Noji, Prof. Atsushi Nakagawa and Prof. Katsuyuki Tanizawa in Osaka University for evaluating this work.

I am deeply grateful to Assistant Prof. Tohru Minamino for teaching me a lot of techniques of biochemical and genetic experiment, discussion and encouragement. I am grateful to Assistant Prof. Takayuki Kato and Dr. Tomoko Miyata for teaching me a lot of techniques of electron microscopy, discussion and encouragement. I am also indebt to Dr. Masafumi Shimada and Dr. Ken-ichi Kazetani who gave me guidance, invaluable comments and warm encouragements.

I am also grateful to Dr. Nobutaka Shimizu and Dr. Masahide Kawamoto at SPring-8, Japan Synchrotron Radiation Research Institute (JASRI) for technical help of the data collection in the use of beamline BL41XU.

I cannot find any words to express my sincere gratitude to all the members of the Protonic NanoMachine Laboratory, including its former members, for a lot of technical help, extensive discussion and continuous encouragement.

In closing, I thank my parents, Toshio and Naomi Ibuki and my sisters for their heartwarming encouragement and support.

September, 2010 Tatsuya Ibuki

Reference

Abrahams, J.P., Leslie, A.G.W., Lutter, R. and Walker J.E. (1994) Structure at 2.8 Å resolution of F1-ATPase from bovine heart mitochondria. *Nature* **370**, 621-628.

Auvray, F., Ozin, A.J., Claret, L. and Hughes, C. (2002). Intrinsic membrane targeting of the flagellar export ATPase FliI: interaction with acidic phospholipids and FliH. *J. Mol. Biol.* **318**, 941–950.

Berg, H.C. (2003) The rotary motor of bacterial flagella. *Annu. Rev. Biochem.* **72**, 19-54.

Berg, H.C. and Anderson, R.A. (1973) Bacteria swim by rotating their flagellar filaments. *Nature*. **245**, 380-382.

Brünger, A.T. *et al*. (1998) Crystallography and NMR system: a new software suite for macromolecular structure determination. *Acta Crystallogr.* **D54**, 905-921.

Cheayen, N.E. (1997) The role of oil in macromolecular crystallization. *Structure* **5**, 1269-1274.

Claret, L., Susannah, C.R., Higgins, M. and Hughes, C. (2003) Oligomerization and activation of the FliI ATPase central to bacterial flagellum assembly. *Mol. Microbiol*. **48**, 1349-1355.

Collaborative Computational Project, Number 4 (1994) The CCP4 suite: programs for protein crystallography. *Acta Cryst.* **D50**, 760-763.

DePamphilis, M.L. and Adler, J. (1971a) Purification of intact flagella from *Escherichia coli* and *Bacillus subtilis*. *J Bacteriol.* **105**, 376-383.

DePamphilis, M.L. and Adler, J. (1971b) Fine structure and isolation of the hook-basal

body complex of flagella from *Escherichia coli* and *Bacillus subtilis*. *J Bacteriol.* **105**, 384-395.

Dunn, S.D., McLachlin, D.T. and Revington, M. (2000) The second stalk of Escherichia coli ATP synthase. *Biochem Biophys Acta.* **1458**, 356-63.

Emsley, P. Lohkamp, B. Scott, W.G. and Cowtan, K. (2010) Features and development of *Coot*. *Acta Crystallogr.* **D66**, 486-501.

Evans, L.D.B., Stafford, G.P., Ahmed, S., Fraser, G.M. and Hughes, C. (2006) An escort mechanism for cycling of export chaperones during flagellum assembly. *Proc. Natl. Acad. Sci. U.S.A.* **103**, 17474-17479.

Fan, F. and Macnab, R.M.（1996）. Enzymatic characterization of FliI an ATPase involved in flagellar assembly in *Salmonella typhimurium*. *J. Biol. Chem.* **271**, 31981-31988.

Fraser, G.M., González-Pedrajo, B., Tame, J.H.R. and Macnab, R.M. (2003) Interaction of FliJ with the *salmonella* Type III Flagellar Export Apparatus. *J Bacteriol.* **185**, 5546-5554.

Gibbons, C., Montgomery, M.G., Leslie, A.G. and Walker, J.E. (2000) The structure of the central stalk in bovine F_1-ATPase at 2.4 Å resolution. *Nat. Struct. Biol.* **7**, 1055-1061.

González-Pedrajo, B., Fraser, G.M., Minamino, T. and Macnab, R.M. (2002). Molecular dissection of Salmonella FliH, a regulator of the ATPase FliI and the type III flagellar protein export pathway. *Mol. Microbiol.* **45**, 967–982.

González-Pedrajo, B., Minamino, T., Kihara, M. & Namba, K. (2006) Interactions between C ring proteins and export apparatus components: a possible mechanism for facilitating type III protein export. *Mol. Microbiol.* **60**, 984-998.

Hirano, T., Yamaguchi, S., Oosawa, K. and Aizawa, S. (1994) Roles of FliK and FlhB in determination of flagellar hook length in *Salmonella typhimurium*. *J. Bacteriol*. **176**, 5439-5449.

Homma, M., Aizawa, S., Dean, G.E. and Macnab, R.M. (1987) Identification of the M-ring protein of the flagellar motor of *Salmonella typhimurium*. . *Proc. Natl Acad. Sci. U.S.A.* **82**, 7483-7487.

Ibuki, T., Shimada, M., Minamino, T., Namba, K. & Imada, K. (2009) Crystallization and preliminary X-ray analysis of FliJ, a cytoplasmic component of the flagellar type III protein-export apparatus from *Salmonella sp*. *Acta Crystallogr.* **F65**, 47-50.

Imada, K., Minamino, T., Kinoshita, M., Furukawa, Y. and Namba, K. (2010) Structural insight into the regulatory mechanisms of interactions of the flagellar type III chaperone FliT with its binding partners. *Proc. Natl Acad. Sci. U.S.A.* **107**, 8812-8817.

Imada, K., Minamino, T., Tahara, A. and Namba, K. (2007) Structural similarity between the flagellar type III ATPase FliI and F1-ATPase subunit. *Proc. Natl Acad. Sci. U.S.A.* **104**, 485-490.

Imai, Y., Matsushima, Y., Sugimura, T. and Terada, M. (1991) A simple and rapid method for generating a deletion by PCR. *Nucleic Acids Res.* **19**, 2785.

Jones, C.J., Homma, M. and Macnab, R.M. (1987) Identification of proteins of the outer (L and P) rings of the flagellar basal body of *Escherichia coli*. *J. Bacteriol*. **69**, 1489-1492.

Jones, C.J., Homma, M. and Macnab, R.M. (1989) L-, P-, and M-ring proteins of the flagellar basal body of *Salmonella typhimurium*: gene sequences and deduced protein sequences. *J. Bacteriol*. **171**, 3890-3900.

Kazetani, K., Minamino, T., Miyata, T., Kato, T. and Namba, K. (2009) ATP-induced FliI hexamerization facilitates bacterial flagellar protein export. *Biochem. Biophys. Res.*

Comm. **388**, 323-327.

Kubori, T., Shimamoto, N., Yamaguchi, S., Namba, K. and Aizawa, S. (1992) Morphological pathway of flagellar assembly in *Salmonella typhimurium*. *J. Mol. Biol.* **226**, 433-446.

Kutsukake, K. (1994) Excretion of the anti-sigma factor through a flagellar substructure couples flagellar gene expression with flagellar assembly in *Salmonella typhimurium*. *Mol. Gen. Genet*. **243**, 605-612.

Lane, M.C., O'Toole, P.W. and Moore, S.A. Molecular basis of the interaction between the flagellar export proteins FliI and FliH from *Helicobacter pylori*. *J. Biol. Chem.* **281**, 508-17.

Leslie, A.G.W. (2005) The integration of macromolecular diffraction data. *Acta Crystallogr. D Biol. Crystallogr.* **D62**, 48-57.

Ludtke, S.J., Baldwin, P.R. and Chiu, W. (1999) EMAN: Semiautomated software for high-resolution single-particle reconstructions. *J. Struct. Biol.* **128**, 82-97.

Ludtke, S.J. and Chiu, W. (2003) Focal pair merging for contrast enhancement of single praticles. *J. Struct. Biol.* **144**, 73-78.

Macnab, R.M. (2003) How bacteria assemble flagella. *Annu. Rev. Microbiol.* **57**, 77-100.

Macnab, R.M. (2004) Type III flagellar protein export and flagellar assembly. *Biochem. Biophys. Acta.* **1694**, 207-17.

McGuffin, L.J., Bryson, K. and Jones, D.T. (2000) The PSIPRED protein structure prediction server. *Bioinformatics* **16**, 404-405.

Minamino, T., González-Pedrajo, B., Kihara, M., Namba, K. and Macnab, R.M. (2003)

The ATPase FliI can interact with the type III flagellar protein export apparatus in the absence of its regulator, FliH. *J. Bacteriol.* **185**, 3983-3988.

Minamino, T., González-Pedrajo, B., Oosawa, K., Namba, K. and Macnab, R.M. (2002) Structural properties of FliH, an ATPase regulatory component of the Salmonella type III flagellar export apparatus. *J. Mol. Biol*. **322**, 281-290.

Minamino, T., Imada, K. and Namba, K. (2008) Molecular motors of the bacterial flagella. *Curr. Opin. Struct. Biol.* **18**, 693-701.

Minamino, T., Imada, K., Namba, K. (2008) Molecular motors of the bacterial flagella. *Curr. Opin. Struct. Biol.* **18**, 693-701.

Minamino, T., Kazetani, K., Tahara, A., Suzuki, H., Furukawa, Y., Kihara, M. and Namba, K. (2006) Oligomerization of the Bacterial Flagellar ATPase FliI is Controlled by its Extreme N-terminal Region. *J. Mol. Biol.* **360**, 510-519.

Minamino, T. and Macnab, R.M. (1999) Components of the Salmonella flagellar export apparatus and classification of export substrates. *J. Bacteriol.* **181**, 1388-1394.

Minamino, T. and Macnab, R.M. (2000a) FliH, a soluble component of the type III flagellar export apparatus of *Salmonella*, forms a complex with FliI and inhibits its ATPase activity. *Mol. Microbiol*. **37**, 1494-1503.

Minamino, T. and Macnab, R.M. (2000b). Interactions among components of the *Salmonella* flagellar export apparatus and its substrates. *Mol. Microbiol.* **35**, 1052-1064.

Minamino, T. and Namba, K. (2004) Self-assembly and type III protein export of the bacterial flagellum. *J. Mol. Micro. Biotechnol.* **7**, 5-17.

Minamino, T. and Namba, K. (2008) Distinct roles of the FliI ATPase and proton motive force in bacterial flagellar protein export. *Nature* **451**, 485-488.

Minamino, T. and Namba, K. Dual mechanism of bacterial flagellar protein export with and without proton coupling. submitted for publication.

Minamino, T., Ryan, C., Yamaguchi, S. and Macnab, R.M. (2000) Role of FliJ in Flagellar Protein Export in *salmonella*. *J. Bacteriol.* **182**, 4207-4215.

Minamino, T., Shimada, M., Okabe, M., Saijo-Hamano, Y., Imada, K., Kihara, M. and Namba, K. (2010) Role of the C-terminal cytoplasmic domain of FlhA in bacterial flagellar type III protein export. *J. Bacteriol*. **192**, 1929-1936.

Minamino, T., Tame, J.R., Namba, K. and Macnab, R.M. (2001) Proteolytic analysis of the FliH/FliI complex, the ATPase component of the type III flagellar export apparatus of Salmonella. *J. Mol. Biol*. **312**, 1027-1036.

Namba, K. and Vonderviszt, F. (1997) Molecular architecture of bacterial flagellum. *Quat. Rev. Biophys.* **30**, 1-65.

Nambu, T. and Kutsukake, K. (2000) The Salmonella FlgA protein, a putativeve periplasmic chaperone essential for flagellar P ring formation. *Microbiol*. **146**, 1171-1178.

Nambu, T., Minamino, T., Macnab, R.M. and Kutsukake, K. (1999) Peptidoglycan-hydrolyzing activity of the FlgJ protein, essential for flagellar rod formation in *Salmonella typhimurium*. *J. Bacteriol.* **181**, 1555-1561.

Noji, H., Yasuda, T., Yoshida, M. and Kinoshita K. (1997) Direct observation of the rotation of F_1-ATPase. *Nature* **386**, 299-302.

Numoto, N., Hasegawa, Y., Takeda, K. and Miki, K. (2009) Inter-subunit interaction and quaternary rearrangement defined by the central stalk of prokaryotic V1-ATPase. *EMBO Rep.* **10**, 1228-1234.

Ohnishi, K., Ohto, Y., Aizawa, S., Macnab, R.M. and Iino, T. (1994) FlgD is a scaffolding protein needed for flagellar hook assembly in *Salmonella typhimurium*. *J. Bacteriol.* **176**, 2272-2281.

Pallen, M.J. Bailey, C.M. and Beatson, S.A. (2006) Evolutionary links between FliH/YscL-like proteins from bacterial type III secretion systems and second-stalk components of the FoF1 and vacuolar ATPases. *Protein Sci*. **15**, 935-941.

Saijo-Hamano, Y., Imada, K., Minamino, T., Kihara, M., Shimada, M., Kitao, A. and Namba, K. (2010) Structure of the cytoplasmic domain of FlhA and implication for flagellar type III protein export. *Mol. Microbiol*. **76**, 260-8.

Schatz, P.J. and Beckwith, J. (1990) Genetic analysis of protein export in *Escherichia coli*. *Annu. Rev. Genet*. **24**, 215-48.

Schoenhals, G.J. and Macnab, R.M. (1996) Physiological and biochemical analyses of FlgH, a lipoprotein forming the outer membrane L ring of the flagellar basal body of Salmonella typhimurium. *J. Bacteriol*. **178**, 4200-4207.

Silverman, M. and Simon, M. (1974) Characterization of Escherichia coli flagellar mutants that are insensitive to catabolite repression. *J. Bacteriol*. **120**, 1196-203.

Terwilliger, T.C. and Berendzen, J. (1999) Automated MAD and MIR structure solution. *Acta Crystallogr. D Biol. Crystallogr.* **D55,** 849-861.

Yamaguchi, S., Fujita, H., Ishihara, A., Aizawa, S. and Macnab, R.M. (1986) Subdivision of flagellar genes of Salmonella typhimurium into regions responsible for assembly, rotation, and switching. *J. Bacteriol*. **166**, 187-93.

Yoshida, M., Muneyuki, E. and Hisabori, T. (2001) ATPsynthase - a marvelous rotary engine of the cell. *Nat. Rev. Mol. Cell. Biol.* **2**, 669-677.

Publication

Original paper

Tatsuya Ibuki, Masafumi Shimada, Tohru Minamino, Keiichi Namba, Katsumi Imada. (2009) Crystallization and preliminary X-ray analysis of FliJ, a cytoplasmic component of the flagellar type III protein export apparatus from *Salmonella. Acta Crytallogra.* **F65**, 47-50.

Tatsuya Ibuki, Katsumi Imada, Tohru Minamino, Takayuki Kato, Tomoko Miyata and Keiichi Namba (2010) Common architecture between the flagellar type III protein export apparatus and F- and V-type ATPases. 投稿中

Conferrence

Poster presentation

○Tatsuya Ibuki, Masafumi Shimada, Tohru Minamino, Katsumi Imada, Keiichi Namba.「Characterization and crystallization of FliJ, a cytoplasmic component of the flagellar type III protein export apparatus of *Salmonella*.」第 45 回日本生物物理学会年会, ポスター番号 2P183, パシフィコ横浜, Dec. 21-23, 2007.

○伊吹達也, 島田賢史, 南野徹, 今田勝巳, 難波啓一「サルモネラ菌べん毛タイプIII輸送装置構成蛋白質FliJの性質とX線結晶構造解析」第14回べん毛研究交流会, ポスター番号P8, 関西セミナーハウス, Mar. 3-5, 2008.

○伊吹達也, 島田賢史, 南野徹, 今田勝巳, 難波啓一「Characterization and X-ray analysis of FliJ, a cytoplasmic component of the flagellar type Ⅲ protein export apparatus of *Salmonella*.」第8回日本蛋白質科学会年会, ポスター番号2P011, タワーホール船堀, Jun. 10-12, 2008.

○伊吹達也, 島田賢史, 南野徹, 今田勝巳, 難波啓一「Characterization and X-ray analysis of FliJ, a cytoplasmic component of the flagellar type Ⅲ protein export apparatus of *Salmonella*.」特定領域研究「生体超分子の構造形成と機能制御の原子

機構」第4回ワークショップ, ポスター番号25, 兵庫県立 淡路夢舞台国際会議場, Jun. 16-18, 2008.

○伊吹達也, 島田賢史, 南野徹, 今田勝巳, 難波啓一「Characterization and X-ray analysis of FliJ, a cytoplasmic component of the flagellar type Ⅲ protein export apparatus of *Salmonella*.」特定領域研究「膜超分子モーターの革新的ナノサイエンス」第3回班会議 ポスター番号1P-18, 名古屋大学・野依記念学術交流館, Jun. 27-28, 2008.

○Tatsuya Ibuki, Masafumi Shimada, Tohru Minamino, Katsumi Imada, Keiichi Namba.「X-ray analysis of FliJ, a cytoplasmic component of the flagellar type III protein export apparatus.」XXI congress and General Assembly of the International Union of Crystallography, Poster number P04.01.20, Osaka, Japan, Aug. 23-31, 2008.

○Tatsuya Ibuki, Masafumi Shimada, Tohru Minamino, Katsumi Imada, Keiichi Namba.「Structure of FliJ, a cytoplasmic component of the flagellar type Ⅲ protein export apparatus of *Salmonella*.」第 46 回日本生物物理学会年会, ポスター番号2P041, 福岡国際会議場, Dec. 3-5, 2008.

○Tatsuya Ibuki, Masafumi Shimada, Tohru Minamino, Katsumi Imada, Keiichi Namba.「Structure of FliJ, a cytoplasmic component of the flagellar type Ⅲ protein export apparatus of *Salmonella*.」BLAST X, cuernavaca Mexico, Jan. 18-23, 2009.

○伊吹達也, 南野徹, 風谷謙一, 難波啓一, 今田勝巳「べん毛III型輸送蛋白質FliJと輸送ATPase FliIの相互作用」第9回日本蛋白質科学会年会, ポスター番号1P002, 熊本全日空ホテルニュースカイ, May 20-22, 2009.

○伊吹達也, 南野徹, 風谷謙一, 難波啓一, 今田勝巳「べん毛III型輸送蛋白質FliJと輸送ATPase FliIの相互作用」特定領域研究「膜超分子モーターの革新的ナノサイエンス」第4回班会議 ポスター番号P-4, 沖縄、万国津梁館, Jun. 17-19, 2009.

○Tatsuya Ibuki, Tohru Minamino, Tomoko Miyata, Takayuki Kato, Keiichi Namba,

Katsumi Imada.「Common architecture between the flagellar export apparatus and F_1-ATPase revealed by the structure of FliI and FliJ.」 International Symposium "Innovative Nanoscience of Supermolecular Motor Proteins" Poster number P-13, Shirankaikan, Kyoto university, Japan, Sep. 8-10, 2009.

○Tatsuya Ibuki, Tohru Minamino, Tomoko Miyata, Takayuki Kato, Keiichi Namba, Katsumi Imada.「Common architecture between the flagellar export apparatus and F_1-ATPase revealed by the structure of FliI and FliJ.」第 47 回日本生物物理学会年会, ポスター番号 2P029, 徳島文理大学, Oct. 30-Nov. 5, 2009.

○伊吹達也, 南野徹, 宮田知子, 加藤貴之, 難波啓一, 今田勝巳 「FliI と FliJ の構造より明らかとなったべん毛輸送装置と F1-ATPase における共通の構造」 特定領域研究「生体超分子構造」第 6 回シンポジウム, ポスター番号 P7, 千里ライフサイエンスセンター Dec. 1-2, 2009.

○伊吹達也, 南野徹, 宮田知子, 加藤貴之, 難波啓一, 今田勝巳「べん毛 III 型輸送蛋白質 FliJ の輸送 ATPase FliI に及ぼす影響」日本生体エネルギー研究会第35回討論会, ポスター番号 P11, 旭川医科大学, Dec. 18-20. 2009.

○伊吹達也, 南野徹, 宮田知子, 加藤貴之, 難波啓一, 今田勝巳 「Control mechanism of ATP hydrolysis reaction in the flagellar type III protein export apparatus.」 第10回日本蛋白質科学会, ポスター番号 P2-013, 札幌コンベンションセンター, Jun. 16-18, 2010.

Verbal presentation

○伊吹達也, 島田賢史, 南野徹, 今田勝巳, 難波啓一 「Structure of FliJ, a cytoplasmic component of the flagellar type Ⅲ protein export apparatus of *Salmonella*.」 特定領域研究「生体超分子構造」第５回シンポジウム, つくば国際会議場（エポカルつくば）Dec. 18-19, 2008.

○伊吹達也, 島田賢史, 南野徹, 今田勝巳, 難波啓一「サルモネラ菌べん毛タイプ III 輸送装置構成蛋白質 FliJ の構造」第 15 回べん毛研究交流会, 秋保グラン

ドホテル, Mar. 9-11, 2009.

Prize

「The Crystallographic Society of Japan Poster Award」XXI congress and General Assembly of the International Union of Crystallography, Osaka, Japan, Aug. 31, 2008.

「ポスター賞」第 9 回日本蛋白質科学会年会, 熊本全日空ホテルニュースカイ, May 20-22, 2009.